Morphologie von Polymerwerkstoffen

Analyse von Polyethylenlaufflächen und duromeren Bandbeschichtungen

Dissertation

von

Jörg Fischer

erstellt

bei der Polymer Competence Center Leoben GmbH

eingereicht

am Institut für Werkstoffkunde und Prüfung der Kunststoffe der Montanuniversität Leoben

Betreuung:	Ao.Univ.-Prof. Dipl.-Ing. Dr.mont. Gernot M. Wallner
Begutachtung:	Ao.Univ.-Prof. Dipl.-Ing. Dr.mont. Gernot M. Wallner
	o.Univ.-Prof. Dipl.-Ing. Dr.mont. Clemens Holzer

Leoben, März 2009

Ich erkläre an Eides statt, dass ich diese Arbeit selbstständig verfasst, andere als die angegebenen Quellen und Hilfsmittel nicht benutzt und mich auch sonst keiner unerlaubten Hilfsmittel bedient habe.

Leoben, März 2009 Jörg Fischer

Danksagung

An erster Stelle danke ich von ganzem Herzen meinem Betreuer und Erstbegutachter am Institut für Werkstoffkunde und Prüfung der Kunststoffe der Montanuniversität Leoben, Herrn Ao. Univ.-Prof. Dipl.-Ing. Dr.mont. Gernot M. Wallner. Er stand mir im Laufe der vergangenen Jahre sowohl wissenschaftlich als auch freundschaftlich zur Seite und wusste dabei stets meine Stärken auszubauen und meine Schwächen auszugleichen. Ich bin in der Lage zu behaupten, aus unseren Diskussionen, egal ob beruflich oder privat, mit einer Erweiterung des Geistes hervorgegangen zu sein.

Mein besonderer Dank gilt dem Vorstand des Institutes für Kunststoffverarbeitung der Montanuniversität Leoben, Herrn o.Univ.-Prof. Dipl.-Ing. Dr.mont. Clemens Holzer, für seine Bereitschaft zur Begutachtung dieser Dissertation.

Dem Vorstand des Institutes für Werkstoffkunde und Prüfung der Kunststoffe der Montanuniversität Leoben und Initiator und ehemaligen wissenschaftlichen Geschäftsführer der Polymer Competence Center Leoben GmbH, Herrn o.Univ.-Prof. Dipl.-Ing. Dr.mont. Reinhold W. Lang, danke ich für die Ermöglichung und das Zustandekommen dieser wissenschaftlichen Arbeit.

Weiters gilt mein Dank den Mitarbeitern des Institutes für Werkstoffkunde und Prüfung der Kunststoffe und der Polymer Competence Center Leoben GmbH für den fachlichen Austausch aber auch die persönliche Unterstützung. Insbesondere bedanke ich mich bei Dipl.-Ing. Dr. mont. Katharina Resch und Dipl.-Ing. Dr. mont. Markus Wolfahrt für ihre Freundschaft, ihre Aufrichtigkeit und ihren Beistand. Ferner gilt mein Dank den studentischen Mitarbeitern Sonja Kahr, Laura Kregl, Sylvana Wetscher, Christof Haingartner und Dominik Haselwanter.

Für die Bereitstellung von Formmassen und Halbzeugen für Skilaufflächen sowie für die Herstellung von Ski-Bauteilen danke ich der Firma Fischer Sports GmbH (Ried im Innkreis, A). Mein besonderer Dank gilt dabei Herrn Dipl.-Ing. Alois Pieber und Herrn Dipl.-Ing. Johann Stroi. Zudem danke ich den Firmen

voestalpine Stahl GmbH (Linz, A) und BASF Coatings AG (Münster, D) für die Bereitstellung freier Lackfilme und beschichteter Bleche. Insbesondere bedanke ich mich bei Herrn Dr. Bernhard Strauß (voestalpine Stahl GmbH) und Herrn Dr.-Ing. Lothar Jandel (BASF Coatings AG).

Meiner Familie, und hier ganz besonders meiner Mutter, danke ich für die Unterstützung auf meinem Lebens- und Bildungsweg. Das Wissen jederzeit gestützt zu werden und einen Sicherheitsfallschirm zu besitzen, gibt mir die Kraft mein Leben zu leben.

Schließlich bedanke ich mich bei meiner Frau und besten Freundin Annemarie für ihre Liebe, Geduld, Unterstützung und ihren Glauben an mich. Unsere Hochzeit ermöglichte mir die Einfahrt in meinen Heimathafen. Durch unsere Liebe wurde das für mich bis dato wertvollste Geschenk auf Erden hervorgebracht, unsere Tochter Lara Maria. Ihr möchte ich dafür danken, dass sie mir jeden Tag erneut dabei hilft, das Wesentliche zu erkennen.

Die vorliegende Dissertation wurde an der Polymer Competence Center Leoben GmbH (Projekte II-2.06 und II-2.07) im Rahmen des Kompetenzzentren-Programms K_{plus} des Bundesministeriums für Verkehr, Innovation und Technologie, unter Beteiligung des Institutes für Werkstoffkunde und Prüfung der Kunststoffe der Montanuniversität Leoben und den Firmen Fischer Sports GmbH, voestalpine Stahl GmbH und BASF Coatings AG erstellt und mit Mitteln des Bundes und der Länder Steiermark und Oberösterreich gefördert.

Inhaltsverzeichnis

Kurzfassung

Da die Eigenschaften von Polymerwerkstoffen durch die Morphologie mitbestimmt werden, ist die morphologische Analyse von zentraler Bedeutung für die Etablierung von Struktur/Eigenschafts-Beziehungen. Für aussagekräftige morphologische Analysen wurden Methodenkombinationen entwickelt, wobei insbesondere die Raman-Spektroskopie und -Mikroskopie zunehmende Bedeutung für Polymerwerkstoffe erlangt. Die Hauptzielsetzung der vorliegenden Dissertation lag daher in der systematischen Auslotung der Fernfeld-Raman-Mikroskopie zur Morphologieaufklärung heterogener Polymerwerkstoffe. Dabei wurde einerseits der Schwerpunkt auf Skilaufflächen aus Polyethylencompounds und andererseits auf duromere, wachsgefüllte Bandbeschichtungen gelegt.

Für die morphologische Analyse wurden Mess- und Auswertemethoden zur Bestimmung der Phasenanteile in teilkristallinen Polyethylenen sowie der Additiv- und Pigmentverteilung in Bandbeschichtungen implementiert und angewendet. Bei den Skilaufflächen lag besonderes Augenmerk bei Messverfahren für ungefüllte und gefüllte Polyethylencompounds mit unterschiedlicher Molmasse, wobei die Raman-mikroskopische Methode durch vergleichende thermoanalytische Untersuchungen abgesichert wurde. Für unterschiedlich pigmentierte, wachsgefüllte Bandbeschichtungen wurden zusätzlich licht- und rasterkraftmikroskopische Methoden implementiert und angewendet, um die heterogene Morphologie in einem weiten Größenordnungsbereich qualitativ und quantitativ zu beschreiben.

Für die untersuchten Polyethylencompounds für Skilaufflächen wurde eine signifikante prozessbedingte Abhängigkeit der teilkristallinen Morphologie insbesondere für ultrahochmolekulare Typen unabhängig vom Rußfüllstoff nachgewiesen. Entlang der Prozesskette vom Polymerisat zum strukturierten Skibelag kam es zur Abnahme der kristallinen Anteile einhergehend mit einer Zunahme der amorphen Phase und der Zwischenphase. Nach der Strukturierung der Lauffläche waren signifikante morphologische Unterschiede an der Oberfläche und im Volumen feststellbar.

Die untersuchten Bandbeschichtungen zeigten kugelförmige Wachsdomänen mit Ausdehnungen im Nano- und Mikrometerbereich. In Wachsdomänen mit einem

Durchmesser größer 2 µm waren Spuren des Bindemittels und des Pigments feststellbar. Die heterogene Morphologie der Wachsausprägung war einerseits abhängig von der Formulierung (Pigmentierung und Wachsgehalt). Andererseits wurde ein signifikanter Einfluss der Aushärtebedingungen nachgewiesen.

Abstract

A comprehensive morphological analysis is of prime importance for the establishment of structure/property-correlations for polymeric materials. In the development of advanced morphological characterization methods for materials special emphasis is given to the combined Raman spectroscopy and microscopy. The main objective of this thesis was the systematic evaluation of far-field Raman microscopical techniques for the morphological analysis of heterogeneous polymeric materials. Therefore, semi-crystalline polyethylene compounds for ski bases and thermoset coil coatings were characterized comprehensively.

Measuring and evaluation methods for the three phase morphology of polyethylene and the lubricant and pigment distribution in coil coatings were implemented and used. With regards to ski bases special focus was given to Raman microscopical characterization procedures for polyethylene compounds with varying molar mass. The Raman microscopical approach was corroborated by differential scanning calorimetry. For wax modified coil coatings with varying pigmentation optical light microscopy and Atomic Force Microscopy were further used for the qualitative and quantitative description of the heterogeneous morphology on different scales from the nanometer to the micrometer range.

For the investigated polyethylene compounds for ski bases a significant effect of the processing conditions on the three phase morphology was confirmed especially for grades with ultra high molecular weight. The carbon black filler had a negligible impact on the development of the three phase morphology. Along the process chain from the polymerizate to the structured ski base a decrease of the crystalline fraction associated with an increase of the amorphous fraction and the interphase was found. Structuring leaded to significant different morphologies within the bulk and the surface of the ski base.

For wax modified coil coatings spherical wax domains with dimensions in the nano- and micrometer range were detected. In wax features with diameter above 2 µm residues of binder and pigment were ascertained. The heterogeneous morphology of wax in the coating was on the one hand dependent on formulation

parameters (pigmentation and wax content). On the other hand a significant effect of the curing conditions on the occurrence and distribution of wax was established.

1 Einleitung und Zielsetzung

Das Wort Morphologie leitet sich von den griechischen Wörtern μορφή (morphé = Gestalt, Form) und λόγοζ (lógos = Wort, Lehre, Vernunft) ab und bezeichnet die Formenlehre. In einer Vielzahl unterschiedlichster Wissenschaftsgebiete stellt die Morphologie einen spezifischen Teilbereich dar. So ist dieser Ausdruck beispielsweise in der Astronomie, der Biologie, der Ethnologie, den Geowissenschaften, der Mathematik, den Sprachwissenschaften und den Werkstoffwissenschaften zu finden (Brockhaus, 1998).

Polymere oder Makromoleküle bestehen aus einer großen Anzahl von gleichen oder gleichartigen molekularen Einheiten (Monomeren), die durch kovalente Bindungen miteinander verbunden sind. Makromoleküle sind meist organisch aufgebaute Stoffe, deren Monomereinheiten sich aus Kohlenstoff, Wasserstoff, Sauerstoff, Stickstoff, Halogenen etc. zusammensetzen. Polymere bilden wesentliche Bestandteile von Lebewesen und Pflanzen. Synthetische Polymerwerkstoffe oder Kunststoffe werden durch chemische Polyreaktionen (Polymerisation, Polykondensation oder Polyaddition), welche kovalente Bindungen zwischen den Ausgangsstoffen bewirken, hergestellt. Kunststoffe sind vielseitig einsetzbar und weisen Eigenschaften auf, die in einem weiten Bereich variierbar und gezielt einstellbar sind (Stuart, 1955; Wunderlich, 1973; Van Krevelen, 1990; Menges, 1990; Retting und Laun, 1991; Strobl, 1997).

Mit Morphologie bzw. mit morphologischen Strukturen werden in der Polymerphysik alle unveränderlichen und veränderlichen molekularen und übermolekularen Ordnungszustände bezeichnet, welche in Homo- und Copolymerisaten, in Polymermischungen und in Mischungen von Polymeren mit anderen Stoffen auftreten. Die physikalischen und technologischen Eigenschaften von Kunststoffen werden von der Morphologie von Polymerwerkstoffen bestimmt, die wiederum vom chemischen Aufbau der eingesetzten Komponenten sowie von den Herstellungs- und Verarbeitungsbedingungen abhängig ist (Retting und Laun, 1991; Woodward, 1995; Strobl, 1997).

Je nach betrachteter Größenordnung liegen Morphologien in unterschiedlichen Strukturebenen vor. Demnach wird zwischen der Morphologie auf molekularer Ebene, der Morphologie von übermolekularen Strukturen, der Morphologie von mehrphasigen Polymerwerkstoffen und der Morphologie von gefüllten Polymerwerkstoffen unterschieden. Auf molekularer Ebene wird die Morphologie durch unveränderliche Strukturparameter wie chemische Zusammensetzung der monomeren Bausteine, der Kettenstruktur, der Kettentopologie, der Molekulargewichtsverteilung sowie der Dichte der permanenten Vernetzungspunkte bestimmt. Übermolekulare Ordnungszustände, zu denen kristalline Überstrukturen, flüssigkristalline Mesophasen, Leerstellenkonzentrationen, Orientierungen und Defektstellen zählen, sind nach der Polyreaktion veränderbar und durch geeignete Ver- und Bearbeitungsmethoden sowie durch gezielte Nachbehandlungen einstellbar. Die Morphologie mehrphasiger Polymerwerkstoffe wird bei Blockcopolymeren durch den chemischen Aufbau im Copolymerisat und damit durch einen unveränderlichen Parameter beeinflusst. Bei Polymermischungen ist hingegen eine Einflussnahme durch nach der Polyreaktion veränderbare Strukturparameter erzielbar. So ist es möglich, die Mischpartner sowie das Mischungsverhältnis bei der Compoundierung zu variieren. Die Morphologie gefüllter Polymerwerkstoffe ist durch die Wahl von Füll- und Verstärkungsstoffen und durch den Verarbeitungsprozess beeinflussbar (Stuart, 1955; Wunderlich, 1973; Woodward, 1988; Van Krevelen, 1990; Menges, 1990; Retting und Laun, 1991; Cahn et al., 1993; Woodward, 1995; Strobl, 1997).

Die Kenntnis der Wechselwirkung zwischen morphologischen Strukturen und den daraus resultierenden Eigenschaften stellt die Basis für eine gezielte Werkstoffentwicklung dar. Hierzu ist eine exakte Charakterisierung der Polymerstrukturen mit geeigneten physikalischen Mitteln erforderlich. Zur Untersuchung der Morphologie von Kunststoffen werden mikroskopische, thermoanalytische, spektroskopische sowie beugungs- und streuungsanalytische Methoden eingesetzt. Die Mikroskopie, mit der die Darstellung von strukturellen Einzelheiten im Inneren und an der Oberfläche von Proben möglich ist, ist das gängigste Verfahren. Durch den Einsatz der kompletten mikroskopischen Bandbreite, die von der einfachen Lichtmikroskopie über die Elektronen-

mikroskopie (Raster-Elektronenmikroskop (REM) und Transmissions-Elektronenmikroskop (TEM)) bis hin zur Rastersondenmikroskopie (z.B. Rasterkraftmikroskop (AFM)) reicht, ist es möglich, die Morphologie von Polymeren in sämtlichen Strukturebenen zu analysieren. Mit Hilfe der Differentialthermoanalyse (DTA), der dynamischen Differenzkalorimetrie (DSC) sowie der Dilatometrie werden thermoanalytische Strukturuntersuchungen durchgeführt. Durch die Detektion von Phasenübergängen, Schmelzvorgängen und thermischen Ausdehnungen ermöglicht die Thermoanalyse Rückschlüsse auf die Leerstellenkonzentration, die kristalline Struktur teilkristalliner Polymere sowie die Molekülorientierung. Die dafür eingesetzten Untersuchungsmethoden werden demzufolge vorwiegend dazu verwendet, die Morphologie übermolekularer Strukturen zu messen. Das Vorliegen von mehrphasigen Polymerwerkstoffen sowie die Auswirkung von Füll- und Verstärkungsstoffen auf die Überstrukturen in gefüllten Polymerwerkstoffen sind jedoch ebenso ermittelbar. Zur strukturellen Untersuchung von Polymeren mittels Spektroskopie werden die Infrarot-, die Raman-, die Kern-Resonanz-, die Elektronenspin-Resonanz-, die mechanische und die dielektrische Spektroskopie verwendet. Obwohl diese Methoden vorwiegend zur Untersuchung der Morphologie auf molekularer Ebene eingesetzt werden, sind spezifische spektroskopische Messeinrichtungen sehr gut dazu geeignet, die Morphologie in sämtlichen Strukturebenen zu detektieren. Auch beugungs- und streuungsanalytische Methoden eignen sich zur Untersuchung der Morphologien in Strukturebenen unterschiedlicher Größenordnung. Auf molekularer Ebene kommen vorwiegend Elektronen- und Neutronenbeugung zum Einsatz. Durch die Röntgen-Strukturanalyse ist es möglich, sowohl die molekularen als auch die übermolekularen Ordnungszustände unterschiedlicher Polymerwerkstoffe zu untersuchen. Lichtstreumethoden eignen sich zur Analyse der Morphologie von übermolekularen Strukturen (Kämpf, 1982; Woodward, 1988; Retting und Laun, 1993; Woodward, 1995).

Da die Analyseverfahren unterschiedliche Möglichkeiten und Einschränkungen aufweisen, wurde eine Reihe von Methodenkombinationen entwickelt, die eine umfassendere Bestimmung morphologischer Strukturen erlauben. Oftmals werden mikroskopische Analyseverfahren mit komplementären spektroskopischen oder

thermoanalytischen Methoden kombiniert (Coates und Reffner, 1999; Pollock und Hammiche, 2001; Kannan et al., 2006; Lin et al., 2007; Christofferson et al., 2008). Aufgrund der hohen erzielbaren lateralen und vertikalen Auflösung und der ausgezeichneten molekular-strukturellen Sensitivität erlangt die Raman-Mikroskopie, eine Kombination aus Raman-Spektroskopie und Mikroskopie, zunehmende wissenschaftliche Bedeutung. Bei der Raman-Mikroskopie ist zwischen Fernfeld- und Nahfeld-Raman-Mikroskopie zu unterscheiden. Bei der erstgenannten, bereits ausgereiften Methode kommen Messgeräte bestehend aus einer Kombination aus Raman-Spektrometer und Lichtmikroskop (Raman-Mikroskope) zum Einsatz. Die damit erzielbare räumliche Auflösung ist auf etwa 500 nm begrenzt und hängt von der Anregungswellenlänge des Lasers, der Numerischen Apertur der Objektivlinse und der untersuchten Probe ab. Durch Einsatz der beiden sich noch in Entwicklung befindlichen Untersuchungsmethoden zur Nahfeld-Raman-Mikroskopie, der oberflächenverstärkten Ramanstreuung (SERS = Surface Enhanced Raman Scattering) und deren Weiterentwicklung der spitzenverstärkten Ramanstreuung (TERS = Tip Enhanced Raman Scattering), sind hingegen räumliche Auflösungen unter 100 nm möglich (Bailo und Deckert, 2008; Kudelski, 2009).

Die bereits in vielen Bereichen eingesetzten Fernfeld-Raman-Mikroskope eignen sich zur qualitativen und quantitativen Charakterisierung von molekular aufgebauten Proben aller Aggregatzustände. Infolge berührungsfreier Detektion der Schwingungs- und Rotationszustände von polaren aber vor allem von unpolaren Molekülbindungen ermöglicht die Raman-Mikroskopie eine Analyse von anorganischen und organischen Stoffen. Diese Methode eignet sich daher zur Materialcharakterisierung in unterschiedlichsten Anwendungsbereichen und wird derzeit zur Untersuchung der chemischen Zusammensetzung und morphologischen Struktur von Arzneimitteln, Edelsteinen, Farbstoffen, Halbleitermaterialien, Katalysatoren, Mineralien, Polymeren und anderen Materialien eingesetzt (MacCreery, 2000; Weber, 2000). Bei Polymerwerkstoffen dient die Raman-Mikroskopie zur Aufklärung der Morphologie auf molekularer und übermolekularer Ebene sowie zur Ermittlung der Struktur heterogener Polymerwerkstoffe (mehrphasige oder gefüllte Systeme). Neben der Analyse der chemischen

Zusammensetzung, der Kettenstruktur, des Polymerisationsgrades, der Vernetzungsdichte, der teilkristallinen Morphologie, des Kristallinitätsgrades und der Kristallform ist es ebenso möglich, den strukturellen Aufbau von Blockcopolymeren, Polymermischungen sowie von anorganisch und/oder organisch gefüllten Polymerwerkstoffen zu detektieren (Strobl und Hagedorn, 1978; Siesler, 1980; Hendra und Agbenyegba, 1993; Schrader, 1995; Jenkins und Larsen, 2004; Kannan et al., 2006; Koenig und Bobiak, 2007).

Im Rahmen zweier Forschungsprojekte, die an der Polymer Competence Center Leoben GmbH (Leoben, A) und am Institut für Werkstoffkunde und Prüfung der Kunststoffe (Montanuniversität Leoben, A) in Kooperation mit den Firmenpartnern Fischer Sports GmbH (Ried im Innkreis, A), voestalpine Stahl GmbH (Linz, A) und BASF Coatings AG (Münster, D) betrieben werden, wird auf die Erarbeitung eines grundlegenden und umfassenden Verständnisses über Zusammenhänge zwischen strukturellen, werkstofflichen und prozesstechnischen Parametern und den für die Anwendung relevanten Eigenschaften abgezielt. In den Projekten mit den Titeln „Effect of molecular and morphological parameters of PE-UHMW compounds on the performance of ski-running surfaces“ und „Development and characterization of novel two-layer high performance coil coatings for the buildings industry“ wird eine umfassende Charakterisierung von Polyethylen-Skilaufflächen und wachsgefüllten, polyesterbasierenden Bandbeschichtungen durchgeführt. Dabei werden heterogene Polymerwerkstoffe untersucht, in denen aliphatische Kohlenwasserstoffe entweder als Polymermatrix oder als eine in der Polymermatrix verteilte disperse Phase eingesetzt werden. Für die Erarbeitung von Struktur/Eigenschafts-Beziehungen ist eine umfassende morphologische Charakterisierung der vorliegenden Polymerwerkstoffe unumgänglich. Daher liegen die Hauptzielsetzungen dieser Arbeit in der Raman-mikroskopischen Charakterisierung der übermolekularen und heterogenen Struktur von Polyethylen-Skilaufflächen sowie der spektroskopischen und mikroskopischen Analyse der heterogenen Struktur von wachsgefüllten Bandbeschichtungen. Im Rahmen der Dissertation sollen als Basis für die Erarbeitung von Struktur/Eigenschafts-Beziehungen morphologische Strukturparameter ermittelt

werden. Die Ermittlung der Struktur/Eigenschafts-Beziehungen ist aus rechtlichen Gründen nicht Ziel dieser Arbeit.

In Anlehnung an die genannten Zielsetzungen gliedert sich diese Dissertation in die folgenden vier Kapitel:

1 Einleitung und Zielsetzung

2 Morphologie von Polymerwerkstoffen für Skilaufflächen

3 Morphologie von Polymerwerkstoffen für Bandbeschichtungen

4 Zusammenfassung und Ausblick

Im Anschluss an dieses einleitende Kapitel werden in Kapitel 2 die Morphologien von Polyethylen-Skilaufflächen in Strukturebenen unterschiedlicher Größenordnung diskutiert. Das Gleitverhalten von Skilaufflächen hängt von der Auswahl des eingesetzten Materials, von der Art und Menge des verwendeten Füllstoffes und von der an die Schnee- und Umgebungsbedingungen angepassten Strukturierung ab (Stroi, 2003; Colbeck und Perovich, 2004; Isosport, 2009; Fischer Sports, 2009). Die Wahl dieser genannten Parameter beeinflusst jedoch auch die in den Laufflächen vorliegenden Morphologien, weshalb ein Zusammenhang zwischen Gleitverhalten und morphologischer Struktur anzunehmen ist. Einerseits wird in Kapitel 2 der Einfluss der gewählten Polymerwerkstoffe und der Ver- und Bearbeitungsschritte auf die teilkristalline Morphologie der Skilaufflächen erarbeitet und diskutiert. Andererseits wird die Auswirkung der Modifikation mit Ruß auf die Morphologie des gefüllten Polymerwerkstoffes für Skilaufflächen ausgearbeitet und beschrieben.

In Kapitel 3 liegt der Schwerpunkt bei der Darstellung und Beschreibung der morphologischen Struktur von wachsgefüllten Bandbeschichtungen. Damit bei einer Verformung von bandbeschichteten Blechen keine Schädigungen des Lackes auftreten, ist eine Wachsausprägung auf der Oberfläche, die als Gleitmittel bei direktem Kontakt mit dem Verformungsstempel wirkt, erforderlich (Nanetti, 2000; Chvedov und Jones, 2004; Meuthen und Jandel, 2005). Kapitel 3 beschäftigt sich mit der Erarbeitung eines grundlegenden und umfassenden

Verständnisses der Zusammenhänge zwischen Wachsausprägung in Bandbeschichtungen und Lackformulierung bzw. Lackaushärtung.

Die beiden nachfolgenden Kapitel 2 und 3 bestehen aus einer Einleitung zur jeweiligen Thematik und den dazugehörigen Veröffentlichungen. Im einführenden Teil wird der themenspezifische Stand von Wissenschaft und Technik zusammen mit den wesentlichen Erkenntnissen der Publikationen beschrieben. Die angeführten wissenschaftlichen Veröffentlichungen beinhalten detaillierte Beschreibungen der untersuchten Proben, der eingesetzten Untersuchungsverfahren, der wesentlichen Ergebnisse sowie der aus den Resultaten abgeleiteten Schlussfolgerungen.

In Kapitel 4 werden sämtliche Ergebnisse, erhalten aus den wissenschaftlichen Arbeiten, gemeinsam mit Schlussfolgerungen bezüglich der Morphologieausprägung in Polyethylenlaufflächen sowie in duromeren Bandbeschichtungen zusammengefasst. Im Ausblick werden bisher noch nicht behandelte Fragestellungen zusammen mit Vorschlägen für zukünftige wissenschaftliche Arbeiten aufgezeigt.

Die Dissertation besteht aus fünf gemeinsam mit Co-Autoren verfassten Publikationen. In sämtlichen Arbeiten ist der Verfasser dieser Doktorarbeit Erstautor. Alle angeführten Veröffentlichungen wurden für referierte Zeitschriften erstellt und eingereicht. Eine Publikation wurde bereits veröffentlicht (Arbeit 1).

2 Morphologie von Polymerwerkstoffen für Skilaufflächen

Im Laufe einer jahrzehntelangen Entwicklung wurden unterschiedlichste Werkstoffe (Glas, beschichtetes Holz, Keramik, verschiedene Kunststoffe und diverse Metalllegierungen) auf ihre Eignung für Skilaufflächen untersucht. Polyethylen kristallisierte sich nicht nur wegen seiner einfachen Ver- und Bearbeitbarkeit sondern auch aufgrund des hervorragenden Gleitverhaltens auf Schnee und Eis als überlegen heraus. Daher werden zur Herstellung von Skilaufflächen Niederdruck-Polyethylene verwendet, die infolge spezifischer Wahl der Polymerisationsbedingungen mittlere Molmassen zwischen 300.000 und 12.000.000 g/mol aufweisen. Es werden sowohl lineare Polyethylene mit unterschiedlichen Dichten (Polyethylen niedriger, mittlerer und hoher Dichte (PE-LLD, PE-MD und PE-HD)) als auch ultrahochmolekulare Polyethylene (PE-UHMW) eingesetzt. Aufgrund des Einflusses von Struktur und Länge der Molekülketten auf die Kristallisationsfähigkeit von Polymeren hängt die teilkristalline Morphologie der Lauffläche von der Auswahl des Polyethylentyps ab. Da Polyethylen zur Verbesserung der Gleiteigenschaften meist mit Additiven (Paraffine, Silikone, Metallsalze etc.) und Füllstoffen (Ruß, Talkum etc.) compoundiert wird, weisen Skilaufflächen auch morphologische Strukturen heterogener Polymerwerkstoffe auf. Diese werden von der Art und Menge der eingesetzten Stoffe beeinflusst (Schamesberger, 1995; Glenne et al., 1997; Stroi, 2003; Colbeck und Perovich, 2004; Federolf, 2005; Isosport, 2009; Fischer Sports, 2009).

Neben der Zusammensetzung des Ausgangstoffes (Polymer, Additive, Füllstoffe) üben prozessbedingte Faktoren wie Temperatur, Zeit oder mechanische Belastung einen signifikanten Einfluss auf die morphologische Struktur von Polymerwerkstoffen aus (Wallner, 2008). Dementsprechend ist infolge des aus einer Reihe von Einzelschritten bestehenden Skiherstellungsprozesses eine Morphologieänderung der Lauffläche zu erwarten. Im ersten Schritt der Skierzeugung wird das formulierte Polyethylencompound abhängig von der

Fließfähigkeit entweder durch Extrusion (mittlere Molmasse: 300.000 – 600.000 g/mol) oder durch Sinterung (mittlere Molmasse: 3.000.000 – 12.000.000 g/mol) zum Halbzeug verarbeitet. Anschließend findet eine thermisch-mechanische Vorbehandlung des Halbzeuges statt, die eine folgende Verklebung des unpolaren Kunststoffes mit dem laminierten Kern des Skisandwiches ermöglicht. Reste des Klebstoffes, die sich auf der Lauffläche des fertig verklebten Skibauteils befinden, werden durch einen Reinigungsschliff entfernt. Zur Optimierung des Gleitverhaltens wird abschließend mit unterschiedlichen mechanischen Verfahren (Schleifen, Prägen oder Gravieren) eine an die Schnee- und Umgebungsbedingungen angepasste topographische Struktur auf der Oberfläche des Skibelags erzeugt (Schamesberger, 1993; Stroi, 2003; Jordan und Brown, 2006; Schamesberger, 2006; Fischer Sports, 2009).

Zur systematischen Erfassung der Morphologieänderung entlang der Prozesskette sind zerstörungsfreie Messmethoden erforderlich, die gegebenenfalls auch in-situ einsetzbar sind. Was die Untersuchung der Morphologie von Polyethylenwerkstoffen anlangt, so wurden mehrere Arbeiten publiziert, die sich mit der morphologischen Charakterisierung mittels Fernfeld-Raman-Mikroskopie beschäftigen. Eine besondere Aufmerksamkeit erlangte dabei die Analyse der dreiphasigen teilkristallinen Morphologie, die sich aus einer kristallinen Komponente, einer amorphen Komponente und einer imperfekt geordneten Komponente mit anisotroper Beschaffenheit, die oft als Zwischenphase bezeichnet wird, zusammensetzt. Da die berechneten Phasenanteile von der angewendeten Methode zur Spektrenzerlegung abhängen, beschäftigten sich bereits einige Autoren mit der Entwicklung und Anpassung geeigneter Peak-Fit-Prozeduren, welche anschließend zur Analyse von Polyethylencompounds eingesetzt wurden (Strobl und Hagedorn, 1978; Keresztury und Földes, 1990; Failla et al., 1992; Rull et al., 1993; Lin et al., 2007). Unter Verwendung der Raman-Mikroskopie wurden neben der Charakterisierung der drei Phasen von unterschiedlichsten Polyethlyentypen auch die Einflüsse von Abrieb, Alterung, Bestrahlung, Verarbeitung und Verstreckung auf die Morphologie der übermolekularen Strukturen von Polyethylen untersucht (Rodriguez-Cabello, 1998; Bertoluzza et al., 2000; Fagnano et al., 2001; Paradkar et al., 2003; Cherukupalli

und Ogale, 2004; Rodriguez-Perez et al., 2005; Visentin et al., 2006; Reggiani et al., 2006; Kyomoto et al., 2007; Barron und Birkinshaw, 2008). Bisher wurde die Raman-Mikroskopie jedoch noch nie für eine umfassende morphologische Charakterisierung von Skilaufflächenwerkstoffen eingesetzt. Zudem wurden meist ungefüllte Polyethylencompounds untersucht und diskutiert.

Die Hauptzielsetzung des vorliegenden Kapitels liegt daher in der systematischen Aufklärung der Morphologie von Polyethylencompounds für Skilaufflächen unter Berücksichtigung werkstofflicher und prozesstechnischer Einflussfaktoren. Dazu werden ausgehend von der Entwicklung und Implementierung einer Raman-spektroskopischen Mess- und Auswertemethode zur Charakterisierung der dreiphasigen teilkristallinen Morphologie die Raman-Mikroskopie und die dynamische Differenzkalorimetrie (DSC) zur Untersuchung von ungefüllten Polyethylenlaufflächen eingesetzt. Dadurch wird die Eignung der Raman-Spektroskopie zur Untersuchung des kristallinen Phasenanteils und der weiterführenden umfassenden Charakterisierung der teilkristallinen Morphologie überprüft. Hierbei ist zu beachten, dass die untersuchten Skilaufflächen keiner spezifischen Oberflächenbehandlung ausgesetzt werden, um die Vergleichbarkeit zwischen den morphologischen Strukturen im Inneren und an der Oberfläche zu gewährleisten. Darauf aufbauend wird die Morphologie von heterogenen Polymerwerkstoffen an gefüllten Laufflächen sowie die Auswirkung der Oberflächenstrukturierung auf die morphologischen Strukturen der Polyethylen-compounds untersucht und diskutiert.

In Arbeit 1 wurde durch den Einsatz der Raman-Mikroskopie die dreiphasige teilkristalline Morphologie von fünf unterschiedlichen für Skilaufflächen eingesetzten Polyethylentypen auf drei Prozessebenen erarbeitet und diskutiert. Nach der Implementierung eines Mess- und Auswertetools zur Charakterisierung der drei morphologischen Phasen wurden die Raman-spektroskopisch gemessenen Kristallinitätsgrade mit Ergebnissen der DSC-Untersuchungen überprüft. Aufgrund der guten Vergleichbarkeit zwischen den aus den unterschiedlichen Messmethoden erhaltenen kristallinen Phasenanteilen wurde die Eignung der Fernfeld-Raman-Mikroskopie für den Einsatz der morphologischen Charakterisierung von Skilaufflächen bestätigt. Die

Untersuchungen zeigten molmassenspezifische Unterschiede bei der Veränderung der teilkristallinen Morphologie infolge Ver- und Bearbeitung der Lauffläche. Niedermolekularere Polyethylentypen wiesen auf den drei Prozessebenen weitgehend vergleichbare morphologische Strukturen auf. Demgegenüber wurden bei den Polyethylenen mit einer höheren mittleren Molmasse abnehmende kristalline und zunehmende amorphe Anteile nachgewiesen.

Basierend auf den in Arbeit 1 gewonnenen Erkenntnissen wurden in Arbeit 2 die morphologischen Strukturen von gefüllten Polyethylenlaufflächen mittels Raman-Mikroskopie und dynamischer Differenzkalorimetrie untersucht, wobei eine Erweiterung der miteinbezogenen Prozessebenen bis hin zur strukturierten Skilauffläche stattfand. Besonderes Augenmerk lag dabei bei der Auslotung und Implementierung einer adäquaten Raman-spektroskopischen Mess- und Analysemethode für russgefüllte Werkstofftypen. Die umfassende Charakterisierung der heterogenen Morphologie gefüllter Extrusions- und Sinterwaren zeigte, dass die Ermittlung der dreiphasigen teilkristallinen Morphologie lediglich bei gefüllten Sinterwaren möglich ist. Bei russgefüllten Extrusionstypen waren aufgrund der feinen Füllstoffverteilung die Polymer- und Füllstoffphasen nicht eindeutig separier- und analysierbar. Die morphologischen Untersuchungen an Sinterwaren ergaben einen signifikanten Einfluss der Ver- und Bearbeitungsschritte. Entlang der Prozesskette wurden eine Abnahme der kristallinen Phase sowie eine Zunahme der amorphen Phase detektiert. Lediglich nach Strukturierung der Skilauffläche durch Schleifen waren signifikante Unterschiede zwischen der Morphologie im Inneren und an der Oberfläche feststellbar. Dieser abschließende Prozessschritt führte in der obersten Schicht der Lauffläche zu einer signifikanten Abnahme der kristallinen Phase sowie zur Zunahme der amorphen Phase und der Zwischenphase.

2.1 Arbeit 1

J. Fischer, G.M. Wallner, A. Pieber

Spectroscopical investigation of ski base materials

Macromolecular Symposia 265 (2008) 28-36

Spectroscopical investigation of ski base materials

J. Fischer[1], G.M. Wallner[2], A. Pieber[3]

[1] Polymer Competence Center Leoben GmbH, Roseggerstrasse 12, Leoben, 8700, Austria, Tel.: +43 3842 402 2109, Fax: +43 3842 402 2102, E-Mail address: joerg.fischer@pccl.at

[2] Institute of Material Science and Testing of Plastics, University of Leoben, Franz-Josef-Strasse 18, Leoben, 8700, Austria

[3] Fischer Sports GmbH, Fischerstrasse 8, Ried/Innkreis, 4910, Austria

Summary

Raman spectroscopy was applied to perform a comprehensive morphological analysis of polyethylene (PE) ski base materials at different processing levels. The morphological characterization included determination and evaluation of Raman spectra and examination of the crystallinity values by differential scanning calorimetry (DSC). A good agreement between Raman and DSC crystallinity fractions was obtained, thus corroborating the Raman spectroscopy approach. While for the PE grade with the lowest average molar mass no significant morphological changes due to processing from the raw material via the extruded film to the post-treated film was found, higher molar mass PE grades exhibited a decrease of crystallinity, but an increase of the amorphous fraction along the process chain.

Keywords: Raman spectroscopy; polyethylene; morphology; DSC; ski base

Introduction

From a market point of view polyethylene (PE) is the most important commercially used polymer with overall market shares of about 30% [1]. While commodity PE grades are dominating in various industrial sectors, such as the packaging

industry, engineering PE grades have also been developed for technical applications, requiring special functional properties. An outstanding example is ultra-high-molecular-weight polyethylene (PE-UHMW) with advanced tribological behaviour. In the literature many investigations on PE-UHMW are described focusing on the application as bearing material in orthopaedics [2-6]. However, PE grades with special tribological properties are also used for other applications which attract less scientific attention. Regarding the leisure and sports industry PE materials are of special relevance for running surfaces (i.e., bases), which are a key element of alpine and nordic skis determining their glide characteristics. For this application currently polyethylene extrusion grades with molar mass between 300,000 and 600,000 g/mol (linear low, medium and high density polyethylene (PE-LLD, PE-MD and PE-HD)) and sinter grades with molar mass between 3,000,000 and 12,000,000 g/mol (PE-UHMW) are used. The process from the raw material to a finished ski base surface consists of various steps, including the formulation and compounding of the material, the extrusion or sintering of semi-finished films, post-treatment (e.g., flaming) of the film, and production of the ski. To improve the base performance advanced material formulations and surface structuring techniques have been developed, implemented and used. While relationships between the additive content of ski base materials, the topographical structure of ski base surfaces and the gliding characteristics were established, up to now no systematic investigation on the effect of material morphology on the performance of ski base surfaces has been carried out. Hence, the overall objective of our research work is to study the morphology of ski base materials on different processing levels (raw material (compound), semi-finished film and post-treated film) by various techniques.

PE-LLD, PE-MD, PE-HD and PE-UHMW are linear forms of polyethylene with semi-crystalline morphology. Important variable parameters of semi-crystalline polymers are the degree of crystallinity and the semi-crystalline morphology, which is considered as a superposition of three phases, the crystalline component (often lamellae), the melt-like amorphous component and the disordered component of anisotropic nature (interphase) [7].

Relevant parameters of polyethylene are commonly derived by density

measurement, differential scanning calorimetry (DSC), infrared (IR) and Raman spectroscopy, nuclear magnetic resonance spectroscopy (NMR), and wide and small angle X-ray scattering (WAXS and SAXS) techniques. While for most of these methods an adequate sample preparation (i.e., the destruction of the sample) is required, Raman spectroscopy has proved to be an appropriate tool to investigate morphological parameters of PE without any kind of damage. Furthermore, Raman spectroscopy allows for a rather comprehensive description of morphological parameters including the full characterization of the three phase components. Although there are some controversies in the literature concerning the feasibility of Raman spectroscopy for the determination of the disordered phase [8-10], various recent studies [6, 11] have used the three phase model to describe morphology changes due to processing or loading and obtained reasonable results from a polymer physical point of view.

The sliding characteristic of ski bases is mainly affected by structural and morphological parameters of the surface layer, which is in contact with the snow counterpart. Therefore, the primary purpose of this paper is to describe morphological parameters at the surface of PE ski base grades as a function of different processing levels. In addition to the various advantages described above, Raman spectroscopy is a sensitive method with high lateral and vertical resolution to determine the morphology of materials surfaces. Therefore, Raman spectroscopy was applied in this study as the prime method. To corroborate the crystallinity values determined by Raman spectroscopy DSC measurements were also carried out. Regarding DSC special attention was given to the sample preparation. An appropriate technique to cut the sample from the surface layer was implemented and used.

Experimental

Materials

Within this work five polyethylene grades differing in their average molar mass and distribution were selected, compounded with additives but without modifiers (e.g., carbon black) and processed to semi-finished products (ski base film) (Table 1).

The compounds and semi-finished products were supplied by Fischer GmbH (Ried, Austria). Depending on the material grade two different techniques, Extrusion (200-220°C) and sintering (200-230°C, 250 bar, 12 h, heating/cooling rate: 30°C/h) were applied to manufacture the ski base film, which was further treated (post-treated film) by flaming with an oxygen rich (yellow) flame (200-300°C, 0.5-1 s). These processing steps are common before the production of the ski. Due to secrecy reasons further processes after the ski production are not considered within this paper.

Table1. Characteristics of the polyethylenes used in this work

Designation in this work	Material	processing method	Density (g/cm³)	M_W x 10^{-3} (g/mol)
M2	PE-LLD	extrusion	0.914	250
M4	PE-MD	extrusion	0.936	400
H4	PE-UHMW	sintering	0.911	4,000
H9	PE-UHMW	sintering	0.918	9,000
HA	PE-UHMW	sintering	0.918	10,500

Raman spectroscopy

Raman spectra were determined by using a LabRam confocal-Raman spectrometer (HORIBA Jobin Yvon GmbH, Bensheim, D). Excitation of Raman bands was obtained upon irradiating the sample with a frequency doubled Nd-YAG laser of 100 mW operating at 532 nm. All measurements were performed in a backscattering geometry, using a 100x long working distance (3.4 mm) microscope objective with a numerical aperture value of 0.80, providing a lateral resolution of about 800 nm. To obtain a spectral resolution of about 3 cm^{-1} a diffraction grating of 1800 grooves/mm was used. Single point spectra were derived from 5 scans with an accumulation time of 5 s. By measuring on three different positions of a specimen mean and standard deviation values were evaluated.

The Raman spectra were manipulated by smoothing and baseline correction. To determine the areas under the peaks of interest, which was used as the measure for the intensity values (I), a curve-fitting procedure was carried out with the software package PeakFit v4.12 (SeaSolve Software Inc.). Appropriate fitting

results were obtained by peak fitting with freely floating ratios of Gaussian and Lorentzian amounts automatically optimized by the software (Figure 1). The reproducibility of the fit was corroborated by fitting the peaks multiple times.

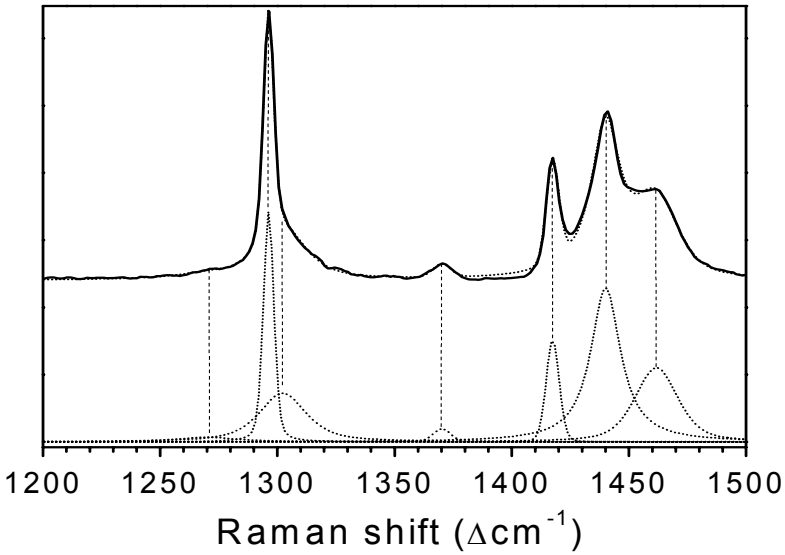

Figure 1. Raman spectra of PE with typical curve fitting results.

To evaluate the degree of crystallinity (α_c) the method devised by Strobl and Hagedorn [7] was used (see Eq. (1)). Because ski bases are produced by at least partial melting and crystallization orthorhombic crystalline structures were assumed.

$$\alpha_c = \frac{I_c}{0.45 \cdot I_T} \cdot 100\% \qquad (1)$$

where I_c is the integrated area of the Raman band representing the orthorhombic crystalline phase, I_T is the integrated area of the CH_2 twisting vibration region (1200-1350 cm^{-1}), which is not affected by the morphology and therefore used as an internal intensity reference and 0.45 is a normalization coefficient, which was found through experiments on 100% crystalline PE [12, 13].

Furthermore the fraction of the amorphous phase (α_a) was calculated by using Eq. (2) [7]:

$$\alpha_a = \frac{I_a}{I_T} \cdot 100\% \qquad (2)$$

where I_a is the integrated area of the Raman band representing the amorphous phase.

Finally, the fraction of the interphase (α_b) is given by Eq. (3) [7]:

$$\alpha_b = 100\% - \alpha_a - \alpha_c \quad (3)$$

Differential scanning calorimetry

The DSC measurements were conducted on a Mettler Toledo DSC 822^e instrument (Mettler Toledo GmbH, Schwerzenbach, CH). Before testing, temperature and heat flow signals from the apparatus were calibrated using indium and zinc. Thermal analyses were carried out in air with PE specimens whose weight ranged between 2 and 3 mg. Samples with a thickness of 0.2 mm and a diameter of 4 mm were prepared from the semi-finished and post-treated films by planning a layer with the defined thickness and by cutting with the defined cross-section (diameter). Each DSC curve was recorded from -30 to 180°C applying a heating rate of 10°C/min. The degree of crystallinity was determined as the ratio between the heat of fusion of the specimen and the heat of fusion of a perfect (100%) crystalline PE (293.6 J/g) [14]. To check possible superimposed melting and crystallization effects due to a low heating rate, various heating rates ranging from 10 to 50°C/min were applied in preliminary investigations. Because no effect of heating rate on the DSC based crystallinity values was found, the standardized rate of 10°C/min was used. By measuring on three different specimens mean and standard deviation values were evaluated.

Results and Discussion

Raman spectroscopy

As discussed in various references [2, 4-7, 11-13, 15-20], in Figure 2 a representative Raman spectrum of PE material H9 is exhibited along with the assignment of the Raman bands to vibration modes. Attributions of Raman bands to morphological phases and to conformational states of the PE chains are well established [2, 4-7, 11-13, 15-20]. In the spectral region from 1000 to 1550 cm^{-1} the bands between 1400 and 1480 cm^{-1} correspond to methylene bending vibrations ($\delta(CH_2)$). The crystalline phase is represented by the peak at 1416 cm^{-1} (crystallinity band) [7]. This band is in conjunction with a crystal field splitting phenomenon, which is resulting from an interaction between the two chains of the

orthorhombic unit cell in all-trans conformation [16]. The crystallinity band at 1416 cm^{-1} has been used to determine the degree of orthorhombic crystallinity of PE samples [2-13, 15, 19]. For the monoclinic crystalline structure, which is a further lattice structure observed in PE, high chain folding energy is required. Hence, a

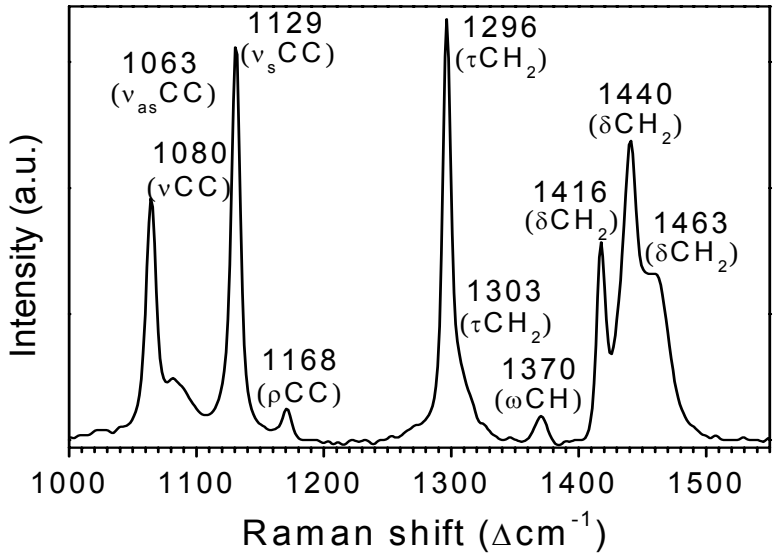

Figure 2. Raman spectrum of PE together with indication of peak wavenumbers and vibration modes.

direct crystallization from the melt into the monoclinic form is impossible [5, 21]. A prerequisite for recrystallization from the orthorhombic to the monoclinic structure is a high energy input (i.e., shear or compression deformation) [22-24]. For melt crystallized PE samples without significant energy input the orthorhombic crystallinity represents the overall crystalline fraction.

The bands at 1080 and 1303 cm^{-1} are assigned to the amorphous phase with PE chains in gauche conformation. Both bands have been used to determine the amount of the amorphous fraction. However, the values of the amorphous content derived from the band at 1303 cm^{-1} (amorphous band) are reported to be more reliable [15]. The Raman peaks at 1063 and 1123 cm^{-1} are attributed to the symmetric and asymmetric C-C stretching vibrations, respectively, occurring in conformational trans sequences longer than 10 all-trans bonds [16, 25]. Because of the highly localized character of the methylene twisting vibrations ($\tau(CH_2)$), the peaks at about 1300 cm^{-1} are almost independent of conformation and

temperature. Therefore, the integrated intensity of the methylene twisting bands is used as an internal intensity standard.

In Figure 3 Raman spectra of the investigated PE samples at the various processing levels are displayed. A qualitative interpretation of the crystalline and amorphous fractions is done by analysis of the spectral regions from 1400 to 1550 cm^{-1} (bending vibrations) and 1250 to 1350 cm^{-1} (twisting vibrations), respectively. For the semi-finished and post-treated films higher intensities of the amorphous band at 1303 cm^{-1} are observable. Hence, due to extrusion or sintering of the raw material an increase of the amorphous phase is established. Concerning the crystallinity band no distinct trends along the process chain are ascertainable. Therefore, a comprehensive analysis of the three phases was carried out. Quantitative data of the crystalline, amorphous and interfacial contents for the investigated PE materials are revealed in Figure 4 and summarized in Table 2. For many of the investigated PE grades the highest crystallinity values but lowest amorphous fractions were obtained for the raw material (exception: M2 grade with the lowest average molar mass value). As an effect of film extrusion, sintering and post-treatment the crystallinity of the samples M4, H4, H9 and HA decreased whereas the content of the amorphous phase increased. Hence, the progresses of the crystallinity and amorphous content for polymers with an average molar mass higher than about 400,000 g/mol are following the same trend. Again, M2 with the lowest average molar mass exhibited a different trend with less significant changes in the crystalline and amorphous fractions. Regarding the interphase the highest values were established for the raw materials. Due to processing a tendency for a decrease of the interfacial content is observable.

As to the effect of average molar mass on the morphology, for the various raw materials the highest crystallinity value was obtained for the extrusion grade M4. For the PE-UHMW grades slightly lower crystallinities, but higher interfacial fractions and thus the lowest amorphous contents were identified. The lowest crystalline fraction determined for the extrusion grade M2 with an average molar mass of only 250,000 g/mol is presumably related to a higher branching density.

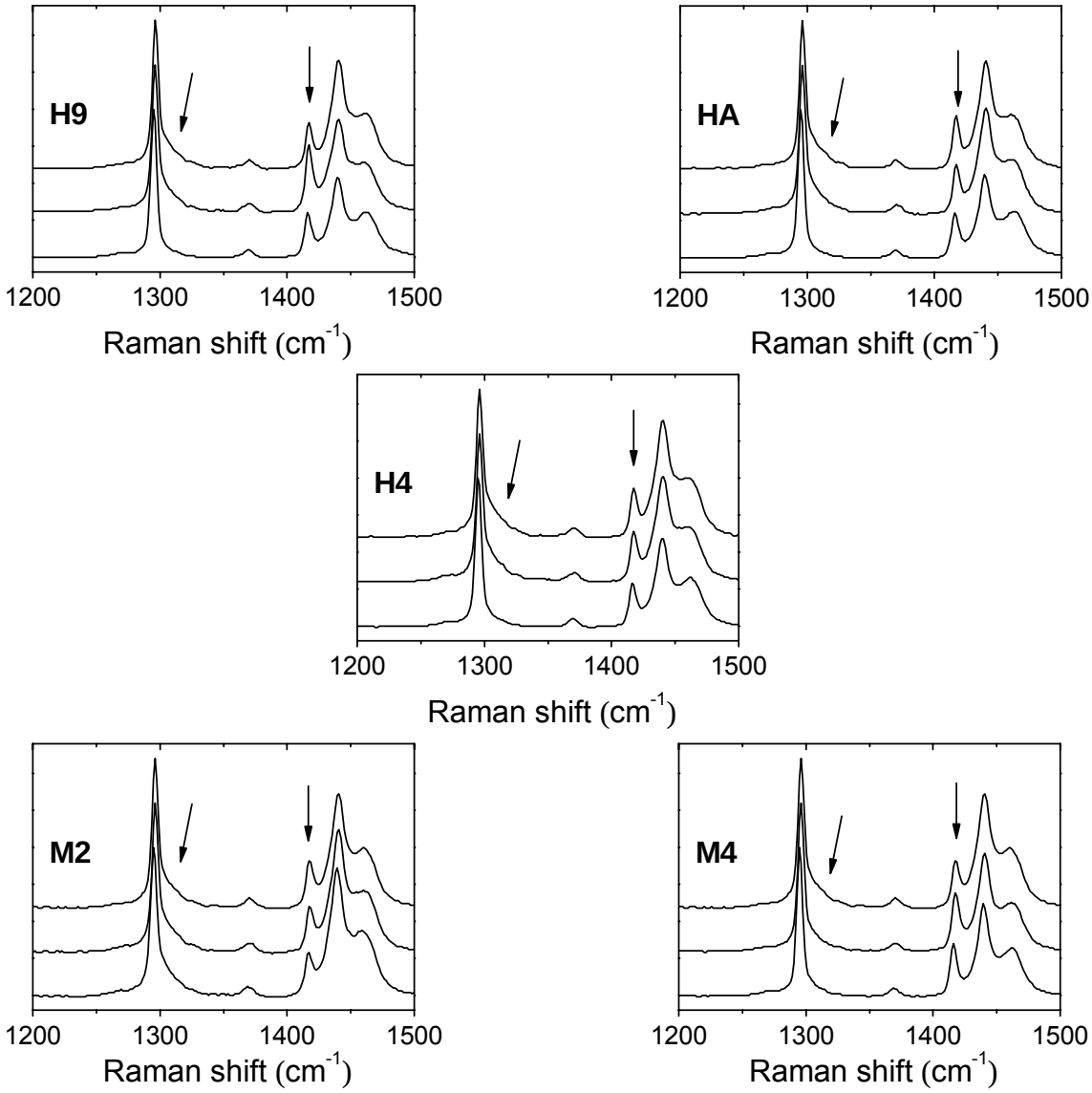

Figure 3. Raman spectra of the investigated PE grades (M2, M4, H4, H9 and HA) at raw material, semi-finished film and post-treated film level (from bottom to top). The spectra are normalized to the internal intensity standard band at 1296 cm^{-1}.

At semi-finished film level it is remarkable that the various PE-UHMW grades investigated exhibit comparable phase fractions. Thus, it can be concluded that the morphology after sintering is not affected by the average molar mass values but by the sinter process. In contrast, after post-treatment different phase fractions were identified for the PE-UHMW samples, which can be related to the differences in the molecular structure.

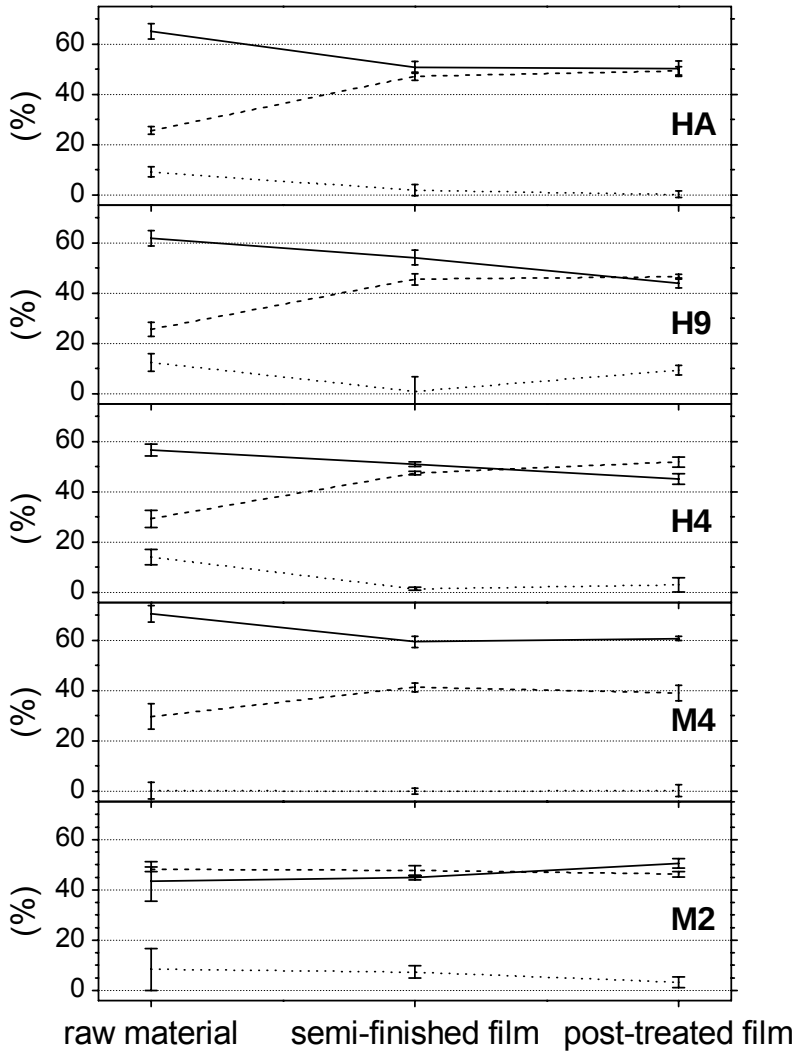

Figure 4. Crystalline ——, amorphous - - - and interfacial ····· fractions as a function of processing level.

Table 2. Mean and standard deviation values (%) of the three phase fractions of the investigated materials.

Sample	raw material			semi-finished film			post-treated film		
	α_a	α_b	α_c	α_a	α_b	α_c	α_a	α_b	α_c
M2	48 ± 1	8 ± 8	43 ± 8	48 ± 2	7 ± 2	45 ± 1	46 ± 1	3 ± 2	50 ± 2
M4	30 ± 5	0 ± 3	71 ± 3	41 ± 2	0 ± 1	59 ± 2	39 ± 3	0 ± 2	61 ± 1
H4	29 ± 3	14 ± 3	57 ± 2	48 ± 1	2 ± 1	51 ± 1	52 ± 2	3 ± 3	45 ± 2
H9	26 ± 3	13 ± 3	62 ± 3	45 ± 2	1 ± 6	54 ± 3	46 ± 1	9 ± 2	44 ± 2
HA	26 ± 2	9 ± 2	65 ± 3	47 ± 2	2 ± 2	51 ± 2	49 ± 2	0 ± 1	50 ± 3

Differential scanning calorimetry

In Figure 5 the DSC traces of the investigated PE grades are shown for the various process levels. While the extrusion grade M2 exhibits the lowest melting

peak temperatures of about 120°C, the values of the second extrusion grade M4 are comparable to the melting peak temperatures of the investigated PE-UHMW polymers. For all grades extrusion or sintering is associated by a significant shift of the melting peak to higher temperatures. This shift is most likely attributed to thicker crystal lamellae. However, because of the lower crystalline and interfacial fractions derived from Raman spectroscopy presumably less crystal lamellae are formed associated with thicker amorphous layers, which can be attributed to the different thermal and process histories during polymerization and film production.

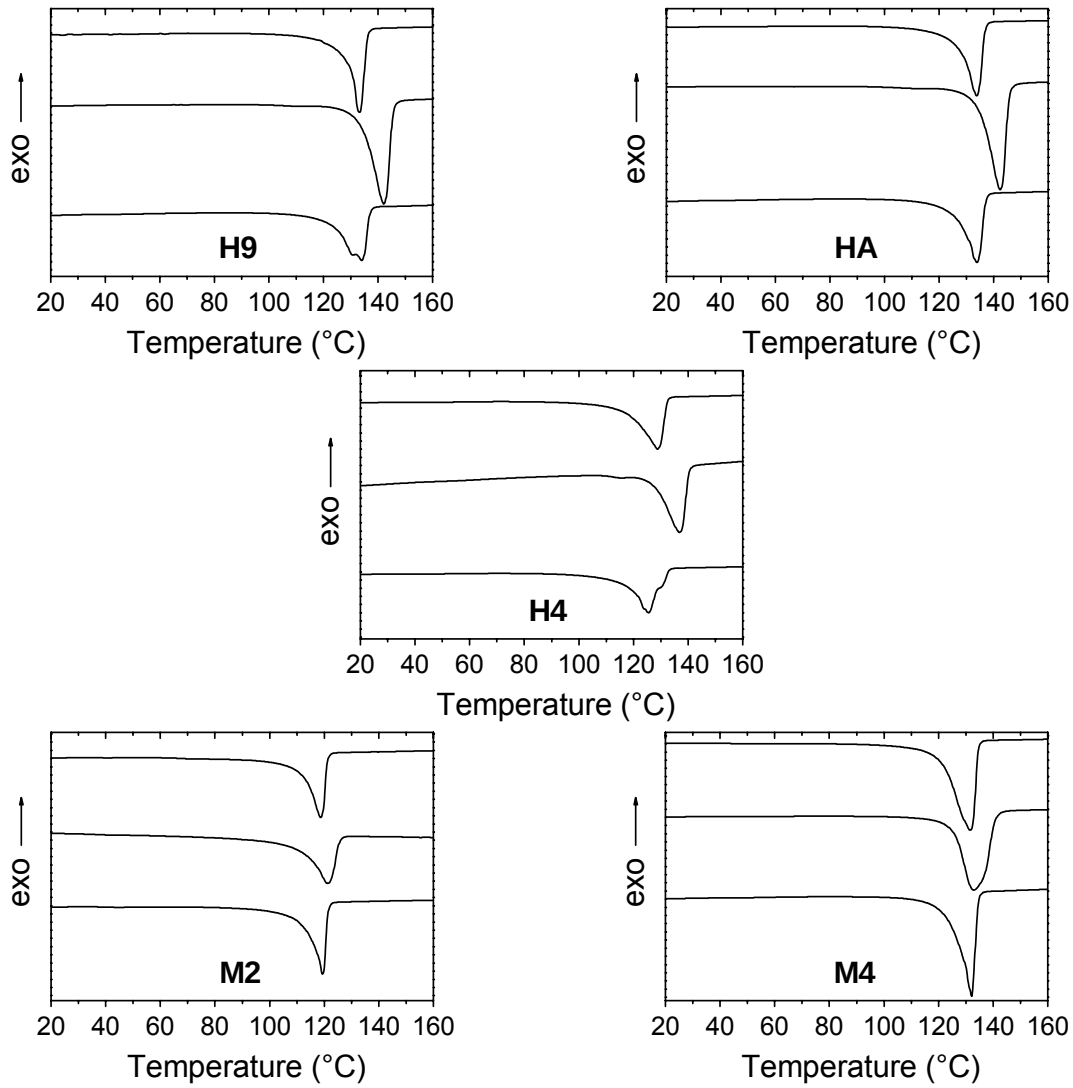

Figure 5. DSC melting endotherms of the investigated PE grades (M2, M4, H4, H9 and HA) at raw material, semi-finished film and post-treated film level (from bottom to top).

For the post-treated films, compared to the semi-finished films, a shift of the melting peak temperatures to lower values is ascertained. Due to flaming the samples were exposed to temperatures above the melting temperature, thus leading to a melting and recrystallization of the film surface. This negative shift is most likely in conjunction with the formation of thinner crystal lamellae. Because of the lower crystalline fractions derived from Raman spectroscopy for many of the investigated PE grades (M4, H4, H9 and HA), a comparable amount of crystal lamellae, but with lower thickness is evolved. The different morphology is probably related to a higher cooling rate during post-treatment.

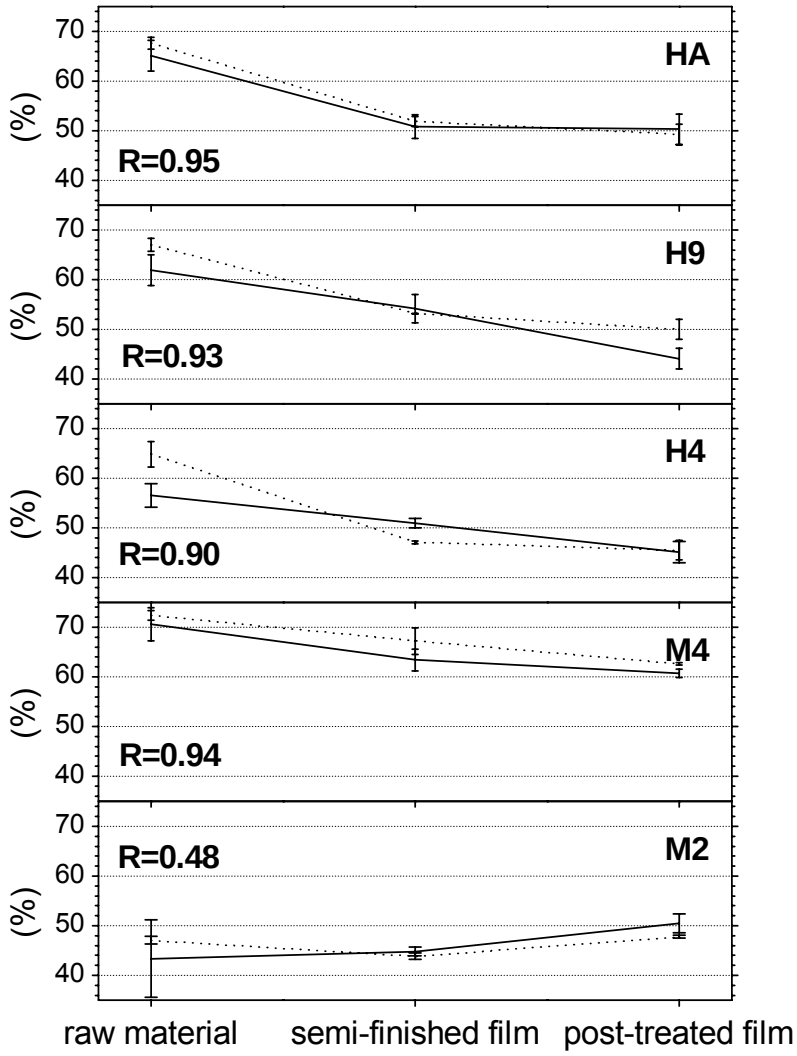

Figure 6. Crystallinity as a function of processing level of the investigated materials determined by Raman spectroscopy ── and DSC ┈┈; R represents the correlation coefficient between Raman and DSC results.

A comparison of the crystallinity values determined by DSC and Raman spectroscopy is revealed in Figure 6 and summarized in Table 3. In general, a good agreement between the DSC and Raman crystallinities was found, thus corroborating the results obtained by Raman spectroscopy and the assumption of an orthorhombic crystalline structure. With exception of the M2 grade the correlation coefficients are equal to 0.90 or higher. The lower correlation coefficient for the M2 grade is related to the fact that the crystallinity values are within a small range. The tendency for lower Raman crystallinity values compared to DSC reported in the literature [5, 11, 19] is confirmed to some extent. As discussed in section Raman spectroscopy the crystallinity values are decreasing significantly for the samples M4, H4, H9 and HA along the process chain. In contrast the crystallinity of the M2 grade is nearly unaffected by the various process steps investigated.

Table 3. Mean and standard deviation of the crystallinity values (%) of the investigated materials obtained by DSC and Raman spectroscopy.

Sample	raw material		semi-finished film		post-treated film	
	DSC	Raman	DSC	Raman	DSC	Raman
M2	47 ± 1	43 ± 8	44 ± 1	45 ± 1	48 ± 0	50 ± 2
M4	72 ± 1	71 ± 3	67 ± 3	63 ± 2	63 ± 0	61 ± 1
H4	65 ± 3	57 ± 2	47 ± 0	51 ± 1	46 ± 2	45 ± 2
H9	67 ± 1	62 ± 3	53 ± 0	54 ± 3	50 ± 2	44 ± 2
HA	68 ± 1	65 ± 3	52 ± 1	51 ± 2	49 ± 2	50 ± 3

Conclusions

For various PE ski base materials it has been demonstrated that Raman spectroscopy allows for a comprehensive morphological analysis obtaining fractions for the crystalline, amorphous and interfacial phase. Crystallinity values derived by Raman spectroscopy are in good agreement with DSC based data, thus corroborating the implemented and used Raman technique. Along the process chain from the raw material to the post-treated extruded or sintered film for many of the investigated PE grades a decrease of the crystalline and interfacial fraction associated by an increase of the amorphous content was detected. PE-UHMW grades with different average molar mass values exhibited morphological differences at raw material and post-treated film level. However, after sintering the phase fractions are comparable and thus independent of the average molar mass.

Acknowledgement

The research work of this paper was performed at the Polymer Competence Center Leoben GmbH (PCCL, Austria) within the framework of the Kplus-program of the Austrian Ministry of Traffic, Innovation and Technology with contributions by the Institute of Materials and Testing of Plastics at the University of Leoben (Austria) and the Fischer GmbH (Austria). The PCCL is funded by the Austrian Government and the State Governments of Styria and Upper Austria. The authors wish to express their acknowledgement to Ao.Univ.-Prof. Dr. Ronald J. Bakker of the Institute of Mineralogy and Petrology at the University of Leoben (Austria) for his cooperation in course of this study.

References

[1] Association of Plastic Manufacturers in Europe [APME], "*The Compelling Facts About Plastics*", **2007**.
[2] A. Bertoluzza, C. Fagnano, M. Rossi, A. Tinti, G.L. Cacciari, *Journal of Molecular Structure* **2000**, *521*, 89.
[3] S. Affatato, G. Bersaglia, D. Emiliani, I. Foltran, P. Taddei, M. Reggiani, P. Ferrieri, A. Toni, *Biomaterials* **2003**, *24*, 4045.
[4] M. Visentin, S. Stea, M. de Clerico, M. Reggiani, C. Fagnano, S. Squarzoni, A. Toni, *J. Biomater. Appl.* **2006**, *21, No. 2*, 131.
[5] M. Reggiani, A. Tinti, P. Taddei, M. Visentin, S. Stea, M. de Clerico, C. Fagnano, *Journal of Molecular Structure* **2006**, *785*, 98.
[6] M. Kyomoto, Y. Miwa, G. Pezzotti, *J. Biomater. Sci. Polymer Edn.* **2007**, *18*, 165.
[7] G.R. Strobl, W. Hagedorn, *J. Polymer Sci.* **1978**, *16*, 1181.
[8] D. Dothée, M. Berjot, W. Marx, *J. Polymer Degradation and Stability* **1988**, *20*, 149.
[9] F. Rull, A.C. Prieto, J.M. Casado, F. Sobron, H.G.M. Edwards, *J. Raman. Spectrosc.* **1993**, *24*, 545.
[10] C.C. Naylor, R.J. Meier, B.J. Kip, K.P.J. Williams, S.M. Mason, N. Conroy, D.L. Gerrrard, *Macromolecules* **1995**, *28*, 2969.
[11] W. Lin, M. Cossar, V. Dang, J. Teh, *Polymer Testing* **2007**, *26*, 814.
[12] L. Mandelkern, R.G. Alamo, M.A. Kennedy, *Macromolecules* **1990**, *23*, 4721.
[13] M.A. Rodríguez-Pérez, R.A. Campo-Arnáiz, R.F. Aroca, J.A. de Saja, *Polymer* **2005**, *46*, 12093.
[14] M. Pyda, *ATHAS DataBank* **2007**, *http://athas.prz.rzeszow.pl*.
[15] G. Keresztury, E. Földes, *Polymer Testing* **1990**, *9*, 329.
[16] J.C. Rodriguez-Cabello, J. Martin-Monge, J.M. Lagaron, J.M Pastor, Macromol. *Chem. Phys.* **1998**, *199*, 2767.
[17] C. Fagnano, M. Rossi, R.S. Porter, S. Ottani, *Polymer* **2001**, *42*, 5871.
[18] J.M. Lagaron, *J. Materials Sci.* **2002**, *37*, 4101.
[19] R.P. Paradkar, S.S. Sakhalkar, X. He, M.S. Ellison, *J. Appl. Polymer Sci.* **2003**, *88*, 545.
[20] M. Zheng, W. Du, *Vibrational Spectroscopy* **2006**, *40*, 219.
[21] T. Yemni, R.L. McCullogh, *J. Polymer Sci.* **1973**, *11*, 1385.
[22] K.M. Furuheim, D.E. Axelson, H.W. Anthonsen, T. Helle, *J. Appl. Polymer Sci.* **2004**, *91*, 218.

[23] L. Kurelec, S. Rastogi, R.J. Meier, P.J. Lemstra, *Macromolecules* **2000**, *33*, 5593.
[24] J.M. Lagaron, N.M. Dixon, W. Reed, J.M. Pastor, B.J. Kip, *Polymer* **1999**, *40*, 2569.
[25] R.J. Meier, *Polymer* **2002**, *43*, 517.

2.2 Arbeit 2

J. Fischer, G.M. Wallner, A. Pieber

Morphology of polyethylene ski base materials

Polymer Engineering and Science, eingereicht

Morphology of polyethylene ski base materials

J. Fischer[1], G.M. Wallner[2], A. Pieber[3]

[1] Polymer Competence Center Leoben GmbH, Roseggerstrasse 12, Leoben, 8700, Austria, Tel.: +43 3842 402 2109, Fax: +43 3842 402 2102, E-Mail address: joerg.fischer@pccl.at

[2] Institute of Material Science and Testing of Plastics, University of Leoben, Franz-Josef-Strasse 18, Leoben, 8700, Austria

[3] Fischer Sports GmbH, Fischerstrasse 8, Ried/Innkreis, 4910, Austria

Abstract

For a comprehensive analysis of carbon black filled polyethylene ski base grades at processing levels from the raw material to the structured ski base high resolution Raman spectroscopy and Differential Scanning Calorimetry were used. Based on Raman mapping the applicability of an advanced evaluation procedure for amorphous, disordered and crystalline phase fractions of polyethylene was checked for PE extrusion and sinter grades. Solely for sinter grades a sufficient segregation between carbon black and PE was confirmed allowing for the comprehensive Raman spectroscopical morphological analysis. Significant morphological changes of PE due to processing from the raw material to the semi-finished film and to the structured ski base were ascertained. Along the processing chain a decrease in crystallinity and an increase in the amorphous phase fraction were found. While the raw material and the sintered semi-finished film exhibited a different but uniform PE morphology, the morphological changes due to structuring of the ski base are limited to the top surface layer. The highest amorphous phase fractions were detected in the surface of the structured ski bases.

Keywords: Raman spectroscopy; polyethylene; morphology; DSC; ski base

Introduction

Polyethylene (PE) is a semi-crystalline polymer, which is widely used for commodity plastics. However, PE grades have also been developed for engineering applications requiring special functional properties. In the leisure and sports industry engineering PE grades are of great importance for running surfaces (i.e., bases). The reasons for the outstanding relevance of PE for ski or snowboard bases are the facile processability and machinability combined with remarkable functional properties, such as gliding, friction or wear behavior. For ski bases polyethylene extrusion grades with molar mass between 300,000 and 600,000 g/mol (linear low, medium and high density polyethylene (PE-LLD, PE-MD and PE-HD)) and sinter grades with molar mass between 3,000,000 and 12,000,000 g/mol (PE-UHMW) are used. To tailor the performance properties of PE ski bases additives or fillers are added on compound level (e.g., carbon black, paraffines, silicones and metal salts), but also applied on component level (e.g., waxing) [1-8].

The manufacturing process from the PE raw material to a finished ski base surface consists of various steps. First, formulated PE compounds are extruded or sintered to semi-finished films, which are further post-treated (e.g., flaming) and glued to the laminated core of the ski sandwich. After production of the ski a special topographical structure is introduced to the running surface by machining (e.g., grinding [5], embossing [9] or engraving [10]). Finally, advanced wax grades are applied, scraped off and brush-finished. Both, the topographical structure and the selected wax grade have to be adjusted to environmental conditions such as type of snow, ambient and snow temperature and relative humidity [5, 8-10].

Along the value chain from the raw material to the finished ski running surface the polyethylene grade used undergoes significant changes in the semi-crystalline morphology. Besides internal parameters (i.e., chemical structure of PE polymer and additives used) the morphology depends significantly on external factors such as time, temperature or mechanical loading. The morphology by itself has a strong effect during structuring and wax finishing of the ski base. Hence, a systematic

description and comprehensive understanding of the morphology is of prime relevance for the development of optimized ski running surfaces [11].

Important variable parameters of semi-crystalline polymers are the degree of crystallinity and the semi-crystalline morphology, which is considered as a superposition of three phase fractions, the fully crystalline component (i.e., perfect lamellae), the melt-like fully amorphous component and the disordered component of anisotropic nature [11-25]. While in the original literature introducing the three phase morphology model for polyethylene the disordered component is postulated to be an interfacial phase between fully crystalline and fully amorphous regions [12-22], more recent studies hypothesize that disordered domains with all-trans conformation also develop within the amorphous phase [23-25], hence calling the disordered phase either intermediate or transitional phase. In the following the phase with lack of lateral order is termed as a disordered phase. To describe morphological parameters of semi-crystalline polymers various analytical techniques such as differential scanning calorimetry (DSC), infrared (IR) and Raman spectroscopy, nuclear magnetic resonance spectroscopy (NMR), and wide and small angle X-ray scattering (WAXS and SAXS) are used. While for most of these methods an adequate sample preparation (i.e., the destruction of the sample) is required, Raman spectroscopy has proved to be an appropriate tool to investigate morphological parameters of PE without any kind of damage. Furthermore, Raman spectroscopy allows for a rather comprehensive description of morphological parameters including the full characterization of the three phase fractions [11-19, 23].

In a previous study at the Polymer Competence Center Leoben GmbH and the Institute of Materials Science and Testing of Plastics at the University of Leoben morphological parameters at the surface of PE ski base grades were determined by Raman spectroscopy for the first time [11]. The crystallinity values determined by Raman spectroscopy were corroborated by Differential Scanning Calorimetry (DSC). Within this work focus was given to various unfilled PE compounds on different processing levels. With regard to the value chain the raw material, the semi-finished film and the post-treated film were considered and analyzed. For the investigated levels a significant effect of polymer type and processing conditions

was established. Hence, the main objective of this paper is to extend the morphological analysis of ski base materials. On the one hand, carbon black filled grades which are of higher importance for ski racing products are considered. On the other hand, further processing levels up to the structured ski base are investigated. In terms of the scientific approach, a Raman spectroscopical method for the analysis of carbon black filled grades has to be adopted and implemented. This high resolution method is applied for a comprehensive characterization of the morphology on the surface of ski base materials on different processing levels. To check potential morphological differences between bulk and surface, furthermore DSC is performed to derive degree of crystallinity values of the bulk which are compared to the crystalline fractions obtained by Raman spectroscopy.

Experimental

Materials

Within this work five polyethylene grades differing in their average molar mass and distribution were selected, compounded with additives and carbon black fillers (Table 1). The compounds were processed either by extrusion or sintering to semi-finished films. Depending on the material grade two different techniques, extrusion (200-220°C) and sintering (200-230°C, 250 bar, 12 h, heating/cooling rate: 30°C/h) were applied to manufacture the ski base film. The semi-finished films were processed to skis using a conventional hot press for skis (time: 10 min, temperature: 120°C and load: 10 bar). The base of the ski was finally structured in a racing stone grinding machine. The samples were manufactured and provided by Fischer Sports GmbH (Ried/Innkreis, Austria).

Table1. Characteristics of the investigated ski base PE grades.

Designation	Material	Processing method	Carbon black content (m%)	PE particle diameter (µm)	$M_W \times 10^{-3}$ (g/mol)
B2	PE-LLD	extrusion	1	4000	250
B4	PE-MD	extrusion	1	1040	400
C4	PE-UHMW	sintering	10	120	4,000
C9	PE-UHMW	sintering	10	140	9,000
CA	PE-UHMW	sintering	10	110	10,500

Raman spectroscopy

Raman spectroscopy was performed on a LabRam HR800 Raman spectrometer (HORIBA Jobin Yvon GmbH, Bensheim, GER) equipped with a confocal aperture. The samples (PE raw material as granule or sinter grain, semi-finished film, unstructured ski base and structured ski base) were mounted on an x, y, z motorized stage. To obtain a spectral resolution of about 1 cm^{-1} a diffraction grating of 1800 grooves/mm was used. Raman spectroscopy was carried out in point illumination mode and in point mapping mode. In point illumination mode the samples were illuminated through a 100x 0.9 NA microscope objective with a HeNe Laser operating at 632.8 nm. Raman spectra in the range from 1200 to 1600 cm^{-1} were collected with an accumulation time of 10 s and were averaged over 5 scans. By measuring on five different positions of a sample mean and standard deviation values were evaluated. For point mapping mode a HeNe Laser, an intensity filter and a 50x 0.75NA microscope objective were used. Spectra were recorded in the wavenumber range from 1000 to 1800 cm^{-1}. 3 scans with an accumulation time of 30 s were performed and averaged. Raman maps were generated by integration of the background-subtracted spectral peaks at 1296 and 1603 cm^{-1}, which are attributable to twisting vibrations of CH_2 groups in PE and to the graphite band in carbon black, respectively. The Raman spectra for quantitative evaluation obtained in point illumination mode were manipulated by baseline correction. To determine the areas under the peaks of interest, which was used as the measure for the intensity values (I), a curve-fitting procedure was carried out with the software package PeakFit v4.12 (SeaSolve Software Inc.). Appropriate fitting results were obtained by peak fitting with freely floating ratios of Gaussian and Lorentzian amounts automatically optimized by the software. The reproducibility of the fit was corroborated by fitting the peaks multiple times [11].

To evaluate the degree of crystallinity (α_c) of PE the method devised by Strobl and Hagedorn, 1978 [12] was used (see Eq. (1)). The prerequisite of orthorhombic crystalline structure was confirmed for the investigated samples by Small Angle X-Ray Scattering (SAXS) [26].

$$\alpha_c = \frac{I_c}{0.45 \cdot I_T} \cdot 100\% \quad (1)$$

where I_c is the integrated area of the Raman band representing the orthorhombic crystalline phase, I_T is the integrated area of the CH_2 twisting vibration region (1200-1350 cm^{-1}), which is not affected by the morphology and therefore used as an internal intensity reference and 0.45 is a normalization coefficient, which was found through experiments on 100% crystalline PE [11, 17].

Furthermore the fraction of the amorphous phase (α_a) was calculated by using Eq. (2) [12]:

$$\alpha_a = \frac{I_a}{I_T} \cdot 100\% \quad (2)$$

where I_a is the integrated area of the Raman band representing the amorphous phase.

Finally, the fraction of the disordered phase (α_b) is given by Eq. (3) [12]:

$$\alpha_b = 100\% - \alpha_a - \alpha_c \quad (3)$$

Differential scanning calorimetry

DSC measurements were performed on a Mettler Toledo DSC 822e instrument (Mettler Toledo GmbH, Schwerzenbach, CH). Temperature and heat flow signals from the apparatus were calibrated using indium and zinc. Thermal analyses were conducted in air with samples of about 2 to 3 mg. From the semi-finished film, the unstructured ski base and the grinded ski base samples with a thickness of 0.2 mm and a diameter of 4 mm were prepared by planning a layer with the defined thickness and by cutting with the defined diameter. Each DSC curve was recorded from -30 to 180°C applying a heating rate of 10°C/min. The degree of crystallinity was determined as the ratio between the heat of fusion of the specimen and the heat of fusion of a perfect (100%) crystalline PE (293.6 J/g) [11]. Possible superimposed melting and crystallization effects due to a low heating rate were checked and falsified in a previous study [11]. By measuring on three different samples mean and standard deviation values were evaluated.

Results and discussion

To evaluate morphological parameters of PE in carbon black filled compounds an appropriate consideration of the filler distribution is important. Hence, exemplary optical micrographs and Raman maps are displayed in Fig. 1 for semi-finished films made of an extrusion grade (B4) and a sinter grade (CA). Morphological parameters of unfilled compounds based on the investigated PE types are described and discussed in a previous paper [11]. In the optical micrograph of the extruded film (grade B4, Fig. 1a) no distinct features are ascertainable. Particularly no indication for the carbon black filler with 1 m% is deducible. In contrast, the optical micrograph of the sintered film (grade CA, Fig. 1b) exhibits a well-defined two phase structure consisting of dispersed dark domains with dimensions up to about 100 µm embedded in a brighter continuous but less pronounced phase. Because the size of the dominating dispersed phase is in good agreement with the mean PE particle diameter (s. Table 1) this phase represents most likely PE.

For explanation of the Raman maps shown in Fig. 1 (c, d) relevant spectra being attributable to the distinct colors white and black of the maps are displayed in Figs. 2 and 3. As shown in Fig. 2, in both spectra being representative for the colors white (Fig. 2a) or black (Fig. 2b) of the Raman map of the sample B4 a superposition of characteristic bands for PE and carbon black is observable. A comprehensive description and explanation of characteristic Raman bands for PE and carbon black is given in the literature (PE: [11-25, 27-29], carbon black: [30, 31]). In the spectrum attributed to white the characteristic strong PE peaks at 1063, 1129, 1296, 1416, 1440 and 1463 cm^{-1} are more pronounced. In contrast, the two broad bands representing the defect peak (maximum at 1360 cm^{-1}) and the graphite peak (maximum at 1600 cm^{-1}) of carbon black are weaker. For the spectrum attributed to black the characteristics are opposite (i.e., PE peaks are weaker and carbon black bands are stronger). Hence, the two components PE and carbon black are not fully separable for the extrusion grade B4 by the applied high resolution Raman microscope. The Raman map of the extruded film (Fig. 1c) indicates a fine distribution of carbon black in the PE matrix (expressed by the dominating gray mixed color) with some inhomogeneities due to agglomerates of

carbon black primary particles (black color) or PE (white color) with residues of the other component.

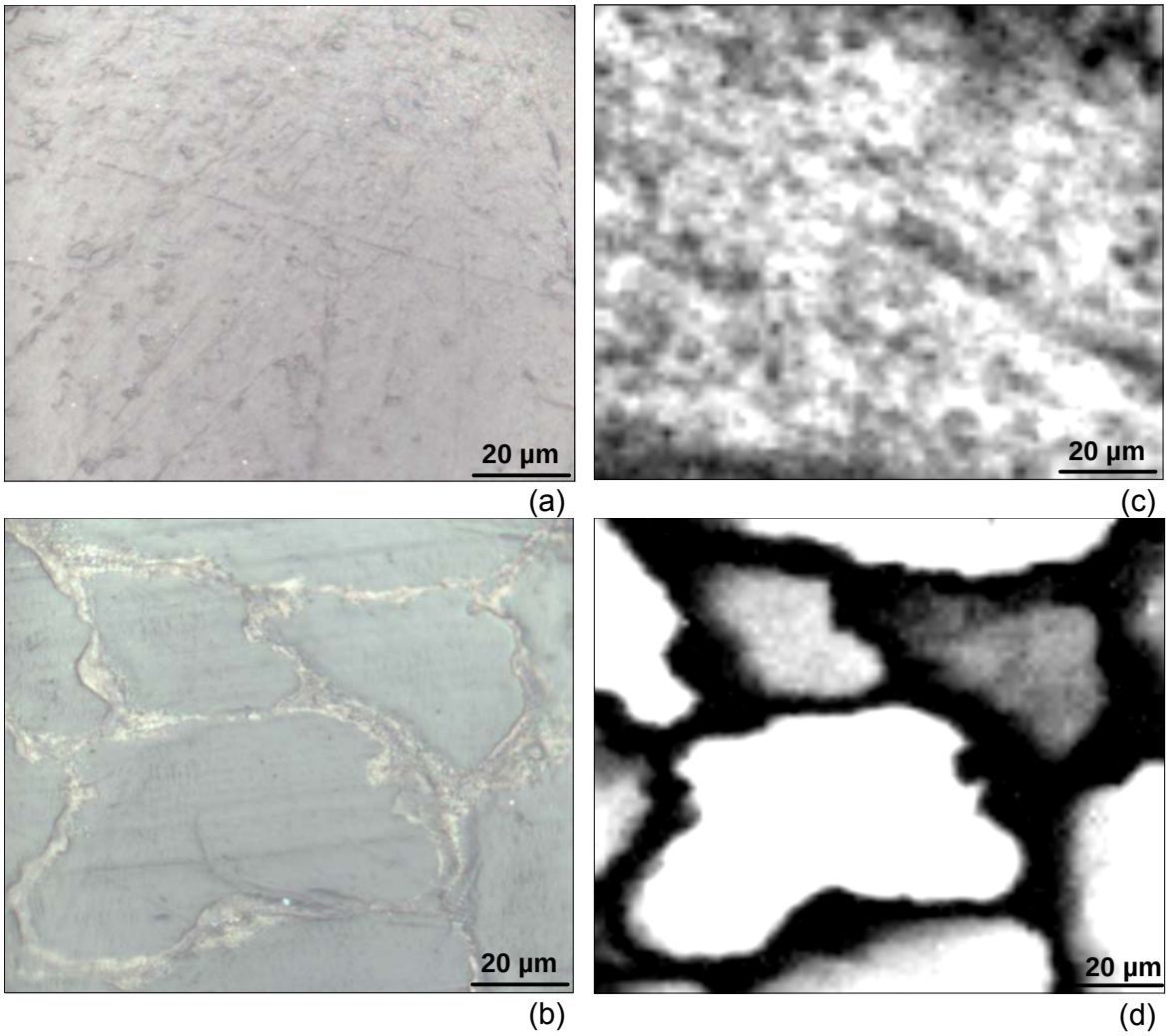

Fig. 1. (a, b) Optical micrographs and (c, d) Raman maps of the semi-finished films based on the (a, c) extrusion compound B4 and the (b, d) sinter compound CA.

Representative spectra for the white and black color of the Raman map in Fig. 1d of the sintered semi-finished film (grade CA) are revealed in Fig. 3. These spectra do not exhibit any superposition of characteristic PE and carbon black peaks. While the spectrum attributed to white consists solely of PE bands, the spectrum attributed to black is explicitly assignable to carbon black. Hence, the two components PE and carbon black are to a large extent separated in the Raman map (Fig. 1d) of the sintered semi-finished film made of grade CA. The haziness at the interface between PE and carbon black (expressed by the gray color) is

related to the fibrillar surface superstructure of the PE-UHMW grain allowing for the partial penetration of carbon black primary particles. Because the development of the dispersed PE phase in the optical and Raman micrographs is comparable, it is usually possible to locate pure PE domains solely by optical microscopy.

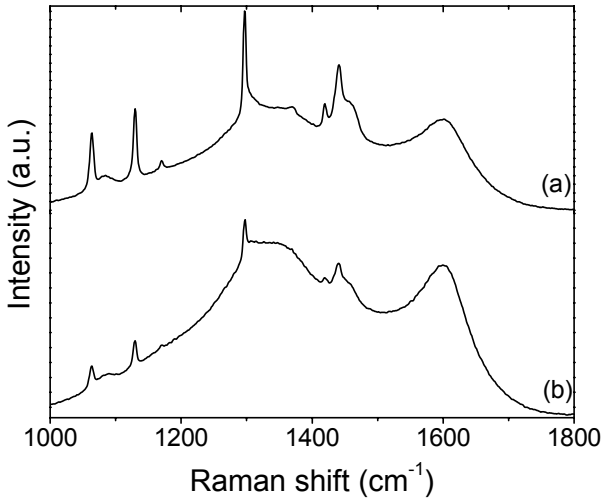

Fig. 2. Raman spectra attributable to the (a) white or (b) black color of the map in Fig. 1c for the extruded semi-finished film of grade B4.

With regard to the quantitative evaluation of morphological parameters of PE in carbon black filled compounds it can be concluded that a reliable quantification by Raman spectroscopy is feasible only for sinter grades (i.e., C4, C9 and CA). For the investigated extrusion grades (i.e., B2 and B4) the methylene twisting band at 1296 cm^{-1} which is used as internal intensity reference is superimposed by the defect band of carbon black. Thus, a reproducible quantitative evaluation of the three morphological fractions (i.e., crystalline, amorphous and disordered phase) is not possible and not within the scope of this paper. In preliminary evaluations of carbon black filled extrusion grades absolute standard deviations up to 20% were obtained which is significantly higher than common values for the disordered fraction [11].

Quantitative data of the amorphous, disordered and crystalline phase contents for the investigated PE-UHMW sinter grades (C4, C9 and CA) are revealed in Fig. 4 and summarized in Table 2. The quantitative data are depicted for the various processing levels from the raw material, to the semi-finished film, to the unstructured ski base and to the structured ski base. In a previous paper with

focus on unfilled PE grades morphological phase fractions are described and discussed for the first and second processing level raw material and semi-finished film. For the raw materials (sinter grain without carbon black) amorphous, disordered and crystalline fractions ranging from 26 to 29%, from 5 to 14% and from 57 to 66% were obtained, respectively. While the investigated PE grades vary only slightly in the amount of amorphous content, significant differences were obtained as to the disordered and crystalline fractions. C4, the PE-UHMW grade with the lowest average molar mass, exhibits the lowest crystalline and the highest disordered phase content. Interestingly, lower disordered fractions associated by higher crystalline fractions were found with increasing average molar mass of the sinter grades.

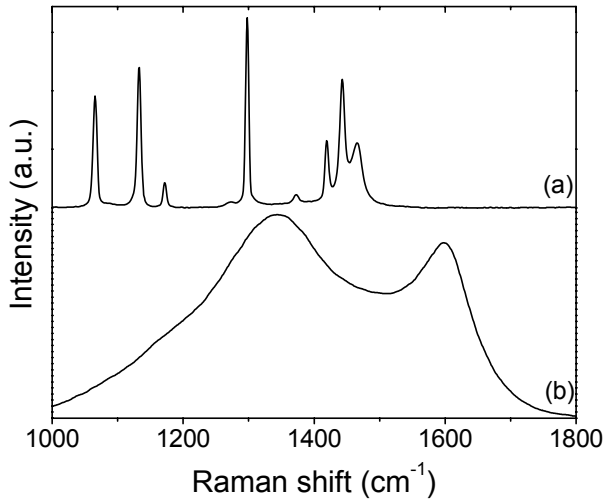

Fig. 3. Raman spectra attributable to the (a) white or (b) black color of the map in Fig. 1d for the sintered semi-finished film of grade CA.

For the semi-finished films significant changes in the amorphous, disordered and crystalline fractions were determined compared to the raw material. While the amount of amorphous phase is increasing, the disordered and especially the crystalline contents are decreasing due to the sinter process. The differences in morphology revealed for the PE-UHMW raw materials level off after sintering. For the investigated semi-finished film samples similar amorphous, disordered and crystalline fractions of about 48, 4 and 48% were obtained, respectively. These values are in agreement with morphological data determined for unfilled semi-finished films in a previous study [11]. A possible reason for the reduced

crystallinities after sintering is the high pressure during melting and crystallization of the PE grades limiting the molecular mobility. As to the raw material it is concluded that the conditions during polymerization favor the crystallizability [32].

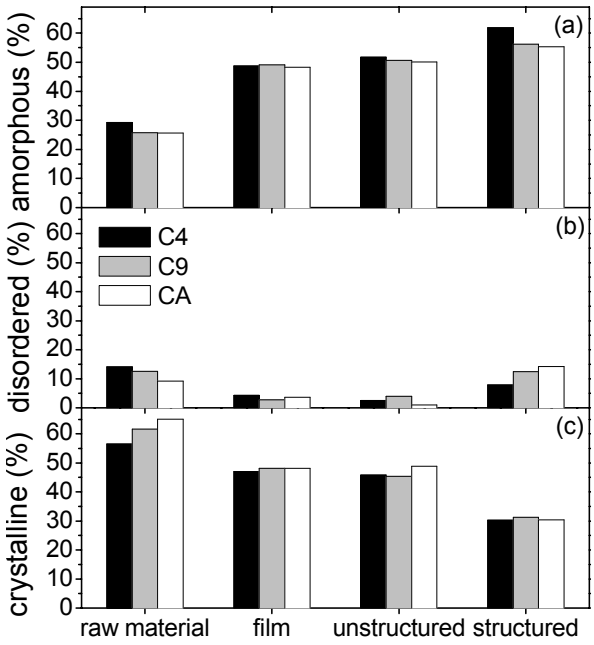

Fig. 4. (a) Amorphous, (b) disordered and (c) crystalline phase fractions of the investigated PE grades (black) C4, (gray) C9 and (white) CA on the levels raw material, semi-finished film, unstructured ski base and structured ski base.

Table 2. Mean and standard deviation values (%) of the three phase fractions (α_a … amorphous, α_b … disordered, α_c … crystalline) of the PE grades C4, C9 and CA at different processing levels.

Sample	raw material			semi-finished film			unstructured ski base			structured ski base		
	α_a	α_b	α_c	α_a	α_b	α_c	α_a	α_b	α_c	α_a	α_b	α_c
C4	29±3	14±3	57±2	49±3	4±4	47±4	52±3	2±3	46±1	62±5	8±5	30±1
C9	26±3	13±3	62±3	49±2	3±3	48±2	51±3	4±1	45±3	56±2	13±4	31±3
CA	26±2	9±2	65±3	48±3	4±4	48±3	50±3	1±4	49±2	55±5	14±5	30±1

As shown in Fig. 4 and in Table 2 the hot pressing of the ski sandwich resulting in the level unstructured ski base has no significant effect on the morphology. The amorphous, disordered and crystalline fractions are only slightly changed with deviations smaller than the statistical uncertainties. Of higher relevance is grinding of the ski base leading to significant morphological changes. Due to structuring of the ski base the amorphous and disordered contents are increased to 55 to 62% and to 8 to 14%, respectively. Accordingly, the fully crystalline phase is reduced to about 30%. These significant changes in the morphology are presumably related

to partly melting and rapid crystallization on the surface during grinding of the ski base. This conclusion is supported by Leevers et al., 1995 who investigated and modeled the fracture mechanisms of PE at high deformation rates [33, 34]. The enhancement of the disordered phase during structuring of the ski base can possibly be attributed to local orientation effects leading to an anisotropic disordered phase where chains are stretched but lack lateral order [19, 21, 23]. Considering the standard deviation a tendency for a higher amorphous and a lower disordered phase fraction was obtained for the PE-UHMW grade C4 with the lowest average molar mass.

To evaluate potential morphological differences between the surface and the bulk of the investigated PE grades on different processing levels thermoanalytical investigations with 200 µm thick film layers planned from the ski base surface were carried out, evaluated and compared to the crystalline phase fractions obtained by Raman spectroscopical local analysis (depth sensitivity of 2 µm) of the ski base surface (s. Fig. 5 and Table 3). For the processing levels raw material, semi-finished film and unstructured ski base a good agreement between Raman and DSC crystallinities was found. Thus, it can be concluded that there is no depth

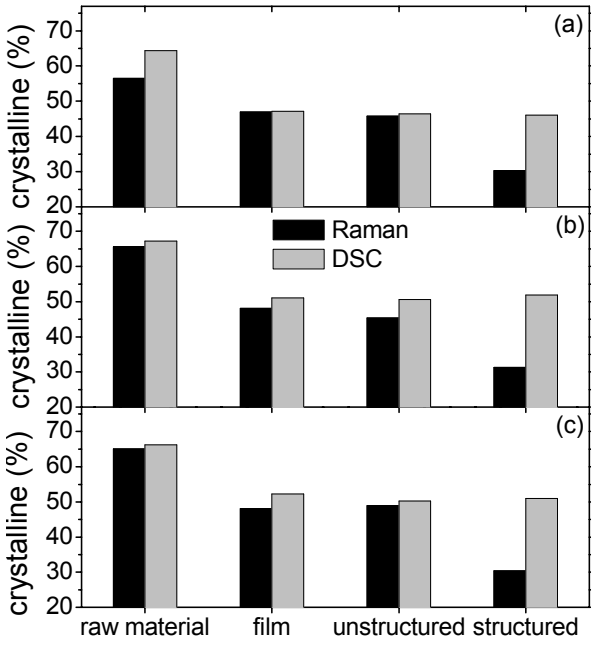

Fig. 5. Crystallinity values of the investigated PE grades (a) C4, (b) C9 and (c) CA on different processing levels obtained by (black) Raman spectroscopy and (gray) DSC.

gradient in the morphology up to the unstructured ski base level. Furthermore, the agreement between Raman and DSC crystallinities corroborates the Raman spectroscopical approach. Interestingly, significant differences in crystallinity were obtained for the structured ski base. While the bulk value derived from DSC remains unaffected after structuring, the local Raman crystallinity on the surface is much lower. Hence, the morphological changes due to grinding of the ski base are confined to the outermost surface layer. To determine the depth gradient of the crystalline fraction comprehensively, in further studies cross-sections of the structured ski base cut perpendicularly to the surface plane will be investigated.

Table 3. Mean and standard deviation of the crystallinity values (%) obtained by Raman spectroscopy and DSC for the PE grades C4, C9 and CA at different processing levels.

Sample	raw material		semi-finished film		unstructured ski base		structured ski base	
	Raman	DSC	Raman	DSC	Raman	DSC	Raman	DSC
C4	57±2	64±1	47±4	47±1	46±1	46±0	30±1	46±1
C9	66±6	67±1	48±2	51±1	45±3	51±1	31±3	52±0
CA	65±3	66±1	48±3	52±1	49±2	50±2	30±1	51±0

Summary and conclusions

Morphological parameters were evaluated for various carbon black filled ski base grades as a function of processing level by Raman spectroscopy and Differential Scanning Calorimetry. The comprehensive morphological evaluation of amorphous, disordered and crystalline phase fractions was only feasible for the investigated PE-UHMW sinter grades. By Raman mapping it was demonstrated that PE extrusion grades exhibit a fine distribution of the carbon black filler. Because of the superposition of relevant PE and carbon black peaks, a quantitative analysis of the morphological parameters of the extrusion grades was disregarded. For the sinter grades a significant effect of processing on the morphological phase fractions was found. The highest crystalline and lowest amorphous phase contents were obtained for the raw material, the sinter grain. While the sinter process results in a significant decrease in crystallinity, hot pressing of the ski does not further affect the morphology. For the raw material, the semi-finished film and the unstructured ski base similar crystallinities were obtained for the bulk and on the surface. The ski base structuring process leads to

a pronounced increase of the amorphous fraction associated by a decrease of the crystalline phase content and an increase of the amount of disordered phase. These morphological changes are restricted to the top layer of the ski base surface. Hence, grinding induced melting and re-crystallization on the surface of the PE ski base were concluded.

Acknowledgement

The research work of this paper was performed at the Polymer Competence Center Leoben GmbH (PCCL, Austria) within the framework of the Kplus-program of the Austrian Ministry of Traffic, Innovation and Technology with contributions by the Institute of Materials Science and Testing of Plastics at the University of Leoben (Austria) and the Fischer Sports GmbH (Austria). The PCCL is funded by the Austrian Government and the State Governments of Styria and Upper Austria.

References

[1] B. Glenne, A. DeRocco, and J. Vandergrift, Cold Regions Sci. Tech., **26**, 35 (1997).
[2] S. Ducret, H. Zahouani, A. Midol, P. Lanteri, and T.G. Mathia, Wear, **258**, 26 (2005).
[3] L. Bäurle, D. Szabó, M. Fauve, H. Rhyner, and N.D. Spencer, Tribology Letters, **24**, 77 (2006).
[4] R. Schamesberger, International Patent, WO 93/05853 (1993).
[5] S.E. Jordan, and C.A. Brown, Wear, **261**, 398 (2006).
[6] S.C. Colbeck, and D.K. Perovich, Cold Regions Sci. Tech., **39**, 33 (2004).
[7] R. Schamesberger, U.S. Patent, 5,466,743 (1995).
[8] I. Rogowski, J.-Y. Gauvrit, D. Léonard, and P. Lanteri, Cold Regions Sci. Tech., **43**, 140 (2005).
[9] J. Stroi, International Patent, WO 03/061783 (2003).
[10] R. Schamesberger, U.S. Patent, US2006/0251486 (2006).
[11] J. Fischer, G.M. Wallner, and A. Pieber, Macromol. Symp., **265**, 28 (2008).
[12] G.R. Strobl, and W. Hagedorn, J. Polym. Sci., **16**, 1181 (1978).
[13] G. Keresztury, and E. Földes, Polym. Testing, **9**, 329 (1990).
[14] M. Failla, R.G. Alamo, and L. Mandelkern, Polym. Testing, **11**, 151 (1992).
[15] F. Rull, A.C. Prieto, J.M. Casado, F. Sobron, and H.G.M. Edwards, J. Raman. Spectrosc., **24**, 545 (1993).
[16] B.H. Stuart, Vibrational Spectrosc., **10**, 79 (1996).
[17] M.A. Rodríguez-Pérez, R.A. Campo-Arnáiz, R.F. Aroca, and J.A. de Saja, Polymer, **46**, 12093 (2005).
[18] M. Kyomoto, Y. Miwa, and G. Pezzotti, J. Biomater. Sci. Polym. Edn., **18**, 165 (2007).
[19] W. Lin, M. Cossar, V. Dang, and J. Teh, Polym. Testing, **26**, 814 (2007).
[20] C. Fagnano, M. Rossi, R.S. Porter, and S. Ottani, Polymer, **42**, 5871 (2001).
[21] R.P. Paradkar, S.S. Sakhalkar, X. He, and M.S. Ellison, J. Appl. Polym. Sci., **88**, 545 (2003).
[22] S.S. Cherukupalli, and A.A. Ogale, Polym. Eng. Sci., **44**, 1484 (2004).

[23] D. Barron, and C. Birkinshaw, Polymer, **49**, 3111 (2008).
[24] J.C. Rodriguez-Cabello, J. Martin-Monge, J.M. Lagaron, and J.M. Pastor, Macromol. Chem. Phys., **199**, 2767 (1998).
[25] R.J. Meier, Polymer, **43**, 517 (2002).
[26] G.A. Maier, internal report (2008).
[27] A. Bertoluzza, C. Fagnano, M. Rossi, A. Tinti, and G.L. Cacciari, J. Mol. Struct., **521**, 89 (2000).
[28] M. Visentin, S. Stea, M. de Clerico, M. Reggiani, C. Fagnano, S. Squarzoni, and A. Toni, J. Biomater. Appl., **21**, 131 (2006).
[29] M. Reggiani, A. Tinti, P. Taddei, M. Visentin, S. Stea, M. de Clerico, and C. Fagnano, J. Mol. Struct., **785**, 98 (2006).
[30] R. Escribano, J.J. Sloan, N. Siddique, N. Sze, and T. Dudev, Vibrational Spectrosc., **26**, 179 (2001).
[31] J.Y. Sze, and B.K. Tay, Surf. Coat. Technol., **200**, 4104 (2006).
[32] J.T.E. Cook, P.G. Klein, I.M. Ward, A.A. Bain, D.F. Farrar, and J. Rose, Polymer, **41**, 8615 (2000).
[33] P.S. Leevers, Int. J. Fracture, **73**, 109 (1995).
[34] P.S. Leevers, and M.-A. Godart, J. Mech. Phys. Solids, **56**, 2149 (2008).

3 Morphologie von Polymerwerkstoffen für Bandbeschichtungen

Für die Beschichtung von metallischen Substraten kommen organische Beschichtungsstoffe zum Einsatz, die sich aus einer komplexen Formulierung organischer und anorganischer Bestandteile zusammensetzen. Die Bandbeschichtungssysteme bestehen aus einem Filmbildner dem je nach Anforderung Weichmacher, Additive, Pigmente, Füllstoffe und Lösemittel beigemengt werden. Der organische Filmbildner (Bindemittel und Vernetzungsmittel) stellt den Hauptbestandteil von Bandbeschichtungen dar und bildet die Matrix des Beschichtungssystems. Für etwa 60% aller Beschichtungssysteme werden Polyester als Bindemittel eingesetzt. Bandbeschichtungssystemen werden anorganische und in geringerem Umfang organische Zusatzstoffe beigemengt, die eine gezielte Einstellung der Eigenschaftsprofile ermöglichen. Anorganische Zusatzstoffe umfassen beispielsweise Entschäumer, Mattierungsmittel, unbunte und bunte Pigmente oder Korrosionsschutzpigmente. Diese liegen innerhalb der Bindemittelmatrix fein verteilt vor und bilden dadurch eine heterogene Morphologie des Lacksystems. Zu den organischen Zusatzstoffen zählen beispielsweise Katalysatoren, Tenside, Entschäumer, UV-Stabilisatoren, Benetzungsmittel, Verlaufsmittel, Gleitmittel, Flammschutzmittel, Konservierungsmittel, optische Aufheller oder bunte Pigmente (Nanetti, 2000; Suzuki und Carrabba, 2001; Meuthen und Jandel, 2005; Fluch, 2009). Für die Verbesserung des Umformverhaltens von Beschichtungen werden bis zu 2 m% Gleitmittel auf Basis von aliphatischen oder teilhalogenierten Wachsen hinzugefügt (Nanetti, 2000; Chvedov und Jones, 2004).

Die Bandbeschichtung von Blechen erfolgt in einem mehrstufigen industriellen Prozess. Ein flaches Substrat aus Stahl- oder Aluminiumblech wird gereinigt, vorbehandelt und ein- oder beidseitig beschichtet. Als erste organische Schicht wird der sogenannte Primer aufgetragen. Dieser wird in einem Einbrennofen getrocknet und vernetzt sowie abgekühlt. Die Aufgabe des Primers liegt in der Haftvermittlung sowie im Korrosionsschutz. In der zweiten Beschichtungsstation

wird der farbgebende Decklack aufgetragen, im Einbrennofen ausgehärtet und abgekühlt. Das Temperaturprofil innerhalb der mit heißer Luft betriebenen Einbrennöfen wird durch Kombination aus Lufttemperatur und Verweilzeit eingestellt (Meuthen und Jandel, 2005; Buder-Stroißnigg, 2008). Ein wichtiger Parameter zur Beschreibung der Temperaturbedingungen im Ofen ist die Einbrenntemperatur (peak metal temperature (PMT)), die üblicherweise zwischen 220 und 250°C liegt (voestalpine, 2008). Durch Variation der Einbrenntemperatur werden der Vernetzungsgrad der Lacksysteme und damit auch die Morphologie auf molekularer Ebene beeinflusst (Perruchot et al., 2003; Gamage et al., 2003). Da die Einbrenntemperaturen signifikant über den Schmelztemperaturen der als Gleitmittel eingesetzten Wachse liegen, ist eine Beeinflussung der morphologischen Strukturen wachsgefüllter Lacke durch Variation der Einbrenntemperatur zu erwarten.

Die Raman-Mikroskopie wurde in der Literatur mehrmals zur Analyse der Morphologie von Lacksystemen auf unterschiedlichen Strukturebenen eingesetzt. Everall (2005a; 2005b) verfasste einen umfassenden aus zwei Artikeln bestehenden Review, der sich mit der Anwendung der Raman-Spektroskopie zur Untersuchung von Lacksystemen unterschiedlichster Zusammensetzung beschäftigt. Das Hauptaugenmerk der bisherigen Analysen lag bei der Untersuchung des Vernetzungsverhaltens der Lacke sowie bei der Bestimmung der Verteilung anorganischer Lacksystemkomponenten (Schrof et al., 1999; Everall, 2005b; Erich et al., 2005; Scholes et al., 2006; Rodriguez et al., 2008). Zur Raman-spektroskopischen Charakterisierung von organischen Zusatzstoffen in Lacksystemen liegen derzeit keine systematischen Arbeiten vor. Der Fokus dieser anwendungsorientierten Arbeiten lag in der Analyse des Einflusses des Wachsgehaltes auf das Reibverhalten der Lacke (Carlsson et al., 2001a; Carlsson et al., 2001b; Bexell et al., 2003; Chvedov und Jones, 2004). Die Bedeutung der morphologischen Struktur für die relevanten Eigenschaften wurde dabei nicht aufgeklärt.

Die Hauptzielsetzung des vorliegenden Abschnittes liegt daher in der systematischen Analyse und Beschreibung der Morphologie wachsgefüllter Bandbeschichtungen als Funktion von Lackformulierung und Aushärtebedingung. Dazu

sollen in einem ersten Schritt Fernfeld-Raman-mikroskopische und lichtmikroskopische Methoden ausgelotet, implementiert und auf unterschiedlich formulierte, heterogene Polymerbeschichtungen mit variablem Wachsgehalt angewendet werden. Darauf aufbauend sollen der Einfluss der Pigmentierung und prozesstechnischer Parameter auf die Morphologie wachsgefüllter Bandbeschichtungen herausgearbeitet werden. Um auflösungsbedingte Grenzen der Raman-Mikroskopie aufzuklären sollen für ausgewählte Bandbeschichtungssysteme rastersondenmikroskopische Methoden mit besserer lateraler Auflösung ausgelotet und den Ergebnissen der Raman-Mikroskopie gegenübergestellt werden. Entsprechend der Hauptzielsetzung werden drei wissenschaftliche Papers ausgearbeitet. In Fortsetzung der Arbeiten 1 und 2 aus Kapitel 2 werden die für diesen Abschnitt relevanten Papers als Arbeiten 3 bis 5 nummeriert.

In Arbeit 3 wurde mittels Raman-Mikroskopie und Lichtmikroskopie die Morphologie von Bandbeschichtungen, deren Formulierung sich bezüglich des eingemischten Wachsgehalts unterschied, untersucht. Neben der spektroskopischen Analyse der chemischen Zusammensetzung der mit einem gering streuenden Weißpigment aus $BaSO_4$ gefüllten Beschichtungssysteme war es möglich, die heterogene Morphologie der wachsgefüllten Polymerwerkstoffe zu ermitteln. Basierend auf den Raman-mikroskopischen Untersuchungen wurde eine einfacher handhabbare Lichtmikroskopie-Technik implementiert und eingesetzt, um eine umfassende Charakterisierung der Wachsauprägung in wachsgefüllten Lacksystemen vorzunehmen. Dabei wurden kugelförmige Wachsdomänen mit Durchmessern zwischen 1 und 32 µm auf der Oberfläche und im Inneren der Beschichtung detektiert. Für den morphologischen Kennwert der mit Wachs bedeckten relativen Fläche ergab sich ein direkter Zusammenhang mit dem eingestellten Wachsgehalt. Letztlich war eine steigende Anzahl an Wachsdomänen mit zunehmender Wachskonzentration feststellbar.

Die in Arbeit 3 entwickelte und implementierte Mess- und Auswertemethode wurde in Arbeit 4 dazu eingesetzt, die Morphologie wachsgefüllter Bandbeschichtungen in Abhängigkeit von den Aushärtebedingungen zu ermitteln. Dazu wurden mit einem stärker streuenden TiO_2 Weißpigment formulierte Bandbeschichtungslacke bei drei Einbrenntemperaturen von 230, 240 und 250°C vernetzt und Raman-

mikroskopisch und lichtmikroskopisch analysiert. Anhand der Raman-spektroskopischen Untersuchungen war es möglich, auf der Oberfläche und im Inneren der Beschichtungen kugelförmige Wachsdomänen festzustellen, in denen Spuren des Bindemittels sowie des TiO_2 Pigments ermittelbar waren. Mit steigender Einbrenntemperatur kam es zu einer Zunahme der mit Wachs bedeckten relativen Fläche sowie der Wachsdomänenanzahl. Damit wurde erstmals gezeigt, dass ein direkter Zusammenhang zwischen Aushärtebedingung und Wachsausprägung an der Oberfläche und im Volumen von Band-beschichtungen besteht.

Basierend auf den vorangegangenen im Mikrometerbereich durchgeführten Arbeiten, wurde die morphologische Charakterisierung in Arbeit 5 in den Submikrometerbereich ausgeweitet. Hierfür wurde neben Raman- und Lichtmikro-skopie auch die Rasterkraftmikroskopie eingesetzt, um einen unpigmentierten, wachsgefüllten Klarlack sowie einen TiO_2 pigmentierten, wachsgefüllten Beschichtung zu analysieren. Beide Bandbeschichtungen zeigten kugelförmige Wachsdomänen an der Oberfläche und im Inneren der Lacke. Mittels Rasterkraftmikroskopie wurden die Raman-mikroskopisch festgestellten Spuren des Bindemittels innerhalb der Wachsdomänen sowie von Wachsdomänen mit Durchmessern kleiner 2 µm innerhalb der Matrix nachgewiesen und somit abgesichert. Außerdem wurden sich von größeren Wachsdomänen ausbreitende Wachsschichten mit Dicken unter 100 nm detektiert. Die mittels Raman-Mikroskopie und Lichtmikroskopie durchgeführte Ermittlung der Wachsverteilung zeigte Unterschiede abhängig von der Pigmentierung. Ein Vergleich der mit Wachs bedeckten relativen Flächen ergab in der Klarlackbeschichtung eine inhomogenere Verteilung zwischen Volumen und Oberfläche. Im Vergleich zur pigmentierten Beschichtung war für die Klarlackbeschichtung eine geringere Wachsausprägung an der Oberfläche einhergehend mit einem höheren Wachsgehalt im Inneren feststellbar.

3.1 Arbeit 3

J. Fischer, G.M. Wallner, B. Strauß, L. Jandel

Raman spectroscopical investigation of wax modified, polyester based coatings

Surface and Coatings Technology, eingereicht

Raman spectroscopical investigation of wax modified, polyester based coatings

J. Fischer[1], G.M. Wallner[2], B. Strauß[3], L. Jandel[4]

[1] Polymer Competence Center Leoben GmbH, Roseggerstrasse 12, Leoben, 8700, Austria, Tel.: +43 3842 402 2109, Fax: +43 3842 402 2102, E-Mail address: joerg.fischer@pccl.at

[2] Institute of Materials Science and Testing of Plastics, University of Leoben, Franz-Josef-Strasse 18, Leoben, 8700, Austria

[3] voestalpine Stahl GmbH, Voest-Alpine-Strasse 3, Linz, 4031, Austria

[4] BASF Coatings AG, Glasuritstrasse 1, Münster, 48136, Germany

Abstract

To analyze coil coatings with improved forming properties lubricant modified top coats were investigated by Raman spectroscopy and optical light microscopy. The formulation of the top coat was varied regarding the lubricant content. From the Raman spectra it was possible to detect the various ingredients (pigment and lubricant) used in the polyester based resins. As to the lubricant dispersed spherical wax domains with diameters ranging from 1 to 32 µm were detected on the surface and within the bulk. The wax domain size distribution was more uniform within the bulk than on the surface. A good correlation between the formulated wax content and the relative area covered by wax was obtained.

Keywords: coil coating, polyester based resin, lubricant, wax, Raman spectroscopy

Introduction

In the coil coating process organic layers are applied on a pre-treated metal strip to achieve protective and decorative coatings with specified aesthetic and functional properties. Depending on the overall requirements, one or more organic layers (i.e., primer, base coat and clear coat) are needed [1-5]. While the main task of the primer is to provide corrosion protection, base or clear coats are the outer surface layers which have to fulfill a number of functional properties including e.g., visual appearance, long-term stability or anti-soiling behavior [3-7]. Furthermore, the surface mechanical properties of base or clear coats are of special relevance allowing for excellent forming of the metal sheet. Metal forming usually involves sliding contact between a soft polymer coating and a hard tool surface [6-11].

Coil coatings are complex formulations including organic and inorganic components. While for the resin matrix different organic molecules (i.e., binder and cross-linking agent) are used, organic and inorganic ingredients are dispersed, partially on a microscopic level. Inorganic ingredients such as oxides, sulfates or phosphates are acting as fillers, coloring agents, UV absorbers, matting agents or corrosion inhibitors. Organic substances are usually added in small quantities to adjust functional properties or to enhance surface mechanical properties. With regards to forming behavior, lubricants based on waxes are of special relevance [7,9-11].

For compositional analysis of organic coatings vibrational spectroscopy such as infrared (IR) and Raman spectroscopy is a versatile tool. Raman spectroscopy is often superior to IR analysis for identifying inorganic substances [12-14]. Furthermore, Raman spectroscopy requires less or no sample preparation and allows for higher spatial resolution and non-contact measurement in compositional mapping. Thus, Raman spectroscopy is gaining more importance for the analysis of organic coatings [12-18]. A comprehensive review on the application of vibrational spectroscopy in coatings research and analysis is given by Everall [12,13]. Up to now Raman spectroscopy has mainly been used for cure analysis [12,13,16-18] and compositional analysis [6,12-15] of organic coatings. With

regards to compositional analysis focus has been given to the investigation of the distribution of pigments [13,14] and other ingredients [5,13,15]. In the literature no studies on the distribution of lubricants in organic coatings are available. However, some application oriented investigations report on a significant effect of the lubricant content on the frictional behavior [6-9].

Hence, the main objective of our work is a systematic analysis of lubricant distribution on the surface and in the bulk of coil coated top coats as a function of lubricant content. For this purpose, model formulations based on polyester resins and common pigments with varying lubricant content were prepared and analyzed by high resolution Raman spectroscopy in point illumination and point mapping mode.

Experimental

Materials

The investigated model top coat systems are based on branched polyester binders and hexamethoxymethyl melamine (HMMM) cross-linking agent. With regard to the pigments, a moderately scattering $BaSO_4$ white pigment was chosen resulting in a translucent coating. The lubricant used was a commercial PE wax with a melting peak temperature of 100°C. Four top coat formulations with lubricant content of 0.0, 0.08, 0.4 and 2.0 m% were prepared by BASF Coatings AG (Münster, GER). The coats were applied on primered steel sheets with a spiral bar coater and cured in an oven for 30 s at an oven temperature of 300°C which corresponds to an industrially relevant peak metal temperature (PMT) of 240°C. The thickness of the coating layer was 22 µm.

Analytical characterization was done on the top coat surface of the coated steel sheet. Furthermore, polished cross-sections of the coated steel sheets were prepared for investigation of the bulk. For identification of the ingredients in the coating, pure $BaSO_4$ filler particles and wax lubricants were characterized as well.

Spectroscopical and microscopical characterization

Raman spectroscopy was performed on a LabRam HR800 Raman spectrometer (HORIBA Jobin Yvon GmbH, Bensheim, GER) equipped with a confocal aperture. The coated metal sheets or the polished cross-sections were mounted on an x, y, z motorized stage. The top coats were illuminated through a 100x 0.9 NA microscope objective with an Ar^+ Laser operating at 514.5 nm. Raman spectra were recorded with an accumulation time of 5 s and were averaged over 5 scans. To obtain a spectral resolution of about 1 cm^{-1} a diffraction grating of 1800 grooves/mm was used. On the one hand, single point spectra were collected over the range from 200 to 3500 cm^{-1}. On the other hand, mapping studies with 1 µm intervals were carried out over the range from 2700 to 3200 cm^{-1}. The Raman map was generated by integration of the background-subtracted spectral peak at 2883 cm^{-1} which is attributable to an asymmetric stretching vibration of CH_2 groups being representative for the wax lubricant.

After identifying the wax domains by Raman spectroscopy, optical light microscopical investigations were performed to determine the particle size distribution and the area of the image covered by wax. An optical microscope BX51 (Olympus Austria GmbH, Vienna, A) was used in reflective mode. Specimens were illuminated through a 50x 0.8 NA microscope objective. The particle size and the relative area covered by the lubricant were determined by recording 10 independent 286 µm x 212 µm surface images and a cross-section of 22 µm x 20000 µm (thickness of top coat x width). For data generation and evaluation the microscope software analySIS auto was used.

Results and discussion

In Fig. 1 a representative optical micrograph of the coating surface formulated with 2.0 m% lubricant (i.e., highest lubricant content investigated) is displayed. The 584 µm x 480 µm image exhibits randomly distributed circular dark domains embedded in the bright matrix. The diameter of the dispersed domains varies from about 2 µm to 32 µm with an average of 9 µm.

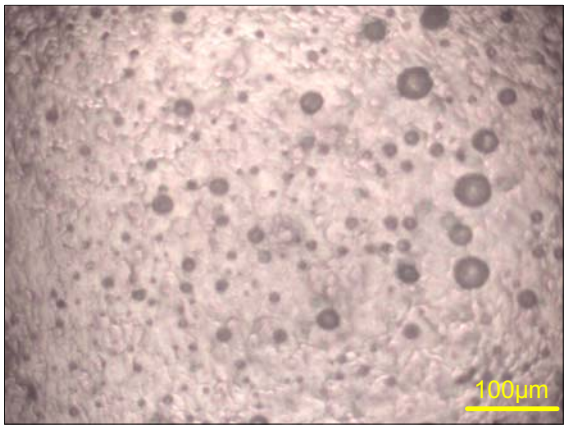

Fig. 1. Optical micrograph of the coating surface formulated with 2.0 m% lubricant.

To analyze the chemical composition of the domains and the matrix Raman spectroscopy was carried out in point illumination mode in the bright and dark areas. Fig. 2 shows a Raman spectrum of the bright area (s. Fig. 1) along with a representative spectrum of the filler $BaSO_4$. At wavenumbers below 1000 cm^{-1} three characteristic peaks with maxima at 460, 617 and 989 cm^{-1} are observable which can be assigned to $BaSO_4$ [5]. Above 1000 cm^{-1} characteristic peaks for the polyester resin at 1620, 1735, 2970 and 3088 cm^{-1} appear [17-21]. While the peak at 1735 cm^{-1} is attributable to the carbonyl stretching vibration, the peaks at 1620 and 3088 cm^{-1} are characteristic for aromatic groups. The strongest band at 2970 cm^{-1} is associated with stretching vibrations of aliphatic CH-groups.

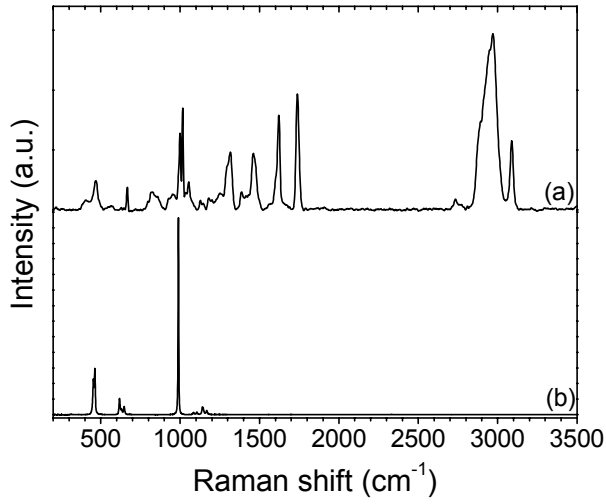

Fig. 2. Raman spectra of (a) the bright area in Fig. 1 and, (b) the $BaSO_4$ filler.

In Fig. 3 a Raman spectrum of the centre of a selected dark domain (s. Fig. 1) with a diameter of about 20 µm is shown along with spectra of the $BaSO_4$ filler and the wax lubricant. In contrast to the spectrum of the bright area an intense broad band is observable in the range from 2800 to 3000 cm^{-1}. By comparison with the spectrum of the wax additive this broad band of the dark domain can unambiguously be assigned to the CH_2 and CH_3 stretching vibrations of the lubricant [22,23]. However, it should be emphasized that in the dark domain also characteristic peaks of the filler and the resin are detectable. Performing a Raman map it was revealed that the whole black domain is covered by the lubricant. Because using a Raman microscope objective with a magnification of 100x and a numerical aperture of 0.9 providing a lateral and vertical resolution of 0.7 and 2.5 µm, respectively [24], it can be concluded that the extension of the investigated dark domain is higher in lateral direction than in vertical direction. Hence, the shape of the investigated dark domain on the surface can be interpreted as spherical cap.

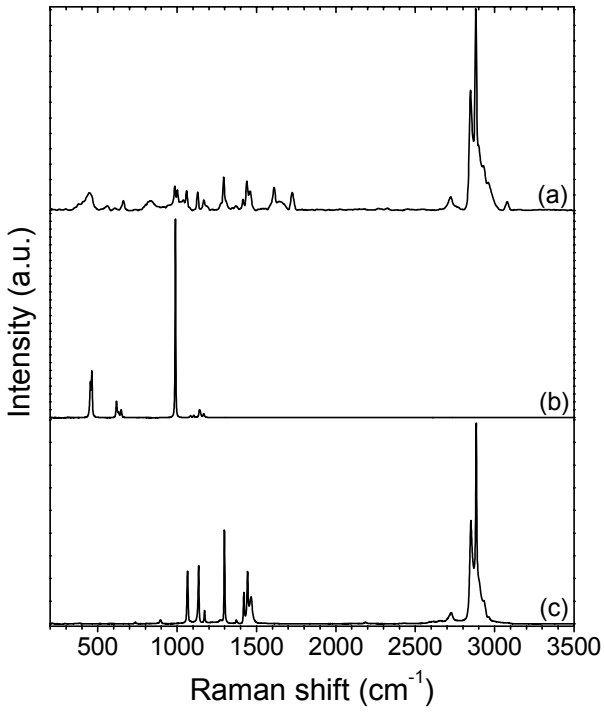

Fig. 3. Raman spectra of (a) the dark domains in Fig. 1, (b) the $BaSO_4$ filler and, (c) the wax lubricant.

To characterize the distribution of the lubricants in the bulk of the top coat polished cross-sections were prepared. In Fig. 4 four representative optical micrographs of

the cross-section are displayed for the top coat formulated with 2.0 m% lubricant. The images with a height of 22 µm, which is equivalent to the thickness of the top coat layer, exhibit bright domains embedded in a grey matrix. The diameter of the dispersed bright domains ranges from about 2 µm to 24 µm with an average of 7 µm. Applying Raman spectroscopy it was ascertained that the bright domains are consisting of wax. Interestingly the wax domains within the bulk reveal the same shape and comparable dimensions as on the surface. Thus, it can be deduced that the wax domains are spherical. By investigating multiple cross-sections it became obvious that the wax particles are preferentially arranged in the bottom section of the top coat adjacent to the primer interface. At the surface of the top coat no bright wax domains were detectable. However, a number of dark spherical caps at the surface of the cross-section and circular dark domains within the bulk were identified. Raman spectroscopy revealed that the dark domains are consisting of resin and $BaSO_4$ filler. By comparing the domain sizes of the spherical caps at the surface of the cross-section with wax domain sizes derived from optical micrographs of the top coat surface a good agreement was achieved. Hence, it can be concluded that the dark domains in the cross-section image are related to wax domains being removed during sample preparation.

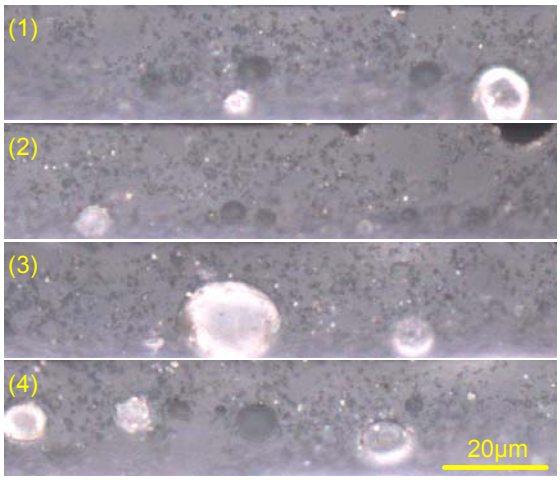

Fig. 4. Four optical micrographs ((1)-(4)) of the polished top coat cross-section formulated with 2.0 m% lubricant (top edge of image: surface of top coat; bottom edge of image: interface between top coat and primer).

To investigate the wax content as a function of lubricant concentration four formulations with 0.0, 0.08, 0.4 and 2.0 m% wax were prepared and investigated by optical and Raman microscopy. By evaluation of ten surface images and 70

cross-section images of each top coat formulation representative values for the minimum, maximum and average area covered by wax on the surface (surface image) and within the bulk (cross-section image) were determined by fitting the circular wax domains with circles. From the area value the particle diameter was derived. With regards to the evaluation of the bulk, spherical cap domains at the surface of the cross-section images were not considered. Moreover these domains were classified as belonging to the surface. In Table 1 the number of identified wax domains on the surface and within the bulk is given along with information regarding the minimum, maximum and average particle diameter and the relative area covered by wax as a function of formulated lubricant content. Furthermore, in Fig. 5 a cumulative histogram for the area covered by wax as a function of wax domain diameter is displayed. The higher the wax concentration the more particle

Table 1 Characteristic values (number; minimum, maximum and average diameter; relative area) of the wax domains on the surface and within the bulk of the investigated top coats with 0.08, 0.4 and 2.0 m% lubricant.

Formulation content (%)	Number (-)		Minimum diameter (µm)		Maximum diameter (µm)		Average diameter (µm)		Relative area (%)	
	Surface	Bulk	Surface	Bulk	Surface	Bulk	Surface	Bulk	Surface	Bulk
0.08	33	18	1	3	12	8	4	5	0.2	0.1
0.4	81	222	1	3	20	12	5	6	1.1	1.3
2.0	166	539	2	2	32	24	9	7	5.7	5.9

domains were found on the surface and within the bulk of the analyzed top coats. The wax domain diameter was ranging from 1 to 32 µm with average values between 4 and 9 µm. For the bulk of the top coat a more uniform wax diameter distribution was yielded. Smallest and biggest domain sizes were obtained for the surface. The higher the wax content the more is the cumulative histogram for the surface and bulk area covered by lubricant shifted to bigger particle size. As to the overall relative area covered by wax (relative wax area) values ranging from 0.1 to 5.9 % were determined. Especially for the formulations with 0.4 and 2.0 m% a good agreement of relative wax area on the surface and within the bulk was obtained with slightly higher relative wax areas within the bulk. In contrast, for the formulation with the lowest lubricant content more relative area is covered by lubricant on the surface than within the bulk. Interestingly, a positive correlation between formulated lubricant content and the relative wax area was found. The

differences in the absolute values for formulated lubricant content and relative wax area are due to density effects.

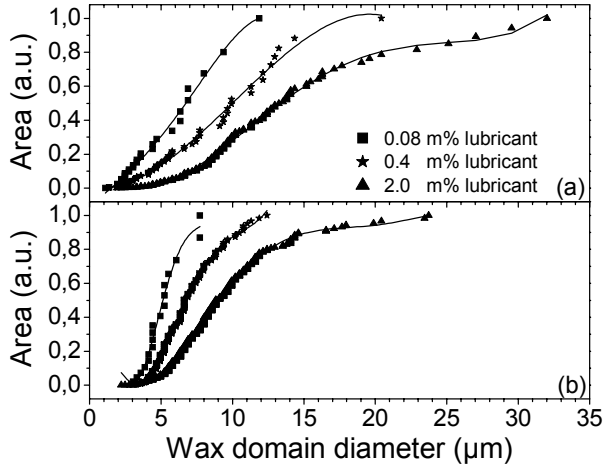

Fig. 5. Cumulative histogram of area covered by wax (a) on the surface and (b) within the bulk as a function of wax domain diameter for top coat formulations with 0.08, 0.4 and 2.0 m% lubricant.

Summary and conclusions

Within this study, a significant effect of the formulated lubricant (wax) content on the formation of wax domains on the surface and within the bulk of coil coatings was established. By optical light microscopy and Raman spectroscopy the distribution of lubricant domains was determined for top coats with 0.08, 0.4 and 2.0 m% of wax. While in the bulk of the coating spherical wax domains were identified, the shape of lubricant domains on the surface was mainly spherical cap. The diameter of the domains was ranging from 1 to 32 µm on the surface and from 2 to 24 µm within the bulk. The higher the lubricant content the higher was the average diameter with values between 4 and 9 µm. By adding up to 2.0 m% of wax, a relative area of up to 5.9 % was covered by dispersed lubricant domains. The relative area of wax on the surface and within the bulk correlated directly with the formulated wax content. For the formulations with 0.4 and 2.0 m% of wax slightly more relative area covered by wax was detected within the bulk compared to the surface. The obtained results imply that the frictional behavior of the investigated coil coatings will differ significantly.

Acknowledgements

The research work of this paper was performed at the Polymer Competence

Center Leoben GmbH (PCCL, Austria) within the framework of the Kplus-program of the Austrian Ministry of Traffic, Innovation and Technology with contributions by the Institute of Materials Science and Testing of Plastics at the University of Leoben (Austria), the voestalpine Stahl GmbH (Austria) and the BASF Coatings AG (Germany). The PCCL is funded by the Austrian Government and the State Governments of Styria and Upper Austria.

References

[1] A.L. Perou, J.M. Vergnaud, Polymer Testing 16 (1997) 19.
[2] M. Delucchi, A. Barbucci, G. Cerisola, Electrochimica Acta 44 (1999) 4297.
[3] K. Adamsons, Prog. Polym. Sci. 25 (2000) 1363.
[4] K. Adamsons, Prog. Org. Coat. 45 (2002) 69.
[5] F.H. Scholes, S.A. Furman, A.E. Hughes, T. Nikpour, N. Wright, P.R. Curtis, C.M. Macrae, S. Intem, A.J. Hill, Prog. Org. Coat. 56 (2006) 23.
[6] A.-S. Jandel, B. Meuthen, Coil Coating; Vieweg / GWV Fachverlage GmbH, 2005.
[7] D. Chvedov, R. Jones, Surf. Coat. Technol. 188-189 (2004) 544.
[8] U. Bexell, P. Carlsson, M. Olsson, Appl. Surf. Sci. 203-204 (2003) 596.
[9] P. Carlsson, U. Bexell, M. Olsson, Wear 251 (2001) 1075.
[10] P. Carlsson, U. Bexell, M. Olsson, Wear 247 (2001) 88.
[11] P. Carlsson, U. Bexell, M. Olsson, Surf. Coat. Technol. 132 (2000)169.
[12] N.J. Everall, JCT CoatingsTech 2 (19) (2005) 38.
[13] N.J. Everall, JCT CoatingsTech 2 (20) (2005) 46.
[14] E.M. Suzuki, M. Carrabba, J. Forensic. Sci. 46 (5) (2001) 1053.
[15] R. Rodriguez, S. Jimenez-Sandoval, M. Estevez, S. Vargas, J. Non-Cryst. Solids 354 (2008) 3623.
[16] W. Schrof, E. Beck, R. Königer, W. Reich, R. Schwalm, Prog. Org. Coat. 35 (1999) 197.
[17] S.J.F. Erich, J. Laven, L. Pel, H.P. Huinink, K. Kopinga, Prog. Org. Coat. 52 (2005) 210.
[18] B. Marton, L.G.J. van der Ven, C. Otto, N. Uzunbajakava, M.A. Hempenius, G.J. Vancso, Polymer 46 (2005) 11330.
[19] J.L. Dupuie, W.H. Weber, D.J. Scholl, J.L. Gerlock, Polym. Degrad. Stab. 57 (1997) 339.
[20] G. Van Assche, E. Verdonck, B. Van Mele, Polymer 42 (2001) 2959.
[21] H.K. Kim, H.T. Ju, J.W. Hong, Eur. Polym. J. 39 (2003) 2235.
[22] H.G.M. Edwards, M.J.P. Falk, Spectrochim. Acta Part A 53 (1997) 2685.
[23] M. Zheng, W. Du, Vib. Spectrosc. 40 (2006) 219.
[24] L. Baia, K. Gigant, U. Posset, R. Petry, G. Schottner, W. Kiefer, J. Popp, Vib. Spectrosc. 29 (2002) 245.

3.2 Arbeit 4

J. Fischer, G.M. Wallner, B. Strauß, L. Jandel

Effect of curing conditions on the morphology of wax modified coil coatings

Progress in Organic Coatings, eingereicht

Effect of curing conditions on the morphology of wax modified coil coatings

J. Fischer[1], G.M. Wallner[2], B. Strauß[3], L. Jandel[4]

[1] Polymer Competence Center Leoben GmbH, Roseggerstrasse 12, Leoben, 8700, Austria, Tel.: +43 3842 402 2109, Fax: +43 3842 402 2102, E-Mail address: joerg.fischer@pccl.at

[2] Institute of Material Science and Testing of Plastics, University of Leoben, Franz-Josef-Strasse 18, Leoben, 8700, Austria

[3] voestalpine Stahl GmbH, Voest-Alpine-Straße 3, Linz, 4031, Austria

[4] BASF Coatings AG, Glasuritstrasse 1, Münster, 48136, Germany

Abstract

Raman spectroscopy and optical light microscopy were applied to analyze the morphology within the bulk and on the surface of wax modified topcoats. To vary the processing conditions resin formulations were coated on primed steel sheets and cured at peak metal temperatures of 230, 240 and 250°C. By Raman spectroscopy dispersed, spherical wax domains within the bulk and on the surface were detected. These features revealed residues of the polyester based resin and the TiO_2 pigment. While the size of the identified lubricant features showed only a slight shift to smaller diameters with increasing peak metal temperature, a significant effect of the curing conditions on the overall number of wax domains and the relative area covered by wax was ascertained. A direct linear correlation between peak metal temperature and relative area covered by wax within the bulk and on the surface of the topcoats was established.

Keywords: coil coating, Raman spectroscopy, peak metal temperature, polyester based resin, wax

Introduction

Coil coating resins are complex formulations including organic and inorganic components. While for the resin matrix different organic molecules (i.e., binder and cross-linking agent) are used, organic and inorganic ingredients are dispersed, partially on a molecular level. Inorganic ingredients are acting as fillers, coloring agents, UV absorbers, matting agents or corrosion inhibitors. In contrast, small quantities of organic substances are added to adjust functional properties. Of special relevance for the improvement of the forming behavior of coil coated steel sheets are lubricants based on waxes [1-4]. Commercial resins are typically formulated with aliphatic or partly fluorinated waxes [5] with a broad range of melting temperatures and wax contents ranging from 0.2 to 2.0 m%.

In coil coating lines multi-stage processes are performed. After cleaning and pre-treatment of the metal strip an organic layer is applied on both surfaces by a two or three roll configuration. The coated layer is dried and cured in ovens subsequent to the coating units. The ovens are heated by hot air. An important process variable is the temperature profile in the curing oven. A technological value for the temperature conditions in the oven is the peak metal temperature (PMT). Typical PMT values are ranging from 220 to 250°C [6]. Due to the fact that for commercial coil coated steel sheets a maximum of four layers is required (i.e., primer and topcoat on both surfaces), coil coating lines are usually equipped with two successive units consisting of a coater and a curing oven. After each unit the coated metal strip is rapidly cooled to ambient temperature.

Depending on the retention time in the oven the peak metal temperature is varied. Because the PMT is significantly higher than melting temperatures of commonly used waxes, it is supposable that the PMT might have a significant effect on the development on the morphology of the cured coating (e.g., distribution of waxes within the bulk and on the surface of the coating).

In previous research work with focus on wax modified organic coatings different approaches are described to identify the wax lubricant. While Carlsson et al., 2001 [2] and Bexell et al., 2003 [4] used ToF-SIMS to analyze lubricants on the surface

of organic coating layers, Chvedov and Jones, 2004 [1] determined the wax concentration on the surface by FTIR spectroscopy in ATR mode. From these investigations it was concluded that the whole surface of the coating is covered by a thin layer of wax. The ToF-SIMS and FTIR approaches did not allow for a detailed mapping of the surface in order to determine potential local differences in the appearance of wax. Hence, the authors used in an associated study high resolution Raman microscopy to analyze wax modified polyester based topcoats [7]. The Raman spectroscopical investigations clearly indicated that the wax is dispersed on the surface and within the bulk. Spherical wax domains with diameters from 1 to 32 µm were found to be embedded in the matrix. In the resin matrix it was not possible to detect wax by Raman spectroscopy. Based on the Raman microscopical findings a more versatile light microscopical technique was deduced and used for a comprehensive investigation of coatings with varying wax contents. It was shown that the wax domain size distribution is more uniform within the bulk than on the surface. Furthermore, a good correlation between the formulated wax content and the relative area covered by wax was obtained.

While in the previous paper focus was given to translucent model topcoat formulations with varying wax content, only one processing condition with a peak metal temperature of 240°C was considered [7]. In contrast, the main objective of the present paper is to analyze the effect of different processing conditions (i.e., peak metal temperatures) on the development of wax domains within the bulk and on the surface of topcoats. For this purpose, model formulations based on polyester resins and common pigments were prepared and coated onto metal sheets by systematic variation of the peak metal temperature. The bulk and the surface of the topcoats were analyzed by high resolution Raman spectroscopy and light microscopy.

Experimental

Materials

The investigated model topcoat systems are based on branched polyester binders and hexamethoxymethyl melamine (HMMM) cross-linking agent. With regard to

the pigments, a low concentration (10 m%) of TiO_2 in Rutile form was chosen resulting in a white topcoat. The lubricant used was a commercial PE wax with a melting peak temperature of 100°C. The topcoat formulations with a lubricant content of 0.4 m% were prepared by BASF Coatings AG (Münster, GER). The coats were applied on primed steel sheets with a spiral bar coater. Curing was done in a laboratory oven with an air temperature of 300°C. The retention time in the oven was varied yielding industrially relevant peak metal temperatures (PMT) of 230, 240 and 250°C. The thickness of the topcoats was 22 µm.

Analytical characterization was done on the surface of the coated steel sheet. Furthermore, polished cross-sections were prepared for investigation of the bulk of the topcoat. For identification of the additives in the coating, pure TiO_2 filler particles and wax lubricants were characterized as well.

Spectroscopical and microscopical characterization

Raman spectroscopy was performed on a LabRam HR800 Raman spectrometer (HORIBA Jobin Yvon GmbH, Bensheim, GER) equipped with a confocal aperture. The coated metal sheets or the polished cross-sections were mounted on an x, y, z motorized stage. The topcoats were illuminated through a 100x 0.9 NA microscope objective with a HeNe Laser operating at 632.8 nm. Raman spectra were recorded with an accumulation time of 10 s and were averaged over 5 scans. To obtain a spectral resolution of about 1 cm^{-1} a diffraction grating of 1800 grooves/mm was used. On the one hand, single point spectra were collected over the range from 200 to 3500 cm^{-1}. On the other hand, mapping studies with 1 µm intervals were carried out over the range from 2700 to 3200 cm^{-1}. The Raman map was generated by integration of the background-subtracted spectral peak at 2883 cm^{-1} which is attributable to an asymmetric stretching vibration of CH_2 groups being representative for the wax lubricant.

After identifying the wax domains by Raman spectroscopy, optical light microscopical investigations were performed to determine the particle size distribution and the area of the image covered by wax. An optical microscope BX51 (Olympus Austria GmbH, Vienna, A) was used in reflective mode. Specimens were illuminated through 20x and 50x microscope objectives. The

particle size and the relative area covered by the lubricant were determined by recording 10 independent 717 µm x 532 µm surface images and a cross-section of 22 µm x 20000 µm (thickness of topcoat x width). For data generation and evaluation the microscope software analySIS auto was used.

Results and discussion

In Fig. 1 a representative optical micrograph of the coating surface cured at a peak metal temperature of 250°C is depicted. The 717 µm x 532 µm image reveals randomly distributed circular dark domains embedded in the bright matrix. The size of the dispersed domains is varying significantly. On the one hand a majority of small domains with a diameter below 10 µm is detectable. On the other hand some bigger domains with diameters up to 45 µm are observable.

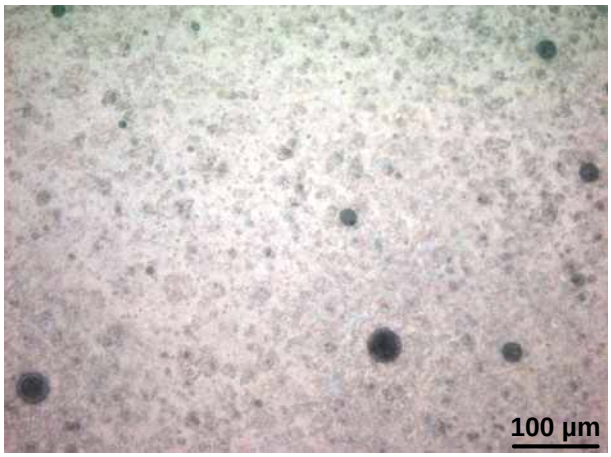

Fig. 1. Optical micrograph of the coating surface cured at a peak metal temperature of 250°C.

The chemical composition of the organic coating surface, the inorganic filler and the organic wax additive used, was analyzed by Raman spectroscopy in point illumination mode. Representative spectra of the bright and dark areas in Fig. 1 and the TiO_2 pigment and the wax ingredient added are displayed in Figs. 2 and 3. By comparison of the spectra of the bright area and the TiO_2 pigment (s. Fig. 2), it can be concluded that the bright areas are dominated by scattering bands being representative for the polyester based resin (at 1003, 1307, 1450, 1620, 1735, 2970 and 3088 cm^{-1} [7-11]) and the TiO_2 pigment (at 451 and 613 cm^{-1} [12, 13]).

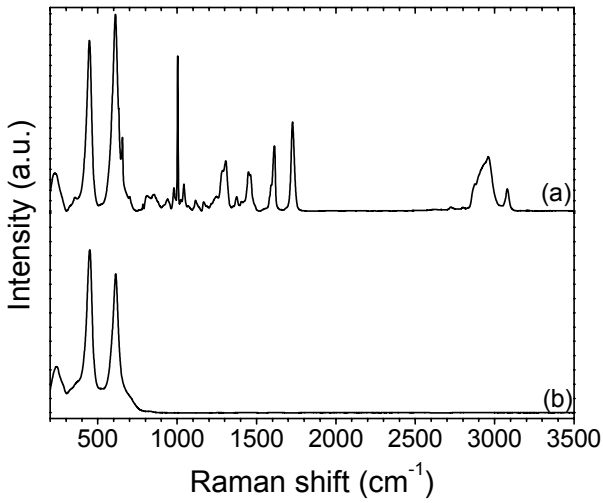

Fig. 2. Raman spectra of (a) the bright area in Fig. 1 and, (b) the TiO_2 filler.

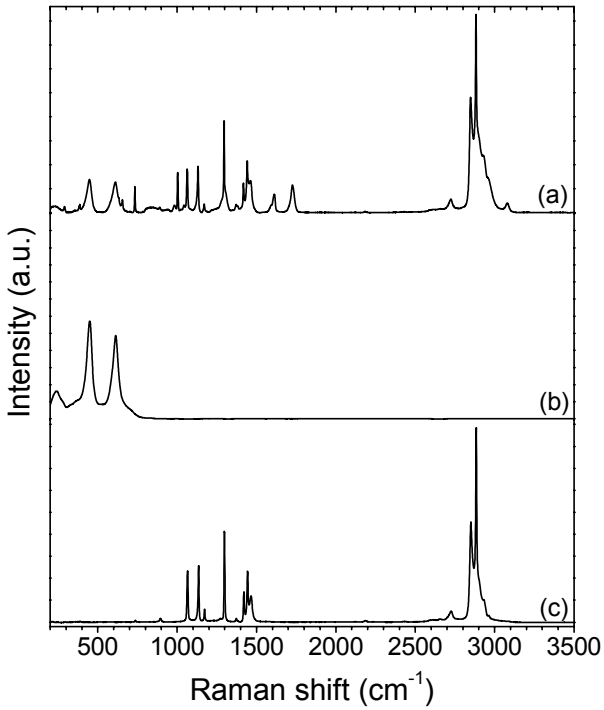

Fig. 3. Raman spectra of (a) the dark domains in Fig. 1, (b) the TiO_2 pigment and, (c) the wax lubricant.

Even at the highest lateral and vertical resolution of the Raman apparatus used it was not possible to record a spectrum with scattering bands of the polyester based resin only. Hence, an excellent dispersion of TiO_2 in the resin matrix was confirmed. In Fig. 3 a Raman spectrum of the centre of a selected dark domain (s. Fig. 1) with a diameter of about 30 µm is shown along with spectra of the TiO_2 pigment and the wax ingredient. In contrast to the spectrum of the bright area the

scattering bands attributable to the wax lubricant (at 1063 and 1129 cm^{-1} (CC stretching vibration), 1296 cm^{-1} (CC twisting vibration), 1416, 1440 and 1463 cm^{-1} (CH bending vibration) and 2850 and 2890 cm^{-1} (CH stretching vibration) [14-16]) are dominating the spectrum of the dark domain. Further scattering bands being relatable to TiO_2 and to the polyester based resin are discernible in the spectrum of the dark domain. Hence, the dark domains of Fig. 1 consist mainly of wax with small amounts of the resin and the pigment. Performing a Raman map it was revealed that the whole black domain is covered by the lubricant. As elaborated in the associated paper, the shape of the investigated dark domain on the surface can be interpreted as spherical cap.

To characterize and to quantify the number, the size and the distribution of the lubricant domains, on the one hand light microscopical surface images were taken and evaluated. On the other hand polished cross-sections of the topcoat were prepared, investigated and evaluated as to the appearance of the lubricant within the bulk. In Figs. 4 and 5 representative optical micrographs are displayed for the surface and the cross-section (bulk) of the topcoats cured at peak metal temperatures (PMTs) of 230, 240 and 250°C. For the different PMTs a majority of small circular wax domains and some larger domains are identifiable on the surface and in the bulk of the topcoat. By qualitative evaluation of the images shown in Figs. 4 and 5 it can be concluded that the number of dark wax domains is increasing the higher the PMT. Furthermore, the surface images indicate that the domains of medium and maximum size are bigger the higher the PMT. With regard to the cross-sectional images for each sample three representative micrographs are displayed in Fig. 5. Independent of PMT small, medium and large wax domains are observable at the top edge, the middle section and the bottom edge (i.e., close to the interface between topcoat and primer) of the cross-sections.

For quantitative evaluation ten 717 µm x 532 µm surface images and about 150 cross-section images covering a cross-section area of 22 µm x 20000 µm were recorded and analyzed quantitatively as to the overall number and the minimum, maximum and average diameter of the wax domains as well as the relative area

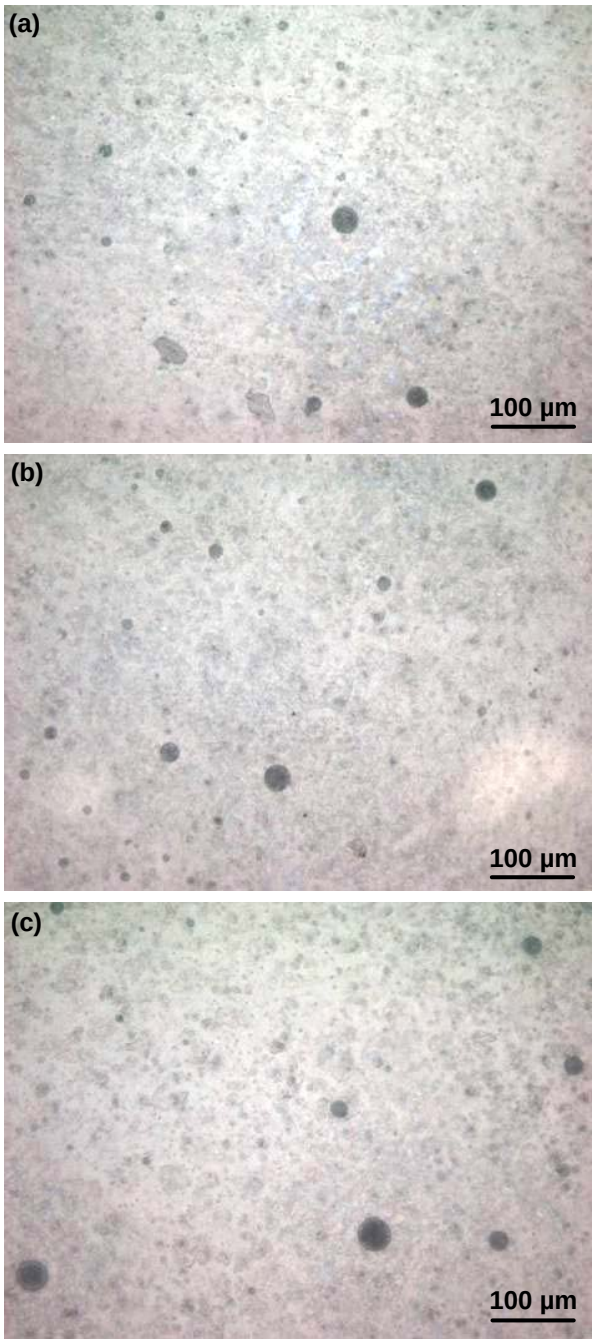

Fig. 4. Optical micrographs of the coating surfaces cured with peak metal temperatures of (a) 230°C, (b) 240°C and (c) 250°C.

covered by wax. Due to the limited lateral resolution of optical light microscopy and the uncertainties in reproducible analysis of wax domains with diameters below 2 µm this wax domain class was not considered for evaluation. Further details and restrictions of the evaluation procedure are described in the associated paper [7]. In Table 1 the number of identified wax domains on the surface and within the bulk

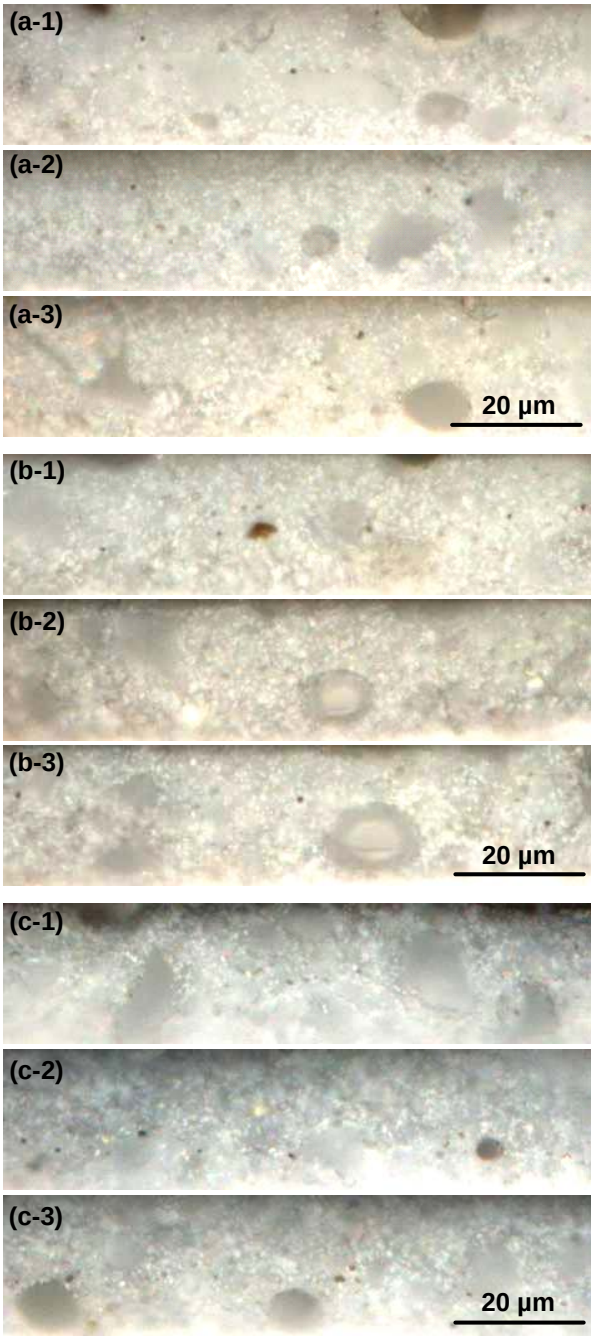

Fig. 5. Optical micrographs of the polished topcoat cross-section cured with peak metal temperatures of ((a-1)-(a-3)) 230°C, ((b-1)-(b-3)) 240°C and ((c-1)-(c-3)) 250°C (top edge of image: surface of topcoat; bottom edge of image: interface between topcoat and primer).

is given along with information as to the minimum, maximum and average particle diameter and the relative area covered by wax as a function of peak metal temperature. The relationship between number of wax domains or relative area

Table 1 Characteristic values (number; minimum, maximum and average diameter; relative area) of the wax domains on the surface and within the bulk of the investigated topcoats cured with peak metal temperatures (PMT) of 230, 240 and 250°C.

PMT	Number (-)		Minimum diameter (µm)		Maximum diameter (µm)		Average diameter (µm)		Relative area (%)	
	Surface	Bulk	Surface	Bulk	Surface	Bulk	Surface	Bulk	Surface	Bulk
230	104	61	3	2	38	16	15	6	0.6	0.5
240	203	57	3	2	37	16	12	8	0.7	0.7
250	276	109	4	2	43	16	12	6	1.1	1.0

covered by wax and the peak metal temperature is depicted in Fig. 6 for surface and cross-section images. Furthermore, in Fig. 7 the frequency distribution of number of wax domains on the surface and within the bulk is plotted as a function of wax diameter class for domains in topcoats cured at a PMT of 230, 240 and 250°C. As shown in Table 1 the number of wax domains is dependent on PMT. The higher the curing temperature the more domains with diameters above 2 µm were found. The differences in the absolute numbers are related to the investigated areas on the surface and in the bulk. While for each coating surface images with an overall area of 3.8E6 µm² were analyzed, the total area of the

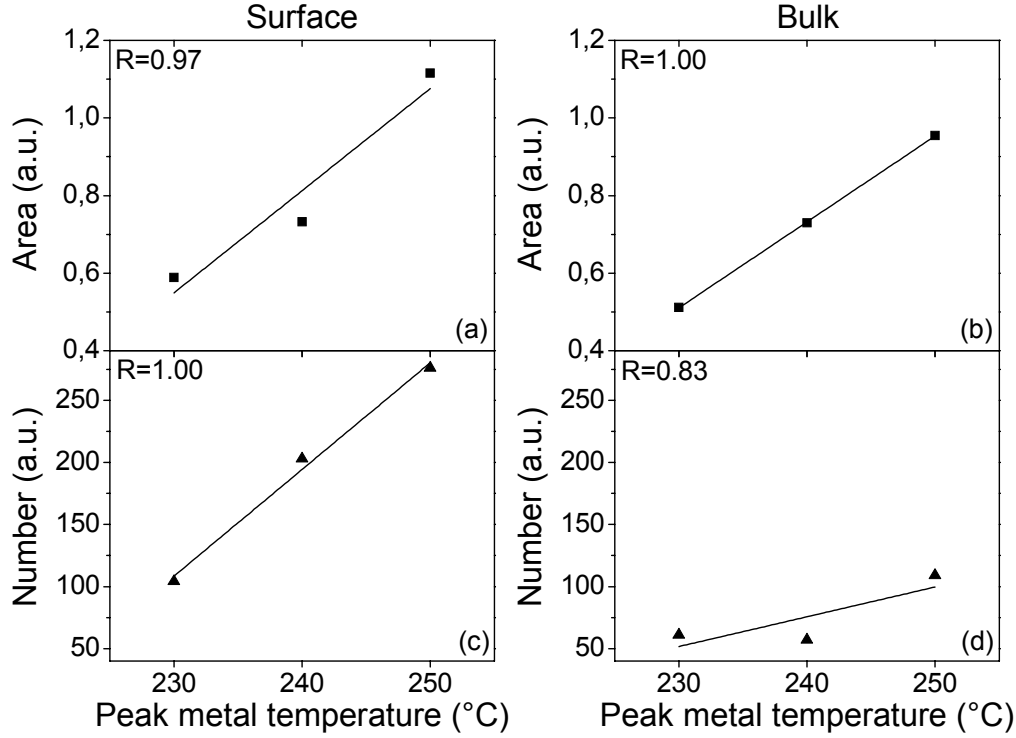

Fig. 6. (a) Surface area and (b) bulk area covered by wax as well as number of wax domains on the (c) surface and (d) within the bulk as a function of peak metal temperature.

investigated cross-section was 4.4E5 µm². Hence, related to the analyzed area much more domains were found in the cross-section. As to the size of the dispersed wax features minimum and maximum values in diameter of 2 and 43 µm were detected. The average feature diameter is ranging from 6 to 15 µm. In general, smaller domains are observable in the bulk than on the surface. In comparison to the previous study the average and the maximum values are higher by about 30 % for the topcoats investigated in the present study. These differences are presumably related to the effect of the pigment (TiO_2 vs. $BaSO_4$). The diameter values are not significantly affected by the PMT. In contrast, the relative wax area on the surface and within the bulk is clearly dependent on PMT. The relative area values are ranging from 0.5 to 1.1 % without significant differences between surface and bulk.

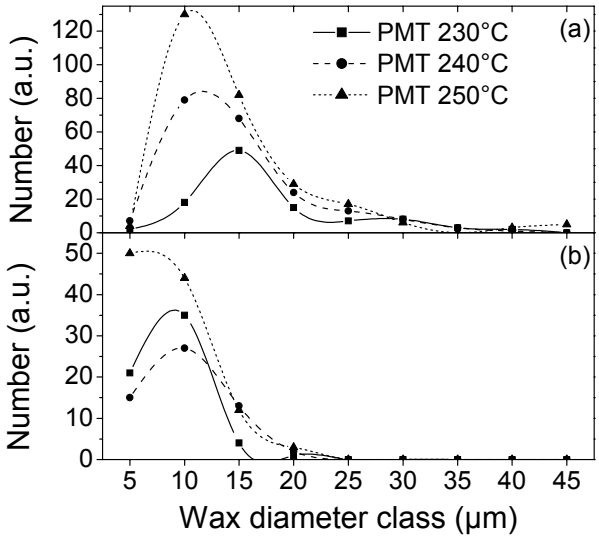

Fig. 7. Frequency distribution of number of wax domains (a) on the surface and (b) within the bulk as a function of wax diameter class for topcoats cured at a peak metal temperature (PMT) of 230, 240 and 250°C.

In Fig. 6 correlations between the number of wax domains or the relative area covered by wax and the peak metal temperature are revealed. Interestingly a linear relationship with similar gradients was found between relative wax area on the surface and within the bulk and PMT. In contrast, the gradient is different for the surface and the bulk for the number of wax domains as a function of PMT. Hence, PMT dependent variations in the distribution of wax domains can be concluded. The frequency distribution of the number of wax domains on the

surface and within the bulk is displayed in Fig. 7 for diameter classes in 5 µm intervals. Different distributions were found for wax domains on the surface and within the bulk. Furthermore, the classified numbers of wax features depend on PMT. In the cross-section mostly wax domains with diameters ranging from 2 to 10 µm were identified. In contrast, on the surface the majority of wax domains has a diameter between 5 and 15 µm. The distribution of number of wax domains on the surface is consistently affected by PMT. The higher PMT the more wax domains in the different diameter classes were found. Furthermore, a shift of the frequency distribution to smaller domains with increasing PMT was detected. The trends obtained for the surface are less significant for the bulk.

Summary and conclusions

Within this study, a significant effect of peak metal temperature on the formation of wax domains on the surface and within the bulk of coil coatings was established. By optical light microscopy and Raman spectroscopy the distribution of lubricant domains with residues of resin and TiO_2 particles was determined for a topcoat formulation with 0.4 m% of wax, applied to a primed metal sheet and cured at peak metal temperatures of 230, 240 and 250°C. In the bulk and on the surface of the cured coating spherical wax domains with diameters ranging from 2 to 43 µm were identified. Independent of curing temperature wax domains were observable in the whole cross-section without any tendency of enrichment near the free surface. Interestingly, the average and maximum diameter of the domains was a factor of about two higher on the surface. The peak metal temperature had a significant effect on the number of lubricant features and on the relative area covered by wax. Linear correlations between the relative area covered by lubricant in the cross-section and on the surface and the peak metal temperature were established. The higher the peak metal temperature the more dispersed wax features were identifiable. Hence, the variation in curing temperature allows for tuning the topcoat morphology. Because higher peak metal temperatures result for a defined formulation in more wax domains within the bulk and on the surface, it can be concluded, that the mechanism of wax formation presumably consists of molecular dissolution of the lubricant and temperature/time-dependent precipitation as dispersed spherical domains.

Acknowledgement

The research work of this paper was performed at the Polymer Competence Center Leoben GmbH (PCCL, Austria) within the framework of the Kplus-program of the Austrian Ministry of Traffic, Innovation and Technology with contributions by the Institute of Materials Science and Testing of Plastics at the University of Leoben (Austria), the voestalpine Stahl GmbH (Austria) and the BASF Coatings AG (Germany). The PCCL is funded by the Austrian Government and the State Governments of Styria and Upper Austria.

References

[1] D. Chvedov, R. Jones, Surf. Coat. Technol. 188-189 (2004) 544.
[2] P. Carlsson, U. Bexell, M. Olsson, Wear 251 (2001) 1075.
[3] P. Carlsson, U. Bexell, M. Olsson, Wear 247 (2001) 88.
[4] U. Bexell, P. Carlsson, M. Olsson, Appl. Surf. Sci. 203-204 (2003) 596.
[5] P. Nanetti, Lackrohstoffkunde, Vincentz, 2000 (ISBN 3-87870-560-3).
[6] Colofer Processing, www.voestalpine.com/stahl/en/site/downloads/product_brochures.html (2008).
[7] J. Fischer, G.M. Wallner, B. Strauß, L. Jandel, Surf. Coat. Technol. (2009) submitted.
[8] B. Marton, L.G.J. van der Ven, C. Otto, N. Uzunbajakava, M.A. Hempenius, G.J. Vancso, Polymer 46 (2005) 11330.
[9] J.L. Dupuie, W.H. Weber, D.J. Scholl, J.L. Gerlock, Polym. Degrad. Stab. 57 (1997) 339.
[10] G. Van Assche, E. Verdonck, B. Van Mele, Polymer 42 (2001) 2959.
[11] H.K. Kim, H.T. Ju, J.W. Hong, Eur. Polym. J. 39 (2003) 2235.
[12] E.M. Suzuki, M. Carrabba, J. Forensic. Sci. 46 (5) (2001) 1053.
[13] W. Schrof, E. Beck, R. Königer, W. Reich, R. Schwalm, Prog. Org. Coat. 35 (1999) 197.
[14] J. Fischer, G.M. Wallner, A. Pieber, Macromol. Symp. 265 (2008) 28.
[15] H.G.M. Edwards, M.J.P. Falk, Spectrochim. Acta Part A 53 (1997) 2685.
[16] M. Zheng, W. Du, Vib. Spectrosc. 40 (2006) 219.

3.3 Arbeit 5

J. Fischer, G.M. Wallner, B. Strauß, L. Jandel

Morphology of wax modified coil coatings without and with pigmentation

Progress in Organic Coatings, eingereicht

Morphology of wax modified coil coatings without and with pigmentation

J. Fischer[1], G.M. Wallner[2], B. Strauß[3], L. Jandel[4]

[1] Polymer Competence Center Leoben GmbH, Roseggerstrasse 12, Leoben, 8700, Austria, Tel.: +43 3842 402 2109, Fax: +43 3842 402 2102, E-Mail address: joerg.fischer@pccl.at

[2] Institute of Material Science and Testing of Plastics, University of Leoben, Franz-Josef-Strasse 18, Leoben, 8700, Austria

[3] voestalpine Stahl GmbH, Voest-Alpine-Straße 3, Linz, 4031, Austria

[4] BASF Coatings AG, Glasuritstrasse 1, Münster, 48136, Germany

Abstract

Wax modified coil coatings without and with white pigmentation were analyzed by optical light microscopy, Raman spectroscopy and Atomic Force Microscopy. By optical light and Raman microscopy dispersed spherical wax domains in the micrometer range were ascertained on the surface and within the bulk of the coatings. By the combined Atomic Force microscopical and Raman spectroscopical approach it was possible to detect resin and pigment residues in the lubricant features with diameters above 2 µm. Vice versa indications for wax inclusions with diameters below 2 µm in the matrix and rather thin wax layers expanding from the spherical lubricant domains onto the surface were obtained. As to the wax distribution evaluated by optical light and Raman microscopy significant differences between clearcoat and white topcoat were detected. The unpigmented coating exhibited smaller wax features and an inhomogeneous distribution with less wax on the surface.

Keywords: coil coating, Raman spectroscopy, AFM, polyester based resin, wax

Introduction

Coil coatings usually consist of two layers, the primer and the topcoat. In a multi-stage process resin formulations are applied on both surfaces of a pre-treated steel sheet and cured in ovens. The main components of the resin formulations are the organic binder and the cross-linking agent, the organic solvent and functional ingredients. While the solvent is a processing aid released in the curing unit, binder, cross-linking agent and ingredients constitute to the coating layer. As ingredients various organic and inorganic substances are dispersed in the matrix of a coating. Inorganic ingredients are acting as fillers, pigments, UV absorbers, matting agents or corrosion inhibitors. In contrast, small quantities of organic substances are added to adjust functional properties. Of special relevance for the improvement of the forming behavior of coil coated steel sheets are lubricants based on waxes [1-4]. Commercial resins are typically formulated with aliphatic or partly fluorinated waxes [5] with a broad range of melting temperatures and wax contents ranging from 0.2 to 2.0 m%.

Previous research work is mainly focused on the investigation and description of application relevant properties of wax modified organic coatings. In various studies [1-4, 6] the friction and wear behavior of coated metal sheets is examined. As the most important result a significant effect of the lubricant content on the frictional behavior is reported [1]. To identify the wax lubricant on the surface of organic coating layers Carlsson et al., 2001 [2] and Bexell et al., 2003 [4] used ToF-SIMS. Chvedov and Jones, 2004 [1] determined the wax concentration on the surface by FTIR spectroscopy in ATR mode. From these investigations it was concluded that the whole surface of the coating is covered by a thin layer of wax. To analyze the appearance of wax on the coatings surface comprehensively, a Raman microscopical technique was developed, implemented and applied for pigmented coatings by Fischer et al., 2009a [7] and Fischer et al., 2009b [8]. In these associated papers it was shown that spherical wax domains with diameters ranging from 1 to 43 µm are distributed randomly on the surface and within the bulk of coatings with $BaSO_4$ or TiO_2 white pigments. In the lubricant domains residues of the polyester based resin and the white pigments were detected by Raman spectroscopy. While in Fischer et al., 2009a a good correlation between

the formulated wax content and the relative area covered by wax was established, in Fischer et al., 2009b a significant effect of the curing conditions on the relative area covered by wax was ascertained. The higher the peak metal temperature the more lubricant was identified on the surface and within the bulk of the investigated white topcoats. Due to the effect of the peak metal temperature a mechanism of wax formation consisting of molecular dissolution of the lubricant and temperature/time-dependent precipitation of dispersed spherical wax domains was concluded.

To establish a sounder basis for the deduction of mechanistic models for wax domain formation, the main objective of this paper is to analyze and investigate a polyester-based model clearcoat without pigments and to check the effect of the TiO_2 white pigment. Furthermore, the experimental approach for the physical and chemical detection of wax domains in coil coatings should be expanded by a further high resolution microscopical technique. For this purpose, coating formulations based on wax modified polyester resins without and with pigments were prepared, coated onto metal sheets and cured at a peak metal temperature of 240°C. The model topcoats were analyzed by light and Raman microscopy and high resolution Atomic Force Microscopy (AFM). The establishment of theoretical models for wax domain formation is not within the scope of this paper.

Experimental

Materials

The investigated model coat systems are based on branched polyester binders and hexamethoxymethyl melamine (HMMM) cross-linking agent. On the one hand, a clearcoat without pigments was formulated. On the other hand, a white topcoat with 10 m% of TiO_2 in Rutile form was prepared. For the clearcoat and the white topcoat a commercial aliphatic wax with a melting peak temperature of 100°C was used. The formulations with a lubricant content of 0.4 m% were prepared by BASF Coatings AG (Münster, GER). The coats were applied on primed steel sheets with a spiral bar coater. Curing was done in a laboratory oven with an air temperature

of 300°C. The retention time in the oven was fixed yielding an industrially relevant peak metal temperature (PMT) of 240°C. The thickness of the coats was 22 µm.

Light and Raman microscopy as well as AFM were done on the surface of the coated steel sheets. To analyze the wax distribution within the bulk by light and Raman microscopy polished cross-sections were prepared.

Microscopical characterization

Optical light microscopy was performed to determine the particle size distribution and the area of the image covered by wax on the surface and within the bulk of the coatings. An optical microscope BX51 (Olympus Austria GmbH, Vienna, A) was used in reflective mode. Specimens were illuminated through 20x and 50x microscope objectives. The particle size and the relative area covered by the lubricant were determined by recording 10 independent 717 µm x 532 µm surface images and a cross-section of 22 µm x 20000 µm (thickness of topcoat x width). For data generation and evaluation the microscope software analySIS auto was used.

Raman spectroscopy was performed on a LabRam HR800 Raman spectrometer (HORIBA Jobin Yvon GmbH, Bensheim, GER) equipped with a confocal aperture. The coated metal sheets or the polished cross-sections were mounted on an x, y, z motorized stage. The coats were illuminated through a 100x 0.9 NA microscope objective with a HeNe Laser operating at 632.8 nm. Raman spectra were recorded with an accumulation time of 10 s and averaged over 5 scans. To obtain a spectral resolution of about 1 cm^{-1} a diffraction grating with 1800 grooves/mm was used. On the one hand, single point spectra were collected over the range from 200 to 3500 cm^{-1}. On the other hand, mapping studies of the coating surface were carried out with 1 µm intervals. To analyze wax domains and TiO_2 white pigments Raman spectra were collected from 2700 to 3200 cm^{-1} and 200 to 1100 cm^{-1}, respectively. While the Raman map of wax was generated by integration of the background-subtracted spectral peak at 2883 cm^{-1} (attributable to vibration of CH_2 groups), for the Raman map of TiO_2 the spectral peak at 450 cm^{-1} (attributable to vibration of TiO_2) was evaluated.

The characterization of wax domains was also done by Atomic Force Microscopy (AFM). Therefore, coated steel sheets were cut to 1 cm x 2 cm samples. To characterize the topography and the morphology of the coating surface AFM was performed in tapping mode (frequency: ~80 kHz) with a MFP 3D (Asylum Research, Santa Barbara, USA). 10 µm x 10 µm height and phase images with a lateral resolution below 0.1 µm were recorded under ambient conditions with the "fast" scan axis parallel to the coating direction. Sharpened Si tips designed for non-contact mode imaging and a high resonance frequency (Si NCH) were used. The tip radius was <10 nm, the opening angle 18°. Due to the fact that an AFM phase image represents the phase lag between the agitating oscillation and the detected cantilever oscillation, the differentiation between harder and softer areas on the coating surface was envisaged.

Results and discussion

In Fig. 1 representative optical micrographs of the surface of the clearcoat and the white topcoat are depicted. The 717 µm x 532 µm images reveal randomly distributed circular dark domains embedded in the bright matrix. While for the clearcoat small black domains with diameters of about 2 µm are dominating, the size of the dispersed black domains in the image of the white topcoat is more uniform distributed ranging from 3 to 37 µm. In both images only few black domains with diameters above 20 µm are observable. To check the chemical composition of selected black domains Raman spectroscopy was carried out. It

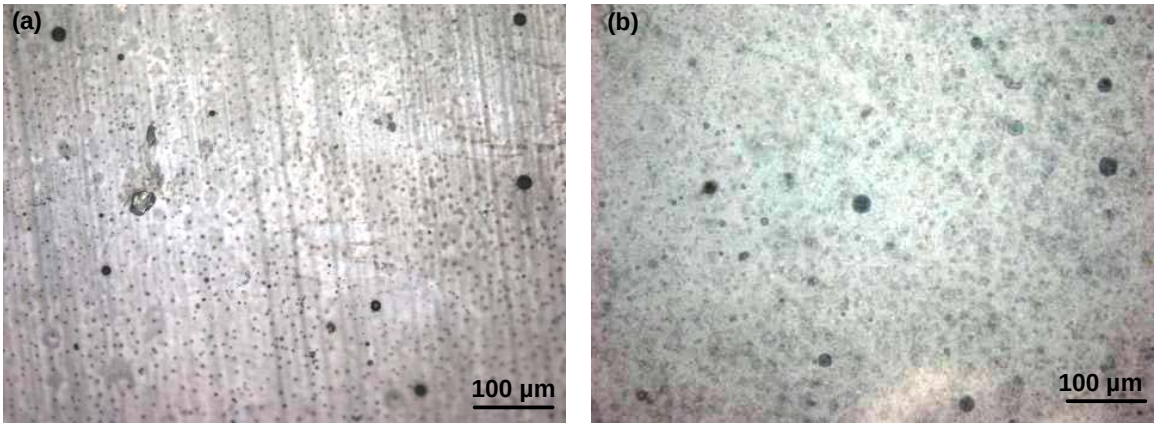

Fig. 1. Optical micrographs of the surfaces of (a) the clearcoat and (b) the white topcoat.

was ascertained that circular black domains with diameters above 3 µm are consisting mainly of aliphatic wax. In contrast, many black features with diameters below 3 µm were identified as resin and are thus interpreted as pinhole defects. Such imperfections are common in coating surfaces and are related to gas release during the coating process [9]. Interestingly, more pinhole defects were detected for the clearcoat surface compared to the white topcoat. Moreover, these defects are found mainly on the surface and hardly in the cross-section of both coatings.

In Fig. 2 100 µm x 74 µm optical micrographs of the clearcoat and white topcoat surface are displayed. In these images representative black wax domains, chosen for high resolution Raman mapping and AFM investigations, are indicated by the 10 µm x 10 µm rectangles. Due to significant height differences in the wax domains, an entire characterization of wax features with diameters above 10 µm was not possible with the AFM setup used. For small wax domains a reproducible positioning in the Raman microscope and the AFM was difficult. Hence, focus was given to high resolution microscopical analysis of wax domains with diameters ranging from 5 to 10 µm.

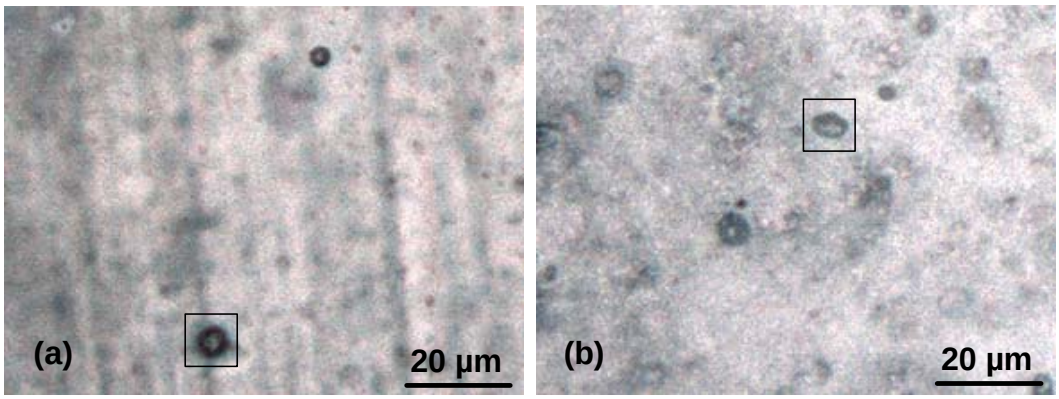

Fig. 2. Optical micrographs of (a) the clearcoat and (b) the white topcoat with indication of typical wax domains by the rectangle (size: 10 µm x 10 µm).

High resolution 10 µm x 10 µm images derived by AFM, Raman mapping and optical microscopy are shown in Figs. 3 to 6 along with Raman spectra measured at representative positions. The spherical wax domain on the surface of the clearcoat (s. Fig. 3) is explicitly discernible by the various microscopical

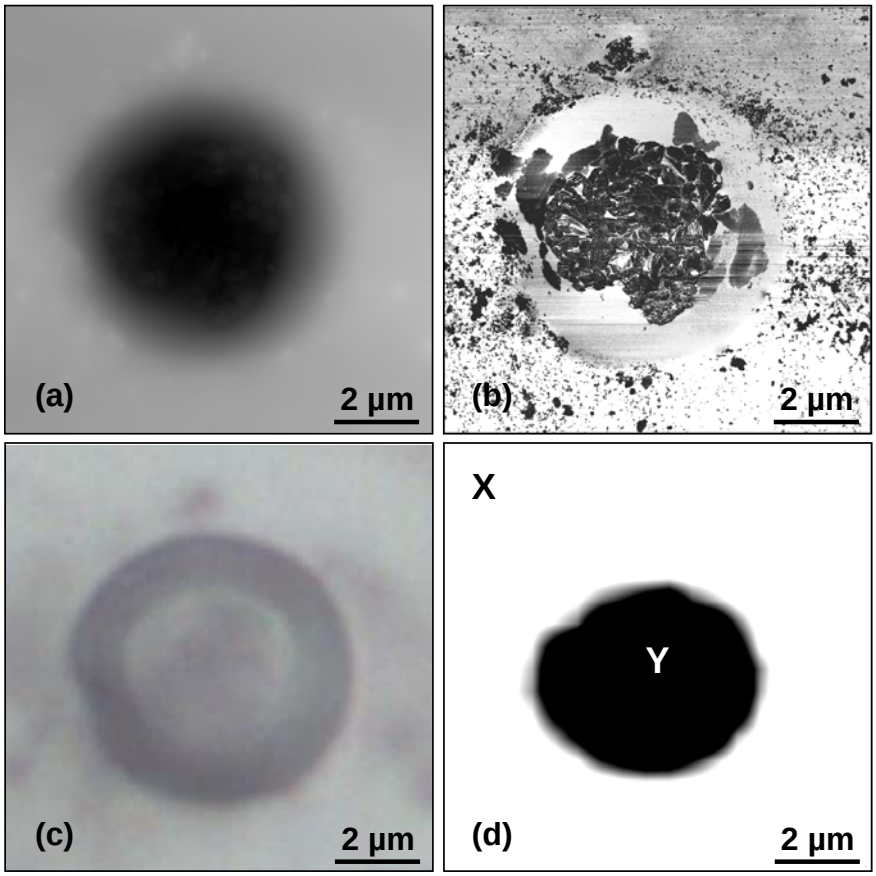

Fig. 3. (a) AFM height image, (b) AFM phase image, (c) optical micrograph and (d) Raman map for wax of the feature designated in Fig. 2a.

techniques applied. The wax domain appears as black feature in the optical micrograph. From the AFM height image in which darker colors indicate depth, it can be concluded that the wax domain represents a depression on the surface. In the transition area from the matrix to the wax domain a depth gradient is observable. For the wax domain with a diameter of about 6.5 µm the maximum height difference between matrix and wax depression is about 1.8 µm. The diameter obtained from the height image is comparable to the value derived from the optical micrograph. In the AFM phase image, in which dark colors represent a smaller phase lag (i.e., soft phase) and bright colors a larger phase shift (i.e., hard phase), the shape of the wax feature is different compared to the height image. While in the center a distinct phase (color) difference compared to the matrix appears, the transition area reveals no phase difference. Presumably, the transition region (shell) around the center is related to a measuring artifact because of the gradient in the outer zone of the wax feature. In both, the matrix

and the wax feature inclusions of the opposite phase (i.e., white in black and vice versa) are recorded and reproduced. This might be an indication for small inclusions of wax with diameters below 2 µm in the matrix and resin in the wax domain.

In the Raman map (s. Fig. 3d) the size of the lubricant domain is slightly smaller compared to the other microscopical images. Furthermore, the Raman map exhibits a brighter shell around the dark center of the wax domain. For mapping the Raman microscope was operated at the maximum achievable resolution (i.e., 100x 0.9 NA microscope objective and confocal hole closed to 200 µm, providing a lateral resolution of about 800 nm and a vertical resolution of about 1 µm). Hence, it can be concluded that the thickness of the outer zone of the wax domain is below 1 µm. Representative Raman spectra obtained at the positions X and Y in Fig. 3d are displayed in Fig. 4. In the center of the wax domain (position Y in Fig. 3d) various Raman peaks are observable. While the majority of the peaks are attributable to the aliphatic wax, few weak peaks at 1620 cm^{-1}, 1735 cm^{-1} and 3088 cm^{-1} are characteristic for the cured resin. Hence, the inclusions of opposite phase (white) in the wax feature of the AFM phase image are most likely related to resin residues within the wax feature confirming the results obtained by AFM. In the matrix (position X in Fig. 3d) various Raman peaks are observable. All of them are representative for the resin. Peaks assignable to the wax are superimposed by

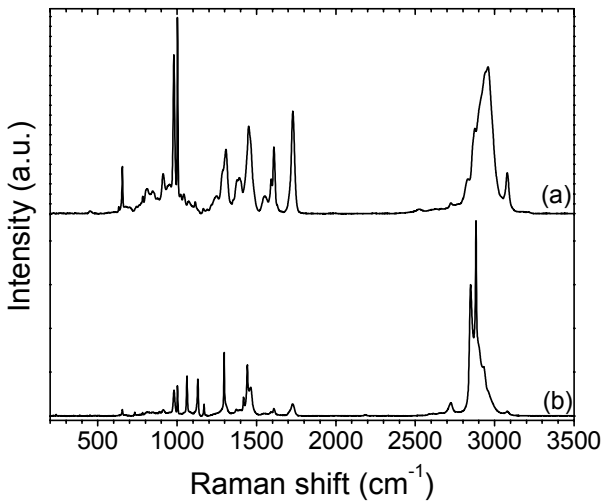

Fig. 4. Raman spectra of the clearcoat (a) outside (X in Fig. 3d) and (b) inside (Y in Fig. 3d) the wax domain.

strong bands of the resin. Therefore, it was not possible to confirm the inclusions of opposite phase (black) in the matrix as wax domains unambiguously. To verify potential wax domains in the matrix with size below 500 nm a combined AFM and Raman technique (e.g., Tip Enhanced Raman Scattering (TERS) [10]) should be used.

In Fig. 5 high resolution 10 µm x 10 µm micrographs derived by AFM height and phase imaging and by Raman mapping are shown for the pigmented topcoat. All micrographs are taken from the same position of the sample with a representative wax feature in the center of the image. In the AFM height image a wax domain with a diameter of about 6.3 µm is discernible. The topography of this wax feature is different compared to the wax domain displayed in Fig. 3. While the outer zone of the wax feature is below the height level of the matrix, the center of the wax domain is protruding. This second kind of wax domain topography is not only

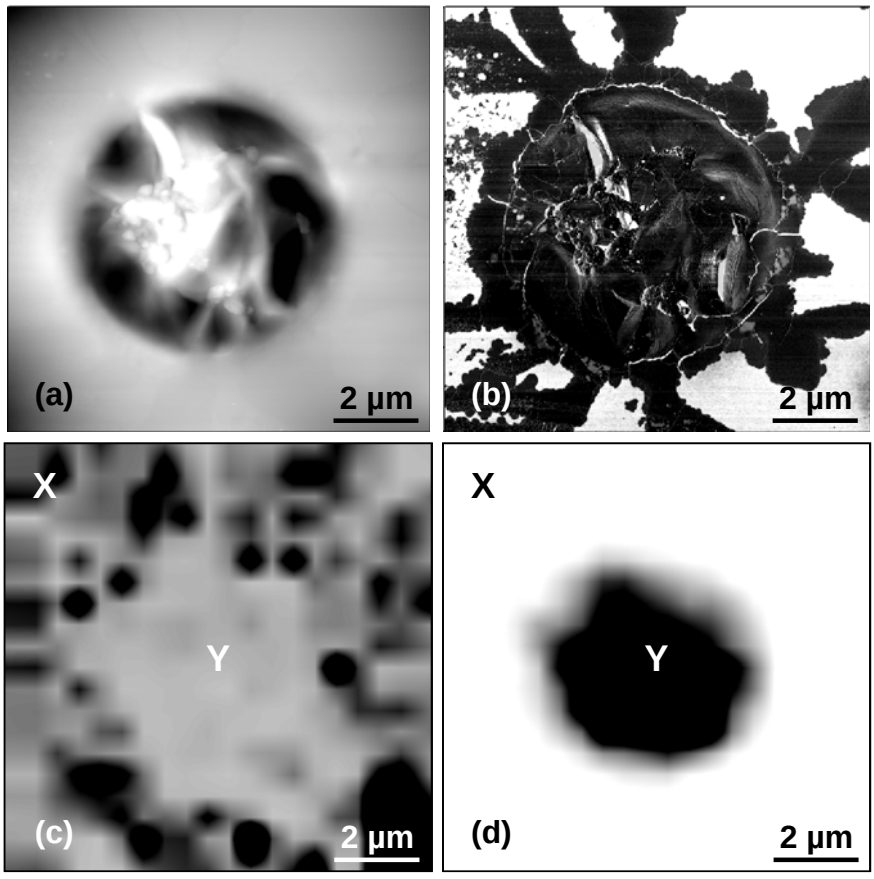

Fig. 5. (a) AFM height image, (b) AFM phase image, (c) Raman map for TiO_2 and (d) Raman map for wax of the feature designated in Fig. 2b.

found in white topcoats. In the clearcoat and the topcoat both kinds of wax domain topography are detectable. The AFM phase image (s. Fig. 5b) is different to the height image. Within the wax feature the black color which is indicating a softer phase is predominant. Only some bright inclusions (i.e., harder phase) are observable. In the matrix bright and dark areas are discernible. Therefore, a layer of wax expanding from the lubricant domain onto the surface of the matrix can be presumed. As described by Weber, 2009 [11] based on crystallization studies on the surface of wax modified UV-cured resins by AFM at elevated temperatures around the melting temperature of the wax, the wax layer expanding into the matrix is significantly dependent on time and temperature.

While in Fig. 5c a Raman map derived by evaluation of the TiO_2 peak is shown, in Fig. 5d the wax peak at 2883 cm^{-1} was examined and used for the map. Fig. 5c reveals an inhomogeneous distribution of TiO_2 within the matrix. The dark areas in Fig. 5c represent clusters of TiO_2 with a diameter of about 1 µm. Interestingly, the TiO_2 clusters are not discernible in the AFM phase image (s. Fig. 5b). Thus, it can be assumed that TiO_2 clusters are covered by the cured resin. In the Raman map with focus on wax (s. Fig. 5d) the size of the lubricant domain is slightly smaller compared to the AFM images. In agreement with conclusions derived for the clearcoat the thickness of the outer zone of the wax domain is below 1 µm. Representative Raman spectra obtained at the positions X and Y in Figs. 5c and 5d are displayed in Fig. 6. In the center of the wax domain (position Y in Figs. 5c and 5d) strong Raman peaks attributable to wax and weaker bands assignable to the cured resin and the TiO_2 pigment (at 450 cm^{-1} and 613 cm^{-1}) are observable. Hence, resin and TiO_2 inclusions within the wax domain are concluded. In the Raman spectrum of position X (i.e., matrix of the coating) scattering peaks attributable to the cured resin and TiO_2 are found. As already described for the clearcoat, no significant wax bands appear in the spectrum of the matrix. Therefore, the dark phase features expanding into the matrix (s. AFM phase image in Fig. 5b) are presumably related to rather thin wax layers not detectable by Raman spectroscopy. For a detailed analysis of these wax layers further microscopical investigations are necessary also considering temperature and time effects.

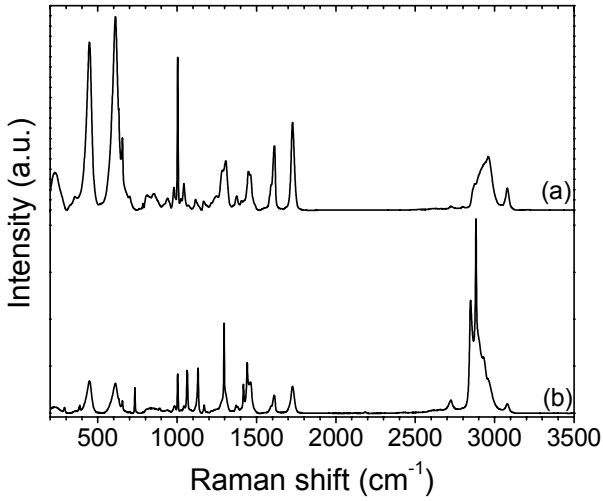

Fig. 6. Raman spectra of the white topcoat (a) outside (X in Figs. 5c and 5d) and (b) inside (Y in Figs. 5c and 5d) the wax domain.

Based on the results of the optical light, Raman and Atomic Force microscopical investigations only spherical wax domains with diameters above about 2 µm can be evaluated reliably. Hence, the distribution of wax domains on the surface and within the bulk was examined by optical light microscopy. For quantitative evaluation ten 717 µm x 532 µm surface images and about 150 cross-section images covering a cross-section area of 22 µm x 20000 µm were recorded and analyzed quantitatively. Further details and restrictions of the evaluation procedure are described in an associated paper [7]. In Table 1 the number of identified wax domains on the surface and within the bulk of the clearcoat and the white topcoat is given along with information as to the minimum, maximum and average particle diameter and the relative area covered by wax. In Fig. 7 the frequency distribution of number of wax domains on the surface and within the bulk of the clearcoat and the white topcoat is shown. While for the clearcoat wax domains with diameters below 10 µm are predominant on the surface and within the bulk, in the white topcoat mainly domains with diameters between 5 and 15 µm were found. Furthermore, significantly less wax domains are detectable in the bulk of the white topcoat compared to the clearcoat. Independent of pigmentation similar maximum domain size values of about 35 µm on the surface, but only about 16 µm within the bulk were obtained. Due to the predominance of smaller domains in the clearcoat the average diameter values on the surface and within the bulk are lower for the

Table 1 Characteristic values (number; minimum, maximum and average diameter; relative area) of the wax domains on the surface and within the bulk of the investigated clearcoat and the white topcoat.

topcoat	Number (-)		Minimum diameter (µm)		Maximum diameter (µm)		Average diameter (µm)		Relative area (%)	
	Surface	Bulk	Surface	Bulk	Surface	Bulk	Surface	Bulk	Surface	Bulk
clearcoat	188	149	3	2	33	17	8	6	0.4	1.2
white topcoat	203	57	3	2	37	16	12	8	0.7	0.7

clearcoat. Regarding the relative area covered by wax significant differences between clearcoat and white topcoat are discernible. For the white topcoat similar fractions of wax were identified on the surface and within the bulk. In contrast, the relative area covered by wax is significantly higher in the bulk of the clearcoat but lower on the surface. Hence, the wax distribution is more uniform for the investigated white topcoat with TiO_2 pigment. This is in agreement with results of a previous study [7] in which a uniform distribution of wax was found for a $BaSO_4$ pigmented coating.

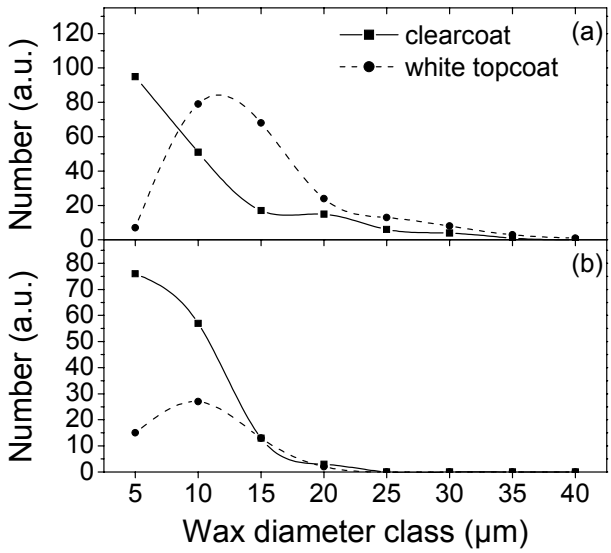

Fig. 7. Frequency distribution of number of wax domains (a) on the surface and (b) within the bulk as a function of wax diameter class for the investigated clearcoat and white topcoat.

Summary and conclusions

In this paper wax modified coil coats without and with pigmentation were analyzed and investigated by optical light microscopy, Raman spectroscopy and Atomic Force Microscopy. Independent of pigmentation spherical wax domains with

diameters ranging from 2 to 37 µm were found on and in the coatings by optical microscopy and confirmed by Raman spectroscopy. Indications for wax inclusions with diameters below 2 µm and rather thin wax layers on the surface were obtained by high resolution AFM. Due to the predominance of Raman bands of the cured resin a Raman spectroscopical confirmation of these indications was not possible. In contrast, inclusions of resin or TiO_2 in lubricant features with diameters above 2 µm were detected. The spherical wax domains with extensions in the micrometer range exhibited two different topographical structures. Both, depressions and small elevations of the center of the wax features compared to the height level of the matrix were obtained for the investigated coatings. For the determination of the wax distribution on the surface and within the bulk of the coatings lubricant domains with diameters above 2 µm could be considered reliably. While the pigmented topcoat revealed a uniform wax distribution on the surface and within the bulk with average domain size of about 10 µm, the wax distribution in the clearcoat was significantly different. A tendency to enrichment of wax within the bulk and to smaller wax features below 10 µm was obtained for the clearcoat. Hence, a significant effect of the white pigment on the wax distribution was ascertained.

Acknowledgement

The research work of this paper was performed at the Polymer Competence Center Leoben GmbH (PCCL, Austria) within the framework of the Kplus-program of the Austrian Ministry of Traffic, Innovation and Technology with contributions by the Institute of Materials Science and Testing of Plastics at the University of Leoben (Austria), the voestalpine Stahl GmbH (Austria) and the BASF Coatings AG (Germany). The PCCL is funded by the Austrian Government and the State Governments of Styria and Upper Austria. The authors wish to express their acknowledgement to Dominik Haselwanter, Katharina Resch and Christian Hofer of the Polymer Competence Center Leoben GmbH for their support in course of the AFM investigations.

References

[1] D. Chvedov, R. Jones, Surf. Coat. Technol. 188-189 (2004) 544.
[2] P. Carlsson, U. Bexell, M. Olsson, Wear 251 (2001) 1075.
[3] P. Carlsson, U. Bexell, M. Olsson, Wear 247 (2001) 88.
[4] U. Bexell, P. Carlsson, M. Olsson, Appl. Surf. Sci. 203-204 (2003) 596.
[5] P. Nanetti, Lackrohstoffkunde, Vincentz, ISBN 3-87870-560-3 (2000).
[6] P. Carlsson, U. Bexell, M. Olsson, Surf. Coat. Technol. 132 (2000)169.

[7] J. Fischer, G.M. Wallner, B. Strauß, L. Jandel, Surf. Coat. Technol. (2009) submitted.
[8] J. Fischer, G.M. Wallner, B. Strauß, L. Jandel, Prog. Org. Coat. (2009) submitted.
[9] B. Meuthen, A.-S. Jandel, Coil Coating, Vieweg, ISBN 3-528-03975-2 (2005).
[10] E. Bailo, V. Deckert, Chem. Soc. Rev. 37 (2008) 921.
[11] A. Weber, ” Anwendung der Rasterkraftmikroskopie (AFM) zur Untersuchung der Streudomänengröße in thermotropen Polymeren”, Bachelor Thesis, Institute of Materials Science and Testing of Plastics, University of Leoben, A (2009).

4 Zusammenfassung und Ausblick

Das übergeordnete Gesamtziel dieser Arbeit bestand in der Erarbeitung morphologischer Strukturparameter von zwei unterschiedlichen Polymerwerkstoffen als Basis für eine anschließende, außerhalb des Rahmens dieser Arbeit stattfindende Ableitung von Struktur/Eigenschafts-Beziehungen. Bei den in dieser Dissertation untersuchten Polymerwerkstoffsystemen handelte es sich um Polyethylen-Skilaufflächen sowie um wachsgefüllte, polyesterbasierende Bandbeschichtungen. Die untersuchten Werkstoffe sind heterogene Systeme, in denen aliphatische Kohlenwasserstoffe entweder als Polymermatrix oder als eine in der Matrix verteilte disperse Phase vorliegen. Zur Aufklärung der Morphologie heterogener Polyethylen-Skilaufflächen und duromerer Bandbeschichtungen wurde eine Kombination aus mikroskopischen und spektroskopischen Methoden mit Schwerpunkt auf Fernfeld-Raman-Mikroskopie implementiert und systematisch eingesetzt.

Bei der Analyse der Morphologie von Polymerwerkstoffen für Skilaufflächen wurde besonderes Augenmerk auf die Beeinflussung morphologischer Strukturen durch werkstoffliche und prozesstechnische Einflussfaktoren gelegt. Am Beginn der Untersuchungen stand die Entwicklung und Implementierung einer Raman-spektroskopischen Mess- und Auswertemethode zur Charakterisierung der in Polyethylen vorliegenden dreiphasigen teilkristallinen Morphologie, die sich aus einer kristallinen, einer amorphen und einer imperfekt geordneten Komponente (Zwischenphase) zusammensetzt. Die Eignung dieser Methode zur Bestimmung des kristallinen Phasenanteils wurde durch Vergleichsmessungen mit der dynamischen Differenzkalorimetrie (DSC) überprüft und bestätigt. Diese Untersuchungen wurden an ungefüllten Skilaufflächenmaterialen auf unterschiedlichen Prozessebenen durchgeführt. Dabei wurde darauf geachtet, dass kein Prozessschritt mitberücksichtigt wurde, bei dem die Lauffläche einer Oberflächenbehandlung ausgesetzt wurde, damit die Vergleichbarkeit der lokalen Raman-Mikroskopie mit der globalen DSC-Analyse gewährleistet war. Die gut übereinstimmenden Ergebnisse beider Messmethoden zeigten molmassen-

spezifische Unterschiede bei der prozessbedingten Veränderung der teilkristallinen Morphologie. Bei den niedermolekularen Polyethylentypen wurde keine signifikante Veränderung der drei Phasenanteile infolge Ver- oder Bearbeitung der Skilaufflächen festgestellt. Demgegenüber führten die Prozessschritte bei den ultrahochmolekularen Polyethylenen (PE-UHMW) zu abnehmenden kristallinen und zunehmenden amorphen Phasenanteilen. Aufbauend auf diesen Untersuchungen wurde die morphologische Struktur von gefüllten Polyethylenlaufflächen unter Berücksichtigung zusätzlicher Prozessschritte einschließlich der Strukturierung durch Schleifen analysiert. Infolge einer umfassenden Charakterisierung der heterogenen Morphologie von russgefüllten Extrusions- und Sintertypen wurde die Raman-mikroskopische Mess- und Auswertemethode für den Einsatz bei gefüllten Systemen ausgelotet. Hierdurch wurde gezeigt, dass diese Methode lediglich bei russgefüllten Sinterwaren einsetzbar ist. Die morphologische Charakterisierung der Sinterwaren entlang der Prozesskette ergab eine prozessbedingte Zunahme der kristallinen Phase und eine damit zusammenhängende Abnahme der amorphen Phase. Anhand des Vergleiches lokaler und globaler Kristallinitätsgrade waren ausschließlich nach der Strukturierung Unterschiede feststellbar. Während volumensensitive thermoanalytische Analysen keine Veränderung des Kristallinitätsgrades nach Strukturierung ergaben, wurde mittels oberflächensensitiver Raman-Mikroskopie eine signifikante Abnahme der kristallinen Phase sowie eine Zunahme der amorphen Phase und der Zwischenphase nachgewiesen. Die signifikante Phasenänderung an der Oberfläche wurde auf lokale Aufschmelz- und Rekristallisationsprozesse infolge des Schleifens zurückgeführt.

Im Rahmen der Analyse von Polymerwerkstoffen für Bandbeschichtungen wurde die Morphologie wachsgefüllter Bandbeschichtungssysteme in Abhängigkeit von Lackformulierung und Lackaushärtebedingung bestimmt. Dabei wurde ausgehend von Raman-mikroskopischen Untersuchungen an mit schwach streuendem $BaSO_4$ pigmentierten und mit unterschiedlichem Wachsgehalt gefüllten Beschichtungen eine einfach handhabbare Mess- und Auswertemethode basierend auf Lichtmikroskopie entwickelt und implementiert. Neben der umfassenden Charakterisierung der chemischen Zusammensetzung der Bandbeschichtungs-

systeme mittels Raman-Mikroskopie wurde durch Lichtmikroskopie eine quantitative Evaluierung der Wachsausprägung an der Oberfläche und im Inneren von Beschichtungen vorgenommen. Die Analyse der unterschiedlich wachsgefüllten Bandbeschichtungen zeigte kugelförmige Wachsdomänen mit Durchmessern bis zu 32 µm innerhalb der Bindemittelmatrix. Außerdem wurde durch Bestimmung der mit Wachs bedeckten relativen Fläche sowie der Detektion der Anzahl an Wachsdomänen ein direkter linearer Zusammenhang zwischen der Wachsausprägung und dem Wachsgehalt festgestellt. Darauf aufbauend wurde die Kombination aus Raman-Mikroskopie und Lichtmikroskopie bei weiteren wachsgefüllten Bandbeschichtungen eingesetzt. An mit stark streuendem Weißpigment (TiO_2) gefüllten und mit unterschiedlichen Einbrenntemperaturen vernetzten Beschichtungen wurden in den kugelförmigen Wachsdomänen Hinweise auf Spuren des Bindemittels und des Pigments abgeleitet. Außerdem wurde eine Zunahme der mit Wachs bedeckten relativen Fläche mit steigender Einbrenntemperatur und somit ein direkter Zusammenhang zwischen Wachsausprägung und Aushärtebedingung etabliert. An einer unpigmentierten Klarlackbeschichtung und einer mit TiO_2 pigmentierten Beschichtung wurde neben der Raman-Mikroskopie und der Lichtmikroskopie eine höher auflösende rasterkraftmikroskopische Methode zur Analyse der heterogenen Morphologie im Submikrometerbereich implementiert und eingesetzt. Zusätzlich zu den kugelförmigen Wachsdomänen mit Durchmessern über 2 µm und den darin befindlichen Spuren von Bindemittel und Pigment wurden innerhalb der Bindemittelmatrix vorliegende Wachsdomänen mit Durchmessern kleiner 2 µm sowie sich von den Wachsdomänen ausbreitende Wachsschichten mit Dicken unter 100 nm nachgewiesen. Verglichen mit der pigmentierten Beschichtung wurde für die Klarlackbeschichtung ein geringerer Wachsanteil an der Oberfläche einhergehend mit einer stärkeren Wachsausprägung im Volumen festgestellt.

Basierend auf den Ergebnissen der Dissertation werden in bilateralen Projekten mit Partnerfirmen sowohl für Polyethylen-Skilaufflächen als auch für wachsgefüllte Bandbeschichtungen Struktur/Eigenschafts/Performance-Beziehungen als Basis für die zielgerichtete Weiterentwicklung von Werkstoffen und Prozessen ausgearbeitet. Dadurch wird die Signifikanz der erarbeiteten morphologischen

Parameter überprüft und gegebenenfalls die Notwendigkeit weiterführender morphologischer Untersuchungen abgeleitet. Aufgrund des dargelegten hohen räumlichen Auflösungsvermögens der Raman-spektroskopischen Methoden sollten sich künftige Arbeiten an Skilaufflächenwerkstoffen beispielsweise mit der Tiefenprofilierung beschäftigen, um so eine umfassendere, tiefenaufgelöste Beschreibung der Morphologie zu ermöglichen. Zudem sollten neben dem Schleifen inklusive gezielter Nachkonditionierung alternative Endstrukturierungsverfahren wie Prägen oder Gravieren untersucht werden. Bei hoher Signifikanz der morphologischen Phasenanteile bietet die Raman-spektroskopische Methode ein hohes Potential für die Entwicklung und Implementierung von in-situ Analyseverfahren zur prozessbegleitenden Qualitätssicherung. Bezüglich der morphologischen Analyse von wachsgefüllten Bandbeschichtungen sollten sich weiterführende Untersuchungen beispielsweise mit Einfluss von Pigmentvariationen (z.B. Schwarzpigment oder Buntpigment) auf die Wachsausprägung beschäftigen. Zudem sollte ein Modell zur Beschreibung der Bildung von Wachsdomänen in der Beschichtung ausgehend von den im Lack dispergierten Wachspartikeln erarbeitet werden. Aus methodischer Sicht wäre die Auslotung und Implementierung der Nahfeld-Raman-Mikroskopie mit deutlich höherer räumlicher Auflösung von besonderem wissenschaftlichem Interesse. Da diese Methode in der Polymerphysik jedoch noch nicht angewendet wurde, müsste eine Reihe grundlegender Fragestellungen gelöst werden.

Literaturverzeichnis

Bailo, E., Deckert, V. (2008). Chem. Soc. Rev. 37, 921.

Barron, D., Birkinshaw, C. (2008). Polymer 49, 3111.

Bertoluzza, A., Fagnano, C., Rossi, M., Tinti, A., Cacciari, G.L. (2000). J. Mol. Struct. 521, 89.

Bexell, U., Carlsson, P., Olsson, M. (2003). Appl. Surf. Sci. 203-204, 596.

Brockhaus (1998). „Brockhaus – die Enzyklopädie 15“, Band 15, Mannheim, D.

Buder-Stroißnigg, M. (2008). „Umformbare polymerbeschichtete Bleche – Polymerphysikalische Charakterisierung und Struktur/Eigenschafts-Beziehungen“, Dissertation, Montanuniversität Leoben, A.

Cahn, R.W., Haasen, P., Kramer, E.J., Thomas, E.L. (1993). „Materials Science and Technology“, Volume 12, VCH, Weinheim, D.

Carlsson, P., Bexell, U., Olsson, M. (2001a). Wear 247, 88.

Carlsson, P., Bexell, U., Olsson, M. (2001b). Wear 251, 1075.

Cherukupalli, S.S., Ogale, A.A. (2004). Polym. Eng. Sci. 44, 1484.

Christofferson, J., Maize, K., Ezzahri, Y., Shabani, J., Wang, X., Shakouri, A. (2008). J. Electron. Packag. 130, 0411011.

Chvedov, D., Jones, R. (2004). Surf. Coat. Technol. 188-189, 544.

Coates, J., Reffner, J. (1999). Spectroscopy 14, 44.

Colbeck, S.C., Perovich, D.K. (2004). Cold Regions Sci. Tech. 39, 33.

Erich, S.J.F., Laven, J., Pel, L., Huinink, H.P., Kopinga, K. (2005). Prog. Org. Coat. 52, 210.

Everall, N.J. (2005a). JCT CoatinsTech 2 (19), 38.

Everall, N.J. (2005b). JCT CoatinsTech 2 (20), 46.

Fagnano, C., Rossi, M., Porter, R.S., Ottani, S. (2001). Polymer 42, 5871.

Failla, M., Alamo, R.G., Mandelkern, L. (1992). Polym. Testing 11, 151.

Federolf, P.A. (2005). „Finite Element Simulation of a carving snow ski“, Dissertation, ETH Zürich, CH.

Fischer Sports GmbH (2009). www.fischer-ski.com, Ried im Innkreis, A.

Fluch, R. (2009). „Charakterisierung verfilmter Coil Coating Lacke mittels dynamisch thermomechanischer Analyse (DTMA)“, Dissertation, Johannes Kepler Universität Linz, A.

Gamage, N.J.W., Hill, D.J.T., Lukey, C.A., Pomery, P.J. (2003). Polym. Deg. Stab. 81, 309.

Glenne, B., DeRocco, A., Vandergrift, J. (1997). Cold Regions Sci. Tech. 26, 35.

Hendra, P.J., Agbenyega, J.K. (1993). „The Raman spectra of polymers“, Wiley, Chichester, USA.

Isosport Verbundbauteile GmbH (2009). www.isosport.at, Eisenstadt, A.

Jenkins, A.L., Larsen, R.A. (2004). Polymer News 29, 71.

Jordan, S.E., Brown, C.A. (2006). Wear 261, 398.

Kämpf, G. (1982). „Die Charakterisierung von Kunststoffen mit physikalischen Methoden“, Hanser, München, D.

Kannan, R.Y., Salacinski, H.J., Vara, D.S., Odlyha, M., Seifalian, A.M. (2006). J. Biomater. Appl. 21, 5.

Keresztury, G., Földes, E. (1990). Polym. Testing 9, 329.

Koenig, J.L., Bobiak, J.P. (2007). Macromol. Mater. Eng. 292, 801.

Kudelski, A. (2009). Surface Science, Article in Press.

Kyomoto, M., Miwa, Y., Pezzotti, G. (2007). J. Biomater. Sci. Polym. Edn. 18, 165.

Lin, S.-Y., Li, M.-J., Cheng, W.-T. (2007). Spectroscopy 21, 1.

Lin, W., Cossar, M., Dang, V., Teh, J. (2007). Polym. Testing 26, 814.

MacCreery, R.L. (2000). „Raman spectroscopy for chemical analysis“, Wiley, New York, USA.

Menges, G. (1990). „Werkstoffkunde Kunststoffe“, Hanser, München, D.

Meuthen, B., Jandel, A.-S. (2005). „Coil Coating“, Vieweg, Wiesbaden, D.

Nanetti, P. (2000). „Lackrohstoffkunde“, Vincentz Network, Hannover, D.

Paradkar, R.P., Sakhalkar, S.S., He, X., Ellison, M.S. (2003). J. Appl. Polym. Sci. 88, 545.

Perruchot, C., Watts, J.F., Lowe, C., Beamson, G. (2003). Int. J. Adhes. Adhes. 23, 101.

Pollock, H.M., Hammiche, A. (2001). J. Phys. D: Appl. Phys. 34, R23.

Reggiani, M., Tinti, A., Taddei, P., Visentin, M., Stea, S., de Clerico, M., Fagnano, C. (2006). J. Mol. Struct. 785, 98.

Retting, W., Laun, H.M. (1991). „Kunststoff-Physik“, Hanser, München, D.

Rodriguez, R., Jimenez-Sandoval, S., Estevez, M., Vargas, S. (2008). J. Non-Cryst. Solids 354, 3623.

Rodriguez-Cabello, J.C., Martin-Monge, J., Lagaron, J.M., Pastor, J.M. (1998). Macromol. Chem. Phys. 199, 2767.

Rodríguez-Pérez, M.A., Campo-Arnáiz, R.A., Aroca, R.F., de Saja, J.A. (2005). Polymer 46, 12093.

Rull, F., Prieto, A.C., Casado, J.M., Sobron, F., Edwards, H.G.M. (1993). J. Raman. Spectrosc. 24, 545.

Schamesberger, R. (1993). International Patent, WO 93/05853.

Schamesberger, R. (1995). U.S. Patent, US95/5466743.

Schamesberger, R. (2006). U.S. Patent, US06/0251486.

Scholes, F.H., Furman, S.A., Hughes, A.E., Nikpour, T., Wright, N., Curtis, P.R., Macrae, C.M., Intem, S., Hill, A.J. (2006). Prog. Org. Coat. 56, 23.

Schrader, B. (1995). „Infrared and Raman spectroscopy“, VCH, Weinheim, D.

Schrof, W., Beck, E., Königer, R., Reich, W., Schwalm, R. (1999). Prog. Org. Coat. 35, 197.

Siesler, H.W. (1980). „Infrared and Raman spectroscopy of Polymers“, Dekker, New York, USA.

Strobl, G.R. (1997). „The Physics of Polymers“, Springer, Berlin, D.

Strobl, G.R., Hagedorn, W. (1978). J. Polym. Sci. 16, 1181.

Stroi, J. (2003). International Patent, WO 03/061783.

Stuart, H.A. (1955). „Die Physik von Hochpolymeren“, Springer, Berlin, D.

Suzuki, E.M., Carrabba, M. (2001). J. Forensic. Sci. 46 (5),1053.

Van Krevelen, D.W. (1990). „Properties of Polymers“, Elsevier, Amsterdam, NL.

Visentin, M., Stea, S., de Clerico, M., Reggiani, M., Fagnano, C., Squarzoni, S., Toni, A. (2006). J. Biomater. Appl. 21, 131.

voestalpine Stahl GmbH (2008). „Colofer Processing“, www.voestalpine.com/stahl/en/site/downloads/product_brochures.html, Linz, A.

Wallner, G.M. (2008). „Polymere Funktionswerkstoffe für die Solartechnik“, Habilitationsschrift, Montanuniversität Leoben, A.

Weber, W.H. (2000). „Raman scattering in materials science“, Springer, Berlin, D.

Woodward, A.E. (1988). „Atlas of polymer morphology“, Hanser, New York, USA.

Woodward, A.E. (1995). „Understanding Polymer Morphology“, Hanser, New York, USA.

Wunderlich, B. (1973). „Macromolecular Physics“, Volume 1, Academic Press, New York, USA.